AlSi system influence on characteristics of power diodes

AlSi system influence on characteristics of power diodes

Ph.d in electronic devices

2/2/2014

Vishay Intertechnology, Inc.
Corrado Sgorlon

Supervisors
Ing. Simone Cianchini
Prof. C.F. Pirri

A Rina, Maria, Bartolo, Giovanni

Table of Contents

Table of Contents 3
1 Thesis overview 6
1.1 Introduction 6
1.2 Thesis structure 6
1.3 Zones of interest in a power diode. 6
1.3.1 Microstructure (chapter 3) 7
1.3.2 Interface between AlSi and silicon substrate (Chapter 4) 8
1.3.3 Amorphous silicon (chapter 5) 9
1.3.4 Interface between amorphous silicon and contact metal. (chapter 6) 9
2 Concepts and techniques overview 10
2.1 introduction 10
2.2 Materials: Silicon and Aluminum 10
2.2.1 Silicon 10
2.2.2 Aluminum 17
2.3 Diode overview 19
2.3.1 Electrical parameters 19
2.3.2 Diode's structure. 20
2.3.3 SIPOS termination 21
2.4 Measurement techniques 22
2.4.1 Schottky barrier height 22
2.4.2 Film stress 23
2.4.3 UV-vis optical characterization. 26
3 Microstructure and crystal structure. 31
3.1 Introduction 31
3.2 Variability of AlSi structure 31
3.3 Experiment 1: Substrate and temperature influence 32
3.3.1 Experimental setup 32
3.3.2 Results 32
3.3.3 Discussion. 36
3.4 OH terminated silicon 38

3.4.1 Experimental 38
3.4.2 Results 39
3.4.3 Discussion and comments 41
3.5 H terminated samples. 44
3.5.1 H terminated samples, experiment 1. 46
3.5.2 Production data collection 47
3.6 Conclusions. 50
4 Silicon substrate / AlSi interaction 51
4.1 Introduction 51
4.2 Schottky barrier with pure aluminum 51
4.2.1 Schottky barrier with oxide at the interface. 51
4.2.2 Thermal treatments 52
4.3 Experimental. 55
4.3.1 Experiment 1: Surface preparation and metal type influence 57
4.3.2 Experiment two: temperature effect 60
4.3.3 Inspection of the interface 62
4.3 Conclusions 66
5 a-Si film deposition 67
5.1 Introduction 67
5.2 Refractive index validation 67
5.2.1 Introduction 67
5.2.2 Experimental. 67
5.2.3 Results and discussion 68
5.3 Amorphous silicon influence on leakage 69
5.4 Sputtered a-Si characterization 70
5.4.1 Introduction 70
5.4.2 Experimental 70
5.4.3 Results and discussion 71
5.4.4 Results summary. 75
5.4.5 Test on production samples 76

5.5 Hydrogen addition on amorphous matrix structure 77
5.5.1 Introduction 77
5.5.2 Experimental 78
5.5.3 Comments 79
5.5.4 Test on Production samples 79
5.6 Conclusions 80
6 Amorphous Silicon and Aluminum interface interactions 81
6.1 Introduction 81
6.2 ALILE: characterization and stress 81
6.3 Experiments on aluminum / amorphous silicon interaction 83
6.3.1 Experiments summary 83
6.3.2 Experiment 1: Identify substrate influence 83
6.3.3 Experiment 2: Furnace response. 87
6.3.4 Experiments 3 and 4: Stress response to interface type 90
6.4 Conclusions 98
7 Closing comments 99
7.1 Results summary 99
7.2 Industrial impact 100
7.3 Future works 100
8 References 101

Ringraziamenti 103

1 Thesis overview

1.1 Introduction

In this thesis we will focus on the behavior of aluminum and silicon. We will study their properties, their interaction and the phenomena occurring at the interfaces between the two materials, having as an objective to explain the impact that those effects have on the structure of a power diode.

We will especially focus on DC sputtered material, and in particular on the deposition of an AlSi (1%Si) alloy and a layer of amorphous silicon.

1.2 Thesis structure

This work will be composed of six chapters: two introductive ones and four experimental

- Introductive chapters
  - The first chapter is an introduction to the whole thesis
  - The second chapter contains some theoretical concepts that will be useful during experimental analysis
- Experimental chapters
  - Chapter three will collect all the experimental work, done to explain the formation and the evolution of the microstructure and crystal structure of the sputtered AlSi Alloy
  - Chapter four contains the studies regarding the interface between crystalline silicon and the sputtered AlSi alloy
  - Chapter five contains the characterization of a sputtered amorphous silicon film
  - In chapter six are collected all the experiments on the interactions between the amorphous silicon film and the AlSi film

1.3 Zones of interest in a power diode.

The four topics, that have been subject of experimental study due to their importance in the processing of power diodes, are highlighted in figure 1.1

We can distinguish two main areas in the device: The active area and the termination. In planar diodes the active area is mainly responsible for the conduction characteristics of the device, such as forward voltage drop. The efficiency of the termination area on the other hand is important to permit the device to reach the maximum breakdown voltage (Vz) determined by the epitaxial layer's thickness.

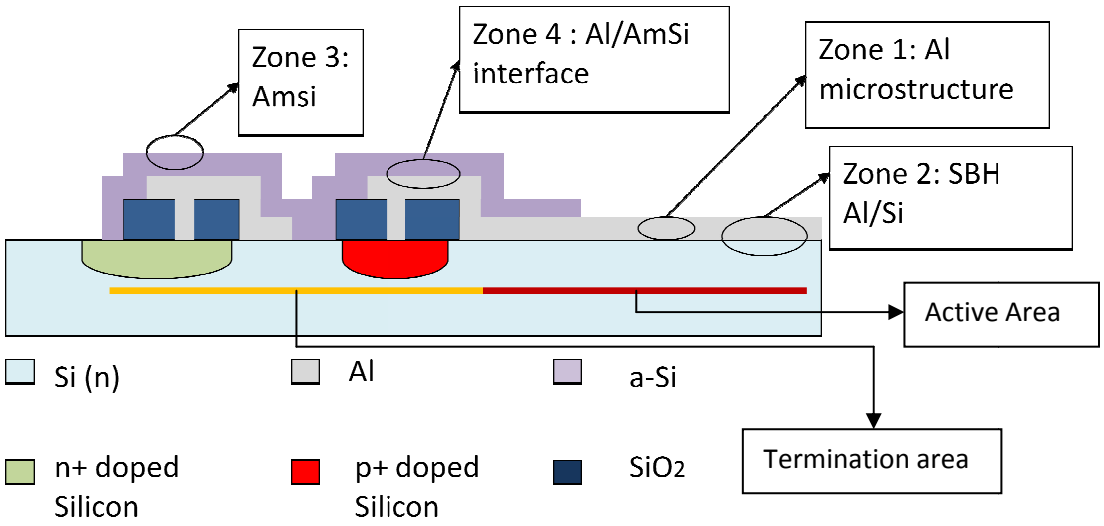

Figure 1.1 schematic representation of a power diode. The areas that have been subject of study have been highlighted.

The influence of the peculiar characteristics of the AlSi system, plays a major role in each of those areas. A deep understanding of the phenomena that occur is crucial, in order to achieve stable processes and repeatable results during devices fabrication.

A brief introduction of each area that will be extensively discussed in a dedicated experimental chapter will be given

1.3.1 Microstructure (chapter 3)

With a microscope analysis is possible to see that AlSi can show many different types of visual aspects. In figure 1.2 is given an example of this high variability. This comprises the presence/absence of a visible grain structure, a high variability in roughness, the presence of peculiar features such as hillocks or cubic formations. All those things can influence not only the material's visual characteristics, but also the mechanical and electrical ones. For this reasons the underlying causes that determine the formation of one structure instead of the other, and the relationship between the microstructure and the corresponding crystal structure, have been investigated.

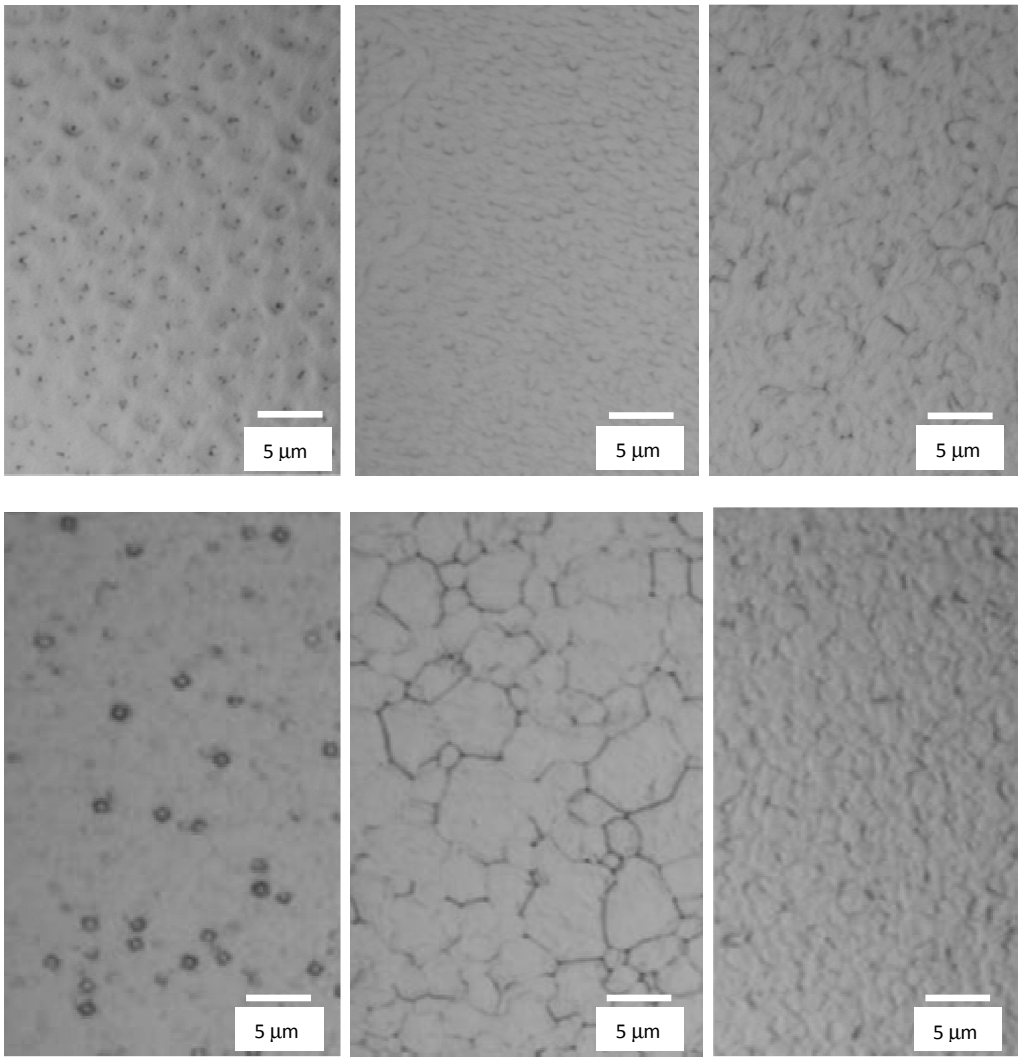

Figure 1.2. Examples of different AlSi microstructures

1.3.2 Interface between AlSi and silicon substrate (Chapter 4)

The second area that has been investigated is the interface between the monocrystalline silicon substrate and the contact metal. This area, depending on the type of device we are dealing with, can act as a simple ohmic contact (in the case of a PN junction diode) or as a schottky barrier, when the contact occurs directly between the metal and the undoped epitaxial substrate. The study of the schottky barrier is of particular interest since, due to the peculiar characteristics of the AlSi alloy and its interaction with the substrate, very high barrier height (over 1eV) can be measured. In the formation of the schottky barrier a major role is also played by oxygen. In chapter 4 we studied how its presence can affect both the selection of microstructure and the stress level. In this chapter it has been studied how it can affect the SBH.

1.3.3 Amorphous silicon (chapter 5)

In order to reach high efficiency of the termination, on high breakdown diodes (600V and more), a film of amorphous silicon is applied. This type of termination is called SIPOS (semi insulating poly silicon) and the electrical properties of the deposited silicon layer have to be tuned carefully.

During this chapter we will characterize a thin layer of amorphous silicon deposited with a DC magnetron sputter, and we compared its performances with an amorphous layer obtained using an e-beam evaporator.

1.3.4 Interface between amorphous silicon and contact metal. (chapter 6)

The last experimental chapter focuses on the interaction between the amorphous silicon in the termination area and the underlying contact metal. Those materials can have strong interactions, and in particular they can trigger an effect called “ALILE”, which is an acronym that stands for Aluminum Induced Layer Exchange. If a thermal budget is given to the system, silicon and aluminum exchange their position and during the exchange silicon can pass from the amorphous form to the polycrystalline one. This effect is associated to a dramatic change in the stress of the a-Si layer. We will investigate the phenomenon focusing our attention on the interface between the two materials.

2 Concepts and techniques overview

2.1 introduction

In this chapter we will give a brief overview of the concepts and techniques that will be used in the next ones to describe and characterize the Al Si system and its impact on power diodes.

Three main topics will be presented:

- An overview of materials: Aluminum and Silicon
- A description of a diode and some details on structural and design concepts that will be used during the analysis of experimental data
- An introduction on the measurement techniques that will be extensively used in the next chapters.

For each topic the main aim will be to highlight those concepts that will be important during the analysis in experimental chapters.

2.2 Materials: Silicon and Aluminum

2.2.1 Silicon

2.2.1.1 Introduction

In the discussion on the materials that constitute the various part of the power diode, we will encounter silicon in both crystalline and amorphous form. Crystalline silicon is the one used as a substrate, while amorphous silicon will be employed in the device termination.

We will introduce some important characteristics of silicon structure paying particular attention to the differences between amorphous and crystalline material.

2.2.1.2 Silicon's structure and properties summary.

Silicon has a diamond structure with a lattice parameter = 5.43 Angstroms. This means that it has a Face Centered Cubic cell with half of the eight tetrahedral sites occupied

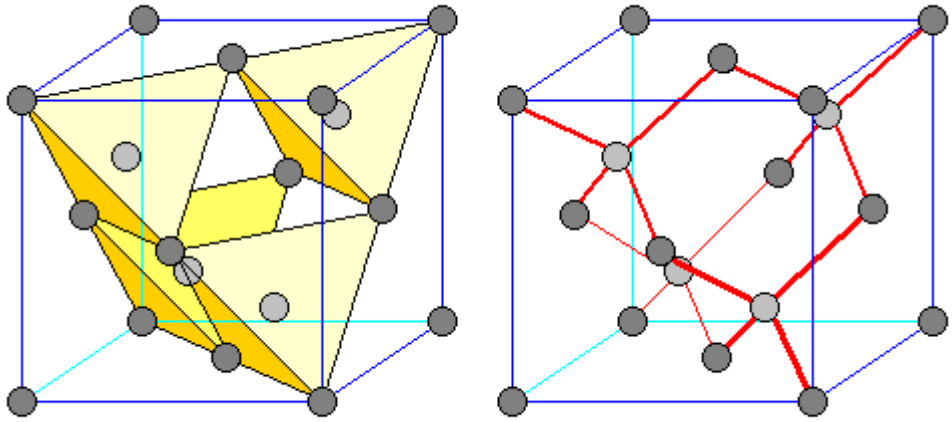

Figure 2.1 diamond structure

Coordination in diamond structure is 4, and the atomic packaging factor is 0.34 (smaller compared to high coordination structures like FCC: 0.74). This limited space filling results in the presence of large channels in the structure on particular crystalline orientation as can be seen in figure 2.2. This property must be taken into account for example when we are making ion implantation.

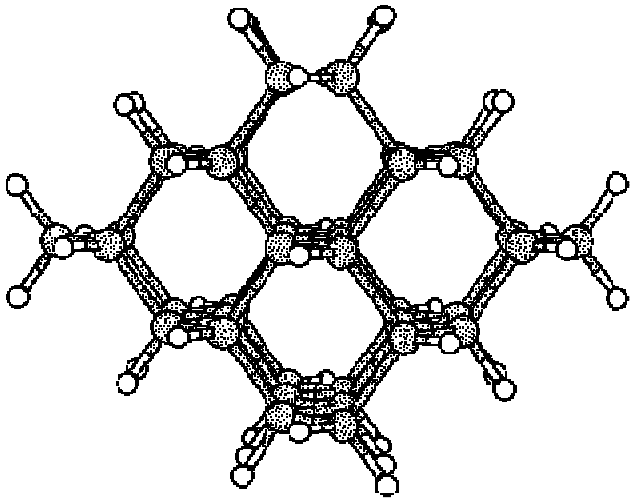

Figure 2.2 Silicon channels

Here below is showed the direct and reciprocal lattice of silicon(in case of a FCC the reciprocal lattice is a BCC). High symmetry points are highlighted with Greek capital letters in reciprocal lattice

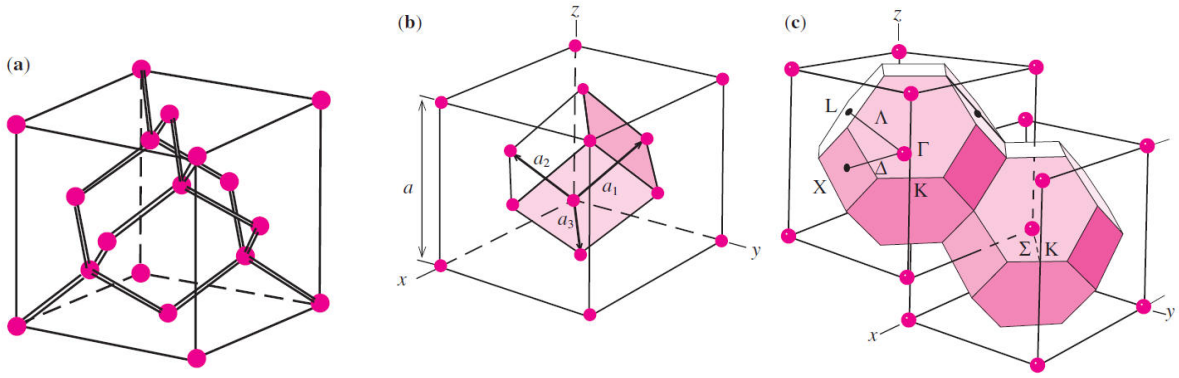

Figure 2.3 (a)silicon diamond structure, Direct lattice (b) and reciprocal lattice (c)

We can calculate the first Brillouin zone using this data, and with the periodical potential the corresponding band structure.

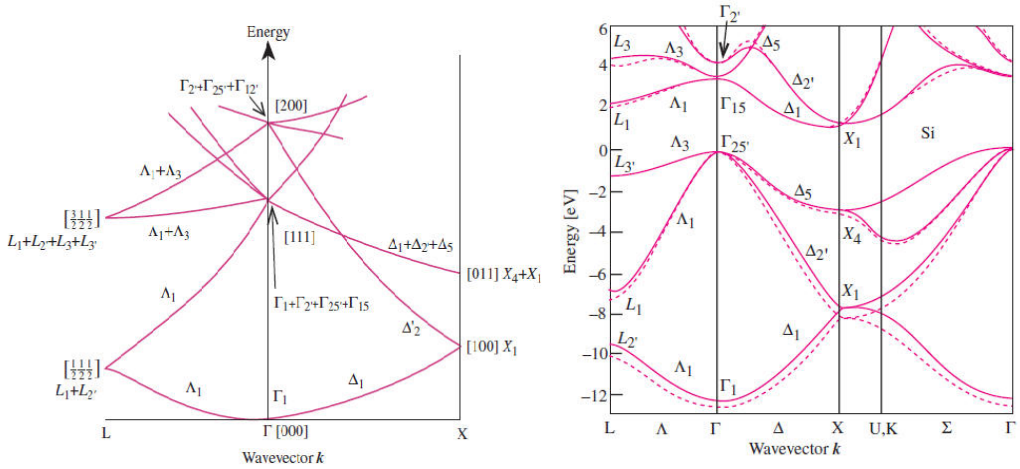

Figure 2.3 Silicon band structure

In figure 2.4 some useful characteristics of this band structure are highlighted. In particular is important to notice the silicon's indirect bandgap (1.15 eV) and two direct transitions that gives clear UV reflectance peaks. The reflectance spectra in the UV region of silicon with the two peaks are shown in figure 2.5

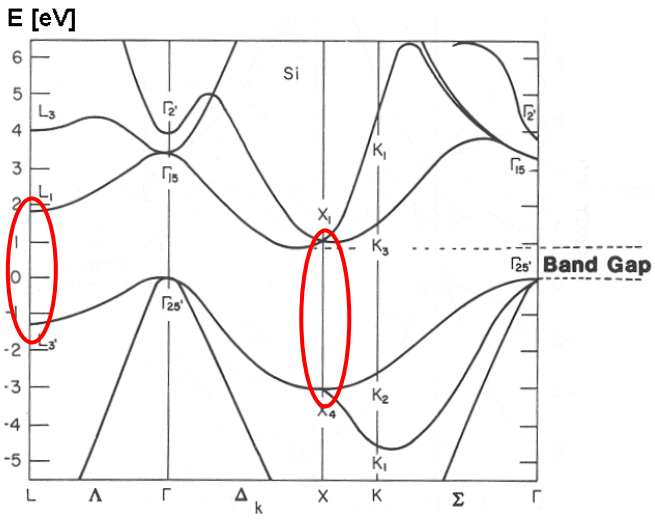

Figure 2.4 Silicon Band structure. Three important features has been evidenced: the indirect bandgap, and two direct transitions, along the L and X direction with an energy of 3.4eV (375 nm) and 4.49 (276 nm)

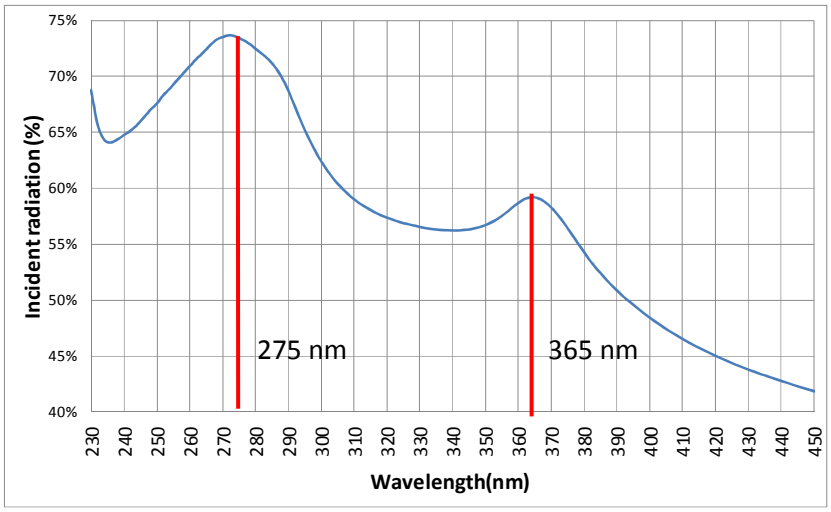

Figure 2.5: UV reflectance spectra of Si

2.2.1.3 Silicon native oxide layer

When exposed to air Silicon immediately oxidizes. For this reason, if no further treatments are done to the material, the surface of the material is composed by a thin (12 to 20 Angstroms) layer of SiO_2 .

This layer can be removed with an HF treatment. After the etch the oxide layer is removed, and hydrogen complexes the dangling bonds. The system in this way is stable and do not oxidize again for some hours. An easy way to see if the surface of silicon is correctly passivated, and no oxide is present

on the surface, is to measure its wettability. Non treated silicon, with the native oxide on top is highly hydrophilic, while H terminated silicon, without native oxide is Hydrophobic.

2.2.1.4 Amorphous material.

The main characteristics of amorphous materials are

- No long range order
- Short range order
- Coordination defects

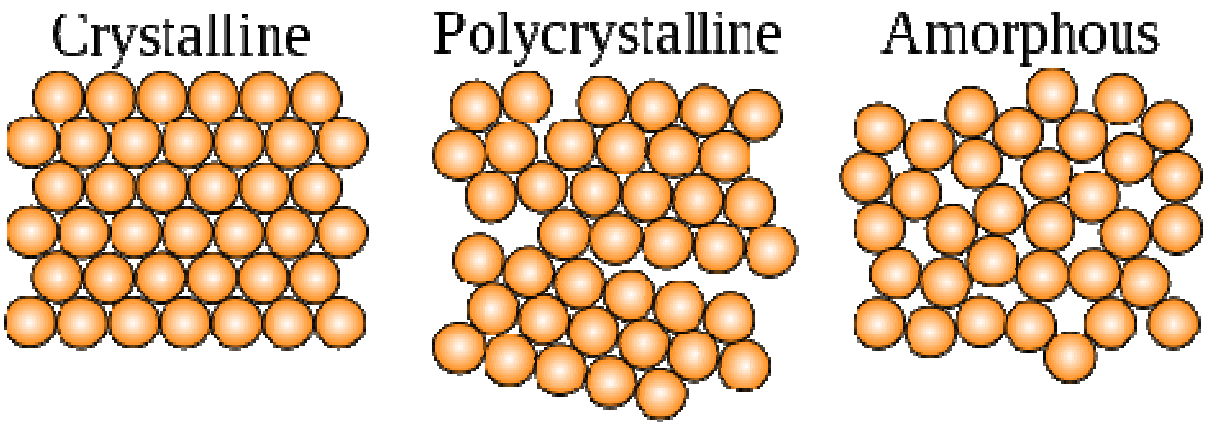

Figure 2.6: comparison between a crystalline, polycrystalline and amorphous material.

The short order results in similar properties of amorphous materials compared to the corresponding crystalline one. Silicon dioxide is always an insulator, and silicon is a semiconductor.

The lack of a long range order otherwise makes the wave function to lose phase coherence over distances of one or two interatomic distances. This gives arise to highly localized stases and large uncertainty in the electron momentum.

$$\Delta k = \frac{\hbar}{\Delta x} \approx \frac{\hbar}{a_0} \approx k \qquad (1)$$

Where Δx is the scattering length and a_0 is the interatomic spacing.

Due to the absence of k conservation, there is not a distinction in amorphous materials between direct and indirect bandgap, and they can all be treated as having direct bandgaps. In place of the E-k dispersion relation, on amorphous materials a Density Of States / Energy distribution is used

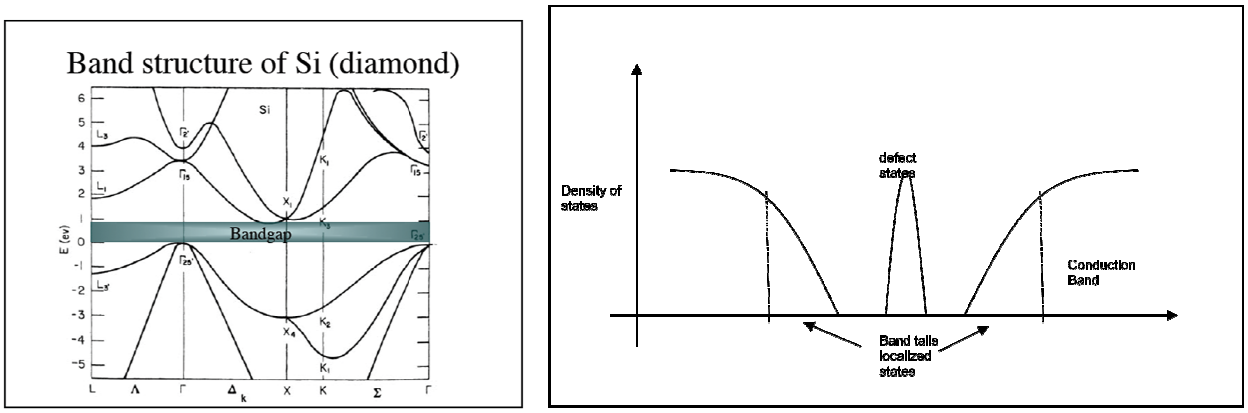

Figure 2.7: comparison between the band diagram description for (a) crystalline and (b) amorphous materials

2.2.1.5 Hydrogen introduction in amorphous silicon

Since in perfect crystalline structure Silicon coordination is 4, and the strong covalent bonds have a precise directionality, in amorphous structure due to the long range disorder, coordination errors are frequent. The consequence is the formation of dangling bonds within the structure that give origin to localized defective states within the bandgap

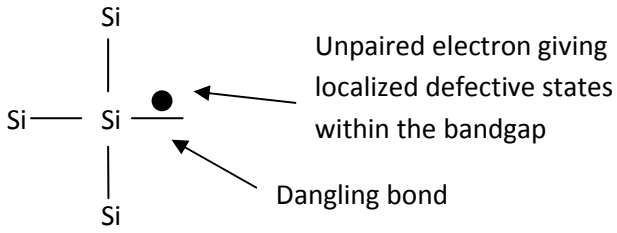

Figure 2.8 dangling bond in silicon

If we add hydrogen to this type of lattice, we can saturate this unpaired bonds, and the effect is a reduction of the defective states as can be seen on figure 2.9

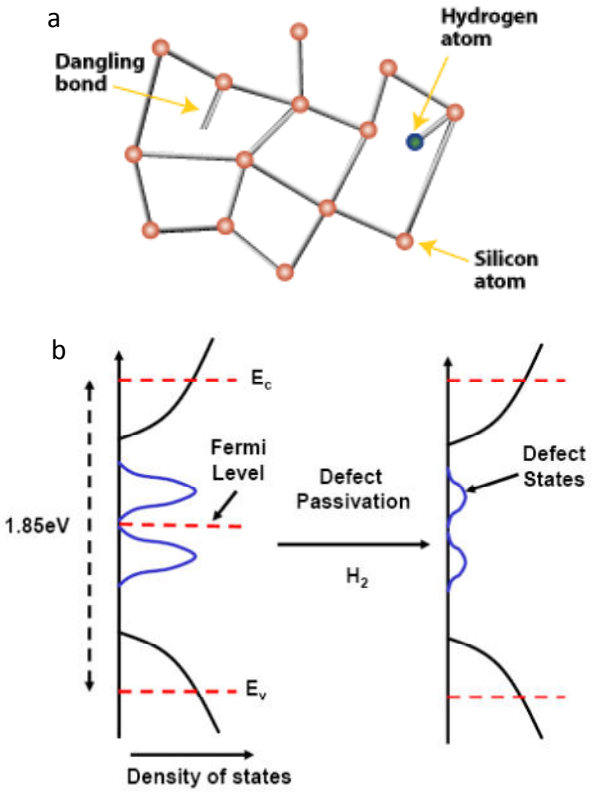

Figure 2.9 effect of hydrogen addition to amorphous silicon structure (a) on the material structure (b) on the reduction of defective states in the bandgap

2.2.1.6 Structural effect of Hydrogen in a-Si

An important effect of the presence of hydrogen in the amorphous silicon is the mobility that hydrogen allows to the otherwise rigid structure (ref 16). Hydrogen can move from one bond to the other, can help to brake coordination defects and, with successive reactions, can relax the structure. See ref XXX for details. On figure 2.10 is possible to see an example of this effect

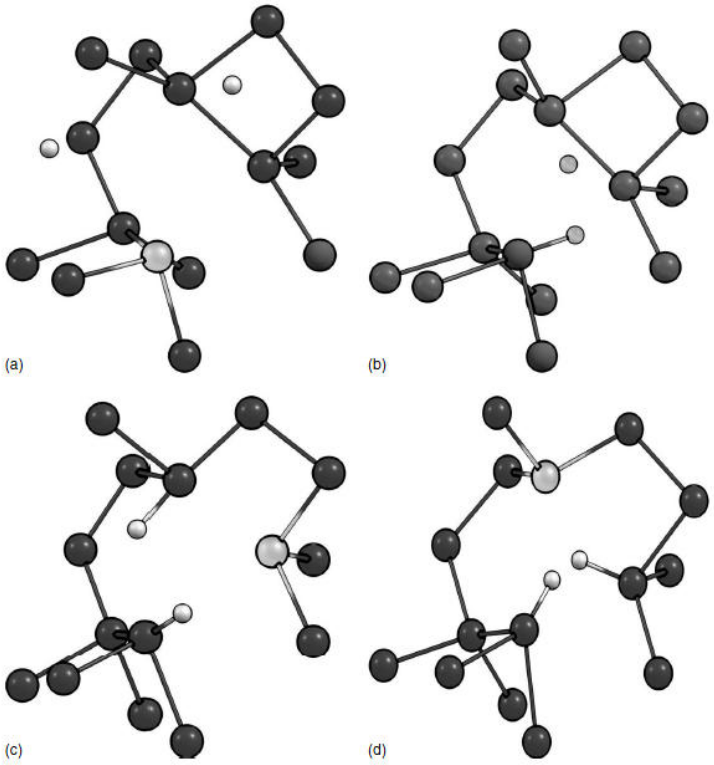

Figure 2.10: Hydrogen reactions in the a-Si structure

2.2.2 Aluminum

2.2.2.1 Introduction

Aluminum is a very important material in the semiconductor industry. in this paragraph we will see an overview of a very important characteristic of aluminum, that will be of crucial importance in its reactivity: the native oxide.

From a crystallographic point of view, aluminum has a face centered cubic structure, with a cell parameter of 4.049 Angstroms

2.2.2.2 Aluminum native oxide

As we have seen for silicon, aluminum surface is always passivated with a native oxide layer. This oxide gives the typical corrosion resistance of aluminum. In our work we are more interested in the structural characteristics of the film rather than its chemical properties.

The natural, colorless oxide thin film is build up from two superimposed layers

- The first compact and amorphous layer, in contact with the metal, is called the barrier layer, because of its dielectric properties. It will form at any temperatures as soon as the liquid or solid

metal comes in contact with air or an oxidizing medium; the temperature acts only on the final thickness. It forms very quickly, within a few milliseconds. The rate of formation is independent of the oxygen partial pressure. In practice , this means that the oxide film will reappear immediately after etching, forming, machining operations have destroyed the natural oxide layer locally, as soon as oxygen is available again. Film growth follows a parabolic kinetics up to 350-400°C and becomes linear at higher temperatures. The maximum thickness of this layer is in the order of 4nm

- The second layer grows on top of the first one, by reaction with the exterior environment, probably by hydratation. Its final thickness will not be reached before several weeks, even months, and depends on the physicochemical conditions (relative humidity and temperature) which favor film growth. This second film is less compact than the barrier layer, is porous and reacts with the external environment. In prolonged contact with water, it tends to grow, expecially at high temperatures, and transforms into bayerite and bohemite. In table 2.11 the properties of this two forms of aluminum oxide are given
-

Species	Crystal structure	Chemical formula	Temperature range of formation	Density
Amorphous alumina		Al2O3	<50-60	3.40
Bayerite	Monoclinic	α-Al(OH)3	60-90	2.53
Bohemite	Orthorhombic	γ-AlOOH	>90	3.01
Corundum	Hexagonal	α-Al2O3	>350	3.98

Table 2.11 Aluminum oxide properties

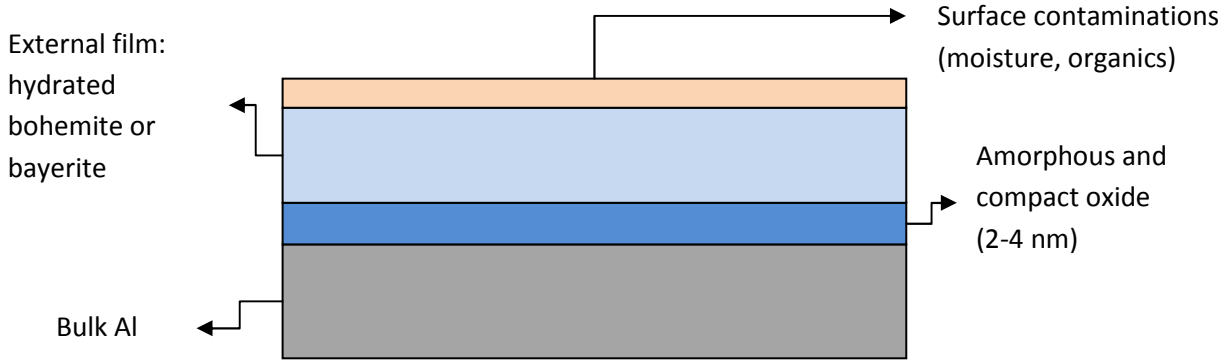

Figure 2.12: Oxide layers on top of aluminum

2.3 Diode overview

2.3.1 Electrical parameters

We will now describe some basic characteristics of a diode. We will focus on the three main electrical parameters that will be used in the following chapters to monitor the impact of the Al-Si system variations: the leakage current, the forward voltage drop and the breakdown voltage

The diode is an electronic device that ideally has a zero resistance when polarized in one direction and infinite resistance in the opposite one.

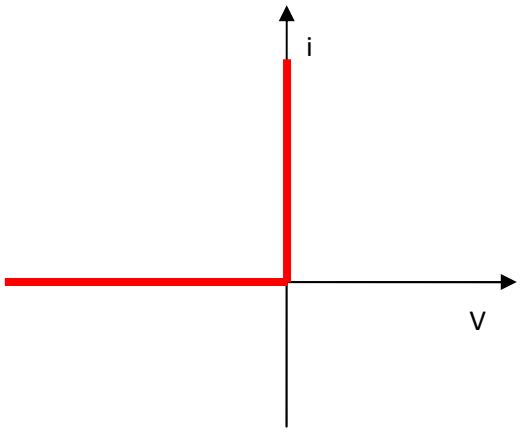

Figure 2.13: ideal diode

In figure 2.13 an ideal diode is presented. A diode performing in this way will not dissipate any power: the device will have no leakage current when is blocking in reverse bias and no tension drop when is polarized in forward bias

A real device performance will be as in figure 2.14

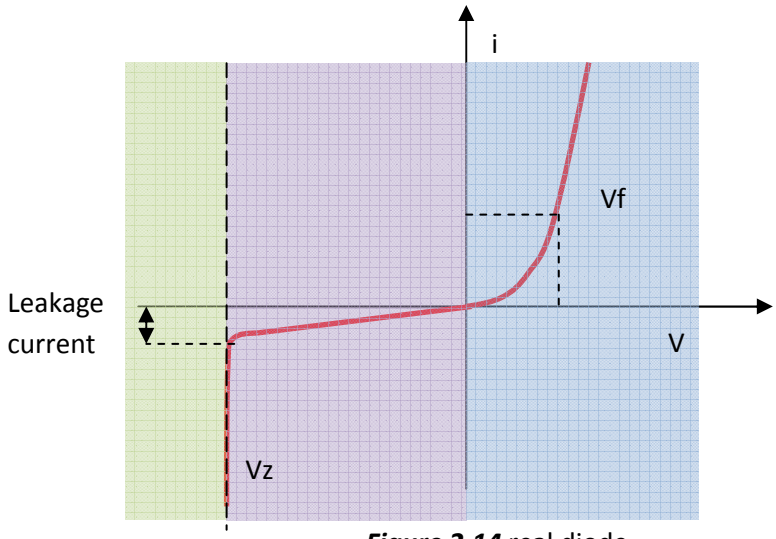

Figure 2.14 real diode

We can distinguish three main areas:

- In forward polarization a certain amount of voltage drop is present. This value is called Vf and is given for a certain amount of current (example Vf at 10A)
- When the device is blocking current we have some current flowing. This current is called leakage current
- A real device is able to sustain a finite amount of potential. This potential is defined breakdown Voltage (Vz)

2.3.2 Diode's structure.

There are many types of diodes, each one with peculiar structure. In figure 2.15. a basic scheme of a planar diode is presented, where have been highlighted two main areas: the active area and the termination. The active area is the central part of the device and is mainly responsible for the conduction of the device in direct bias polarization. The termination on the other hand works when the device is used in reverse bias conditions. Its efficiency represents the ability of the device to reach the maximum breakdown possible. The leakage current can originate either from the active area and from undesired effect in the termination.

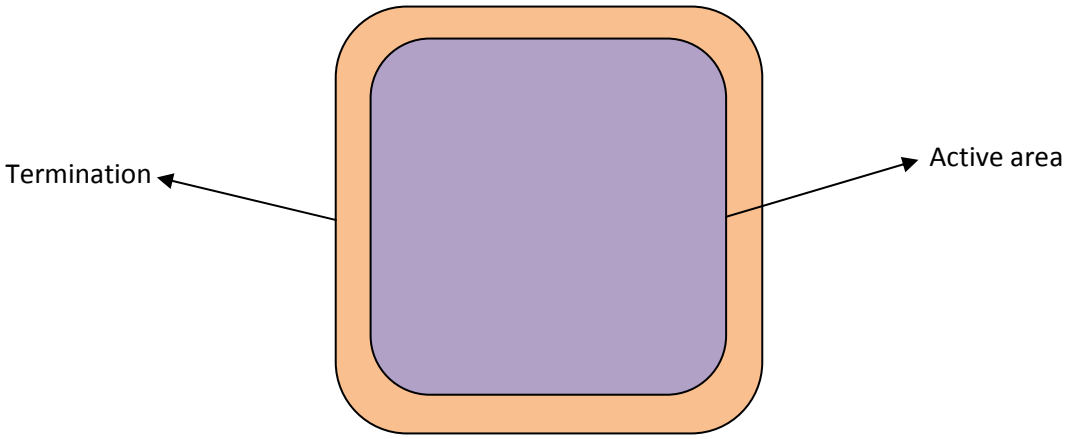

Figure 2.15: Schematic representation of a diode

2.3.3 SIPOS termination

The use of amorphous silicon (or polysilicon) to increase the efficiency of devices termination is known under the acronym of SIPOS (semi insulating poly silicon) termination (ref. 7, 8). The effect of the addition of polysilicon in a structure with more than one guard ring, is to spread the voltage drop across all the termination, and in this way avoiding that the electrical field does not reach high values that can cause a breakdown. A scheme of the SIPOS termination can be seen in figure 2.16. In figure 2.17 is possible to see a simulation of the current flow at the breakdown voltage in the same termination with or without the SIPOS layer on top. As can be seen the current flows in active area if the silicon layer is present, and the termination is able to efficiently block the tension. If the amorphous silicon layer is not present, the termination is not able to block all the reverse bias, and the current starts to flow in the termination area.

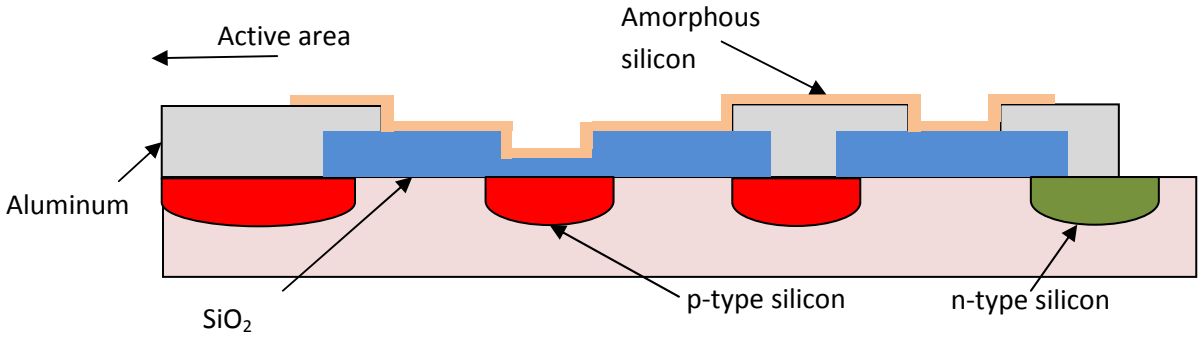

Figure 2.16: a scheme of the SIPOS termination

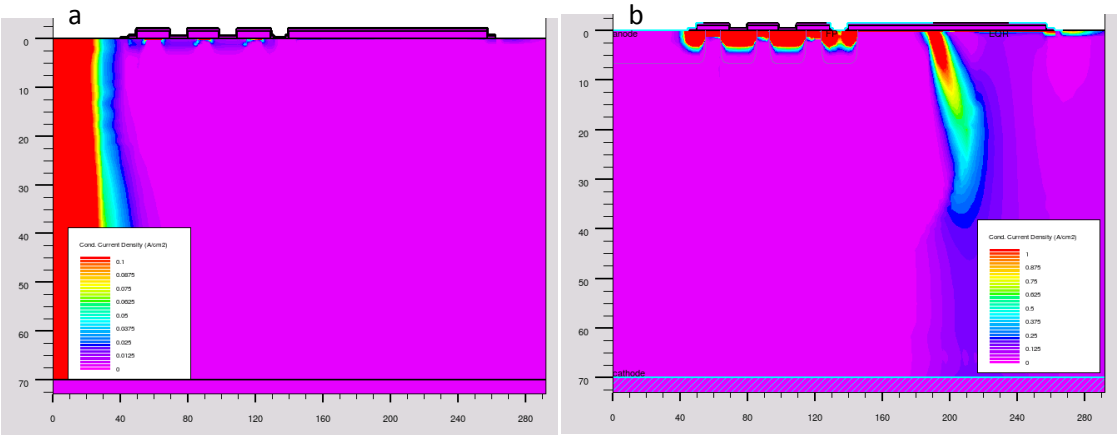

Figure 2.17: Simulation of Current flow at the breakdown in (a) a termination with SIPOS (b) the same termination without SIPOS

2.4 Measurement techniques

2.4.1 Schottky barrier height

We used two types of diodes during our experiments: the PN diodes where the rectifying characteristic is given by the p-n junction, and the schottky diodes, where in the active area a metal / semiconductor interface is present. We will calculate the schottky barrier height (SBH) and the ideality factor for those samples.

The current tension relation derives from the thermionic emission theory, we can write it as follows

$$J = J_0 e^{\left(\frac{qV}{nkT}\right)}\left[1 - e^{\left(\frac{-qV}{kT}\right)}\right] \qquad (2)$$

Where

$$\frac{1}{n} = 1 - \left(\frac{\delta\Phi_e}{\delta V}\right) \qquad (3)$$

Where n is the ideality factor q is the unit charge k is the Boltzmann constant T is temperature, J_0 is the saturation density of current and V is the applied tension.

Equation 2 can be written as

$$J = J_0\left[e^{\left(\frac{qV}{nkT}\right)} - 1\right] \qquad (4)$$

The difference beteen Equation 2 and 4 is negligible if the applied tension V>3kT/q. This last equation permits the calculation of the ideality factor using experimental data from the J-V characteristic. If we use logarithmic coordinates, the graph is linear with a pendency q/nkT.

The SBH is calculated from the J0 value. From this value we have

$$\Phi_B = \frac{kT}{q} \ln\left(\frac{J_0}{A^* T^2}\right) \qquad (5)$$

A* is the Richardson constant

2.4.2 Film stress

Stress measurement using substrate bowing can be a really valuable resource in the definition and control of production processes. It is cheap and non destructive, and the measurement takes only a few seconds. Furthermore it is very simple to perform, so it can be easily taught to line operators and used as a valid statistic process control, in order to monitor a process stability.

Even if stress data acquisition is simple, its interpretation can be very complex, since the final value and its changes depends on many different parameters.

As we will see stress depends on the thermal expansion characteristics of the involved materials, and is possible to link stress response to various types of structural properties and changes, such as phase transitions and material transport along grain boundaries.

During the experimental chapters we will use the film's stress measurement in a lot of different ways: to understand the variability of the sputtering process, to detect structural changes on the material, to find correlations between material's microstructure and electrical parameters.

The total thin film stress σ_f is defined as the algebraic sum of the intrinsic stress (σ_i) and the extrinsic or thermal stress ($\sigma(T)$),

- Thermal: is strictly bounded with the thermal expansion of the involved materials
- Intrinsic: is characteristic of a material and depends on its deposition condition and its internal structure.

$$\sigma_f = \sigma_i + \sigma(T) \qquad (6)$$

$$\sigma_f = \frac{1}{6} \frac{E_s h_s^2}{(1-\nu_s) h_f} \left(\frac{1}{R_2} - \frac{1}{R_1}\right) - (\alpha_s - \alpha_f)(T - T_0) \frac{E_f}{1-\nu_f} \qquad (7)$$

where α_s and α_f are the coefficient of thermal expansion of the substrate and the film respectively, ΔT is the temperature difference between the deposition temperature and the measure temperature, E_f is the Young's module of the film and E_s is the Young's module of the substrate, ν_f is the Poisson's ratio of the film and ν_s is the Poisson's ratio of the film, h_s is the thickness of the substrate and h_f is the thickness of the film; R_2 and R_1 are the curvature after and before the film deposition

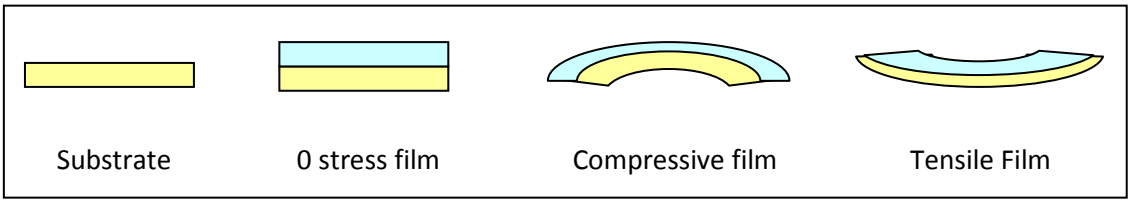

Figure 2.18: Scheme of substrate reaction to different types of films

To better understand why a compressive or a tensile film should bend the substrate in this way is shown in figure 2.18. We will now focus on what intrinsic stress is from a structural point of view.

- In a 0 stress material, the atoms of the material are *averagely* positioned in the lower potential energy distance. For this reason they will not tend to increase or lower their distance and this results in no force applied.

- In a *COMPRESSIVE* film, the atoms are positioned at a lower distance compared to their lower potential energy distance. For this reason they will tend to increase this distance and the resulting bowing is a negative profile. Compressive stress is typical of Film Densification, and involves high energies. Most deposited films at high deposition rates, with very energetic sources such as with Sputters or PECVD, have typical intrinsic Compressive stress.

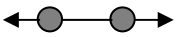

- In a *TENSILE* film, the atoms are positioned at a greater distance compared to their lower potential energy distance. For this reason they will tend to lower their distance and the resulting bowing has a positive value. Tensile stress is typical of crystallization and reticular bonding formation, it may also be connected with a material with a very low density.

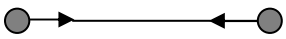

This can be also be seen as a movement on the typical Lennar Jones surface

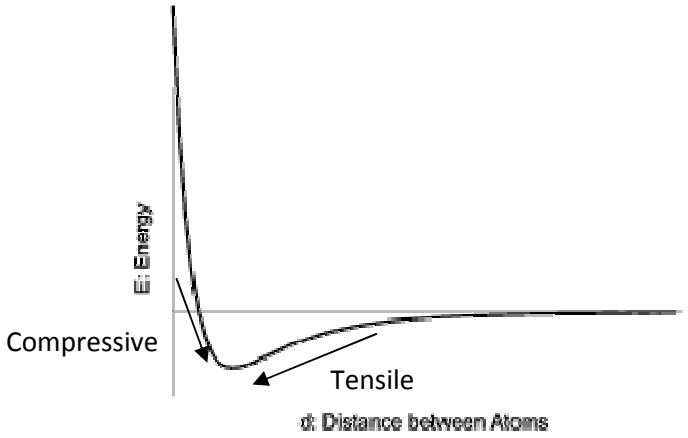

Figure 2.19: stress as a movement with respect to a Lennar Jones curve

The thermal contribution is easy to understand: if the deposited material has a lager expansion coefficient compared to the substrate, while cooling it gains tensile stress (this is the case for example of aluminum on silicon). If it has a smaller expansion coefficient gains compressive stress (for example silicon oxide on silicon).

In table 2.20 there is a summary of various responses on the stress to different factors

Tensile Stress	Compressive stress
Cooling a material with higher thermal expansion coefficient compared to the substrate (example: Al on Silicon)	Cooling a material with Lower thermal expansion coefficient compared to the substrate (example: Silicon Dioxide on Silicon)
Crystallization of a material with higher density on solid state compared to liquid state (exception for materials with very strong covalent bonding such as silicon and germanium)	Crystallization of a material with lower density on solid state compared to liquid state
	Formation of grain structure and void inclusion
	Formation of compounds
	Impurity diffusion

Table 2.20 stress responses

2.4.3 UV-vis optical characterization.

2.4.3.1 Introduction and basic response

Optical , electrical and structural characterics of materials are strictly bond. We will make comparisons between the variations in stress of the materials (expecially for amorphous silicon in chapter 5 and 6) and corresponding variations of the refractive index.

If we consider the complex refraction index

$$N = n - ik \qquad (8)$$

Where N is the complex refractive index, n is the real part and k is the complex part (extinction coefficient).

The absorption coefficient may be expressed as follows

$$\alpha = \frac{4\pi k}{\lambda} \qquad (9)$$

We can now Calculate R (reflectance) A (absorbance) and T (transmittance)

$$R = \frac{(n-1)^2 + k^2}{(n+1)^2 + k^2} \qquad (10)$$

$$T = (1 - R)e^{-\alpha X} \qquad (11)$$

$$A = 1 - (R + T) \qquad (12)$$

X is the material's Thickness.

In figure 2.21 and 2.22 is possible to see the Reflectance, transmittance and absorbance spectra for 1 micron film of aluminum and silicon.

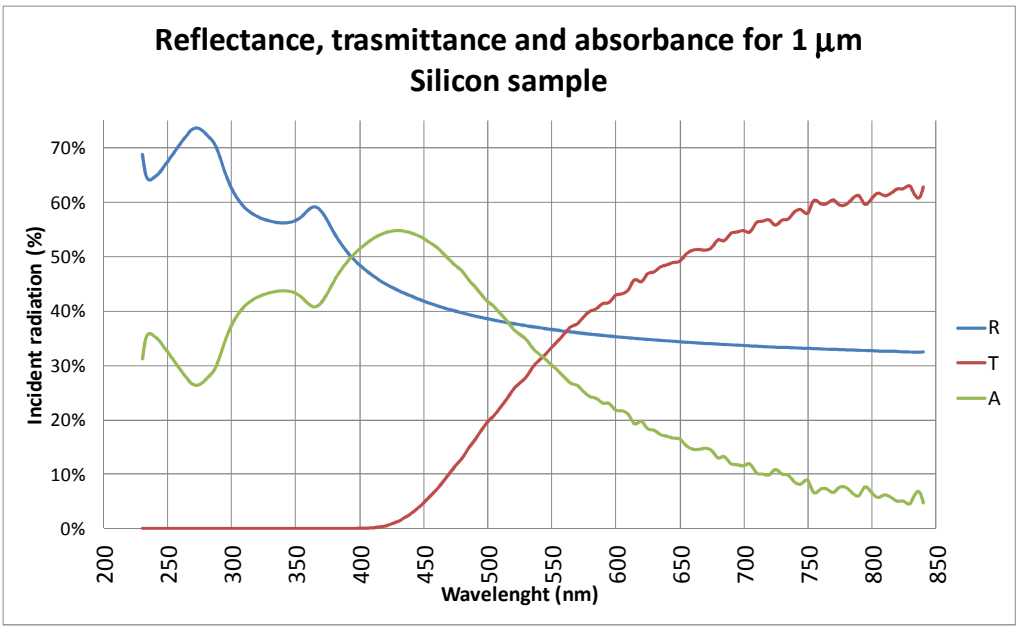

2.21: Optical response for a 1 mm sample of silicon

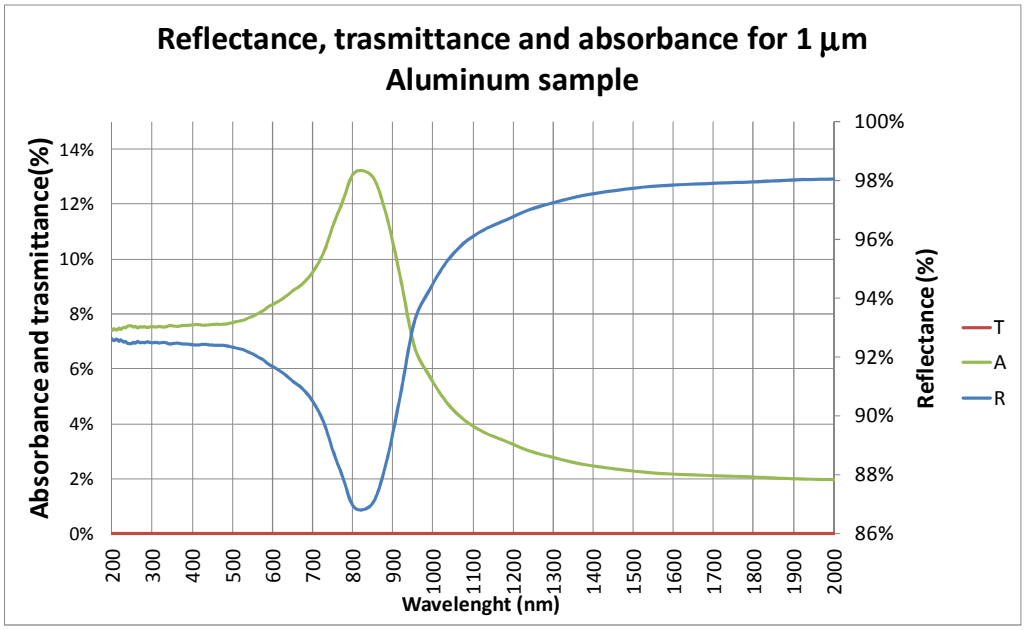

2.22: Optical response for a 1 mm sample of silicon

2.4.3.2 Thickness measurement

2.4.3.2.1 Introduction

We used two tools to measure the thickness of amorphous silicon films: the Nanospec AFT210 and the n&k 1500. We will describe de differences between this two tools.

2.4.3.2.2 Nanospec

When a substrate is present, the multiple reflections inside the film generate a spectra with interferences fringes such as the one proposed in figure 2.23

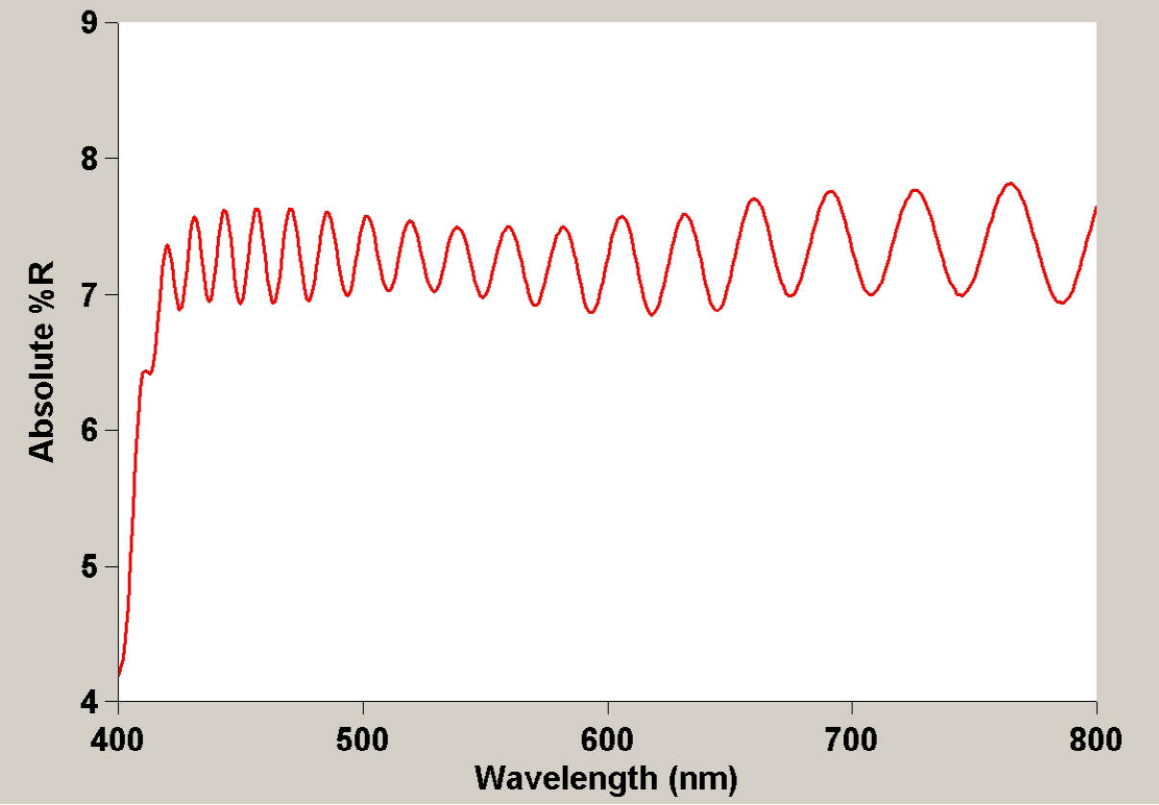

Figure 2.23: Interferences fringes

Since usually the refractive index tends to be constant at large wavelengths (IR), if we consider a material with fixed real part of the refraction index n, we can calculate its thickness using equation 13

$$d = \frac{m}{2D_n\sqrt{(n^2 - \sin^2\theta}} \qquad (13)$$

- d is the material's thickness
- m number of interference fringes

- n real part of the refraction index
- θ angle of incidence
- D_n wavenumber in the considered region (cm^{-1})

This method to estimate the thickness is the one used for example in one of the tools we used (Nanospec AFT210).

2.4.3.2.3 N&k 1500

We used another tool to estimate the thickness of the films: the n&k 1500.

With this tool, from the modelization of the full UV Vis reflectance spectra, is possible to determine many other quantities apart from thickness, such as:

- Index of refraction n
- Extinction coefficient k
- Energy Bandgap, E_g
- Interface roughness, σ

This is done using the Forouhi and Bloomer [ref. 1,2] dispersion equations and uses a broadband (120 nm ~ 1000 nm) reflectance spectrum. Forouhi and Bloomer deduced a physical model for refractive index n and extinction coefficient k in terms of λ and material parameters, applicable to a wide range of semiconductors and dielectric films. This model is valid over the deep ultraviolet – near infrared wavelength range. The Forouhi-Bloomer equations fit experimental data and they require few parameters

$$k(E) = \sum_{i=1}^{q} \frac{A_i(E-E_g)^2}{E^2+B_iE+C_i} \qquad (14)$$

$$n(E) = n(\infty) + \sum_{i=1}^{q} \frac{B_{0i}+C_{0i}}{E^2+B_iE+C_i} \qquad (15)$$

In these equations E is the photon energy related to the wavelength of light according to E=hc/l where h is Planck's constant and c is speed of light in vacuum. E_g is the energy band gap, and A, B, and C are not mere fitting parameters, but are related to electronic structure of the material. The quantities B_0 and C_0 are not independent parameters, but depend on A, B, C and E_g. Amorphous material can be described from equations 1 and 2 by taking only one term of the sum. Polycrystalline and crystalline material can be described by taking more than one term in the sum.

The tool incorporates those equations, together with Fresnel equations and structural parameters such as film thickness and interface roughness to generate a calculated reflectance spectrum R_{cal}. This R_{cal} is then compared to the experimental reflectance spectrum R_{exp} in the entire measurement spectrum range, by means of the non linear least –squares fit:

$$\delta = \sqrt{\frac{1}{N}\sum_{i=1}^{N}[R_{\exp}(\lambda_i) - R_{cal}(\lambda_i)]^2} \qquad (16)$$

During the fitting all the parameters inside the F-B equations are varied to minimize δ.

As can be seen, this method is way more complicated with respect to the simple one used in the Nanospec, and requires a lot of computational power. Furthermore in order to design a recipe all the starting points and many fitting parameters need to be initialized correctly. If a good recipe is developed, the tools allow to gather many information about the system we are inspecting, that can be useful to characterize and tune the materials processing conditions

3 Microstructure and crystal structure.

3.1 Introduction

One of the major issues arising from Al-Si deposition is the great variability of its microstructure. This characteristic is of great interest and is a very important feature of solid materials. Microstructure should be distinguished from crystal structure: while the latter is related to the relationship between unit cells and crystal spacing, and gives a description of what happens in the atomic (angstrom) level, the former is related to the grain distribution (size, shape), the surface topology, the grain orientation and takes in consideration the nm to cm scale. A key technique that can be used in order to investigate the crystal structure is X Ray Diffraction (XRD). XRD diffraction patterns will be used in the following chapters to determine the orientation and the type of crystals present in AlSi films. The microstructure on the other hand, describes the material in a wide range of scales and aspects. Microscope analysis is the best way to detect and describe the microstructure of a material and, depending on the dimension of features we are investigating, we can choose different techniques such as SEM, Optical microscope, AFM. In our work we mainly used optical microscope, with a polarizer filter in order to make the microstructure more visible, and SEM to highlight peculiar structures.

Many important technological characteristics are related to the microstructure. On a macroscopic scale microstructure is responsible for the brightness or for the opacity of a material, as well as for the uniformity of its visual appearance. The compliance of the devices to a repeatable and controlled visual aspect can be important while selling devices to customers. The visual appearance is also important when dealing with automatic inspection tools. Pattern recognition algorithms expect to find always the same type of optical response, and in some cases a fine tuning of the microstructure can help those tools to be faster and more efficient.

Also mechanical and electrical properties can be affected by microstructure.

For all those reasons a good control on the microstructure is of paramount importance in order to achieve stable results, as well as good and predictable production properties.

In this chapter we will investigate both crystal structure and microstructure of a sputtered AlSi (1% Si content) film. The two types of descriptions are complementary and we will see that, in order to understand and give a complete description of microstructure formation, we will need to understand the underlying crystal structure and the parameters influencing it.

3.2 Variability of AlSi structure

As we have seen in chapter 1, the microstructure variability encountered in production on Al-Si films is really wide, either considering an inspection with microscope or with naked eyes.

In order to explain the reasons of this variability and to find the influencing factors, we performed a series of experiments. We can divide those experiments in three main blocks

- *Block1:* in this first screening experiment we investigated the influence of substrate and sputtering temperature, making a correlation between those factors and the crystal structure.
- *Block2:* in this series of experiments, we focused on substrates with native oxide at the interface, analyzing in detail the microstructure and the stress evolution with temperature
- *Block3:* In the last series of experiments we used as substrate silicon without native oxide, and with hydrogen passivation. We describe a phenomenon that we called "marble effect" and making a correlation between this effect and the stress.

3.3 Experiment 1: Substrate and temperature influence

3.3.1 Experimental setup

We deposited an Aluminum Silicon (1% Si content) alloy using a DC magnetron sputtering (Varian 3290). The deposition atmosphere was composed of Argon and the temperature of the stations ranged from room temperature to 200°C. As a substrate we used Cz silicon wafers of [100] orientation. Before the deposition we applied two different types of surface preparations. The first one was the standard sequence used for silicon cleaning: RCA, which is the combination of SC1 (standard cleaning 1) and SC2 (standard cleaning 2). This solutions are used respectively to remove particles and metallic contaminations. SC1 is a mixture of $NH_4OH:H_2O_2:H_20$ 1:5:25 and SC2 is $HCl:H_2O_2:H_2O$ 1:5:25 We used a 10 minutes dip on each bench at the temperature of 60°C. The second preparation is a diluted HF (DHF) bath: a 60" dip at room temperature in a solution of HF and H2O in the proportions of 1:50. We inspected the surfaces after preclean, in order to validate their stability, using Optical Contact Angle measurements

Pictures were taken to all the samples using an optical microscope with a polarizer filter in order to make the microstructure visible. On the major microstructure features we took SEM images.

X-Ray Photoelectron Spectroscopy (XPS) was performed on the Al coated Si samples by means of a PHI 5000 VersaProbe - Physical Electronics system, equipped with an ion gun. In order to investigate the interface region between the Si wafer and the AlSi layer, the surface was sputtered for the time required to reach the interface before starting the acquisition of the spectra. When the interface region was reached, XPS spectra were acquired after each sputtering cycles od 15'' and were elaborated to obtain compositional maps.

3.3.2 Results

The evolution of microstructure is Highly dependent on the interface between substrate and the sputtered material. The two interfaces possible on silicon are shown in figure 3.2, and are respectively the OH one (when a native oxide is present, such as on untreated surfaces or on those where an oxidizing preparation was performed) and the H terminated one (when the oxide is removed and the surface is passivated with H). The H passivation inhibits the formation of native oxide and is stable for a

certain amount of time. On Table 3.1 there are the results of Surface free energy characterization for standard OH passivated silicon (such as the one treated with RCA) and for H passivated silicon generated from a DHF treatment. We then measured again the H passivated sample after 8hrs in order to validate the surface's stability. Since the results after 8 hrs did not change, we can avoid to treat as a variable the time between the preclean and the deposition, which in any case took always less than 30 minutes.

Substrate	SFE Total (mJ/m2)	Polar (mJ/m2)	Disperse (mJ/m2)
Si	71	57	16
Si (HF treatment)	39	21	18
Si (HF treatment + 8 h)	38	25	13

Table 3.1: SFE measurements on the two types of substrates

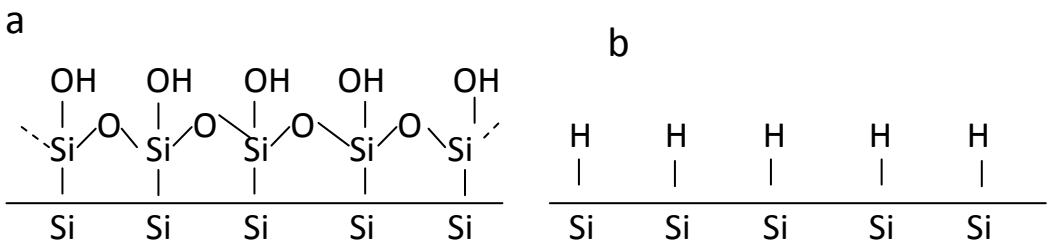

Figure 3.2: different types of Silicon terminations: 1a native surface resulting from air exposure or oxidizing chemicals such as the ones contained in RCA. 1b H passivated surface resulting from DHF treatment.

Figure 3.3 schematizes the experimental matrix. On figure 3.4a to 3.4d the optical microscope pictures are shown, figure 3.5a to 3.5d contains the XRD spectra

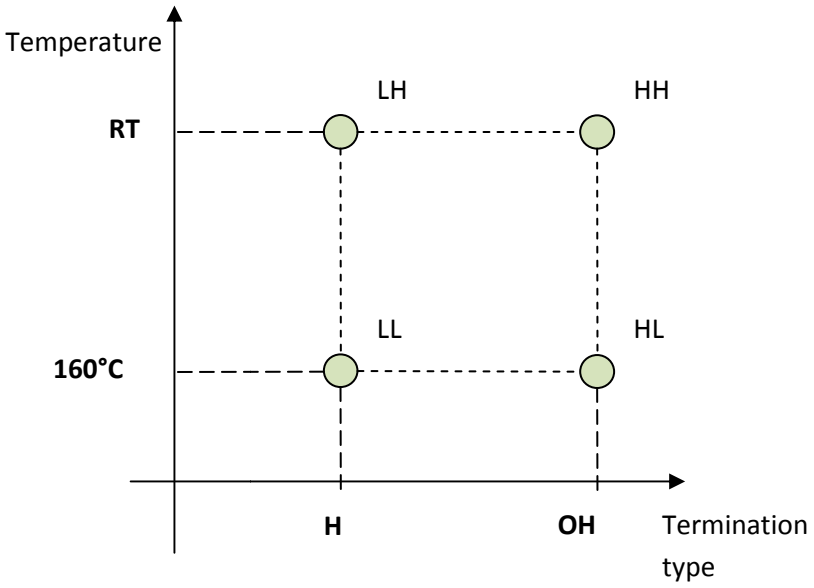

Figure3.3: Experimental matrix

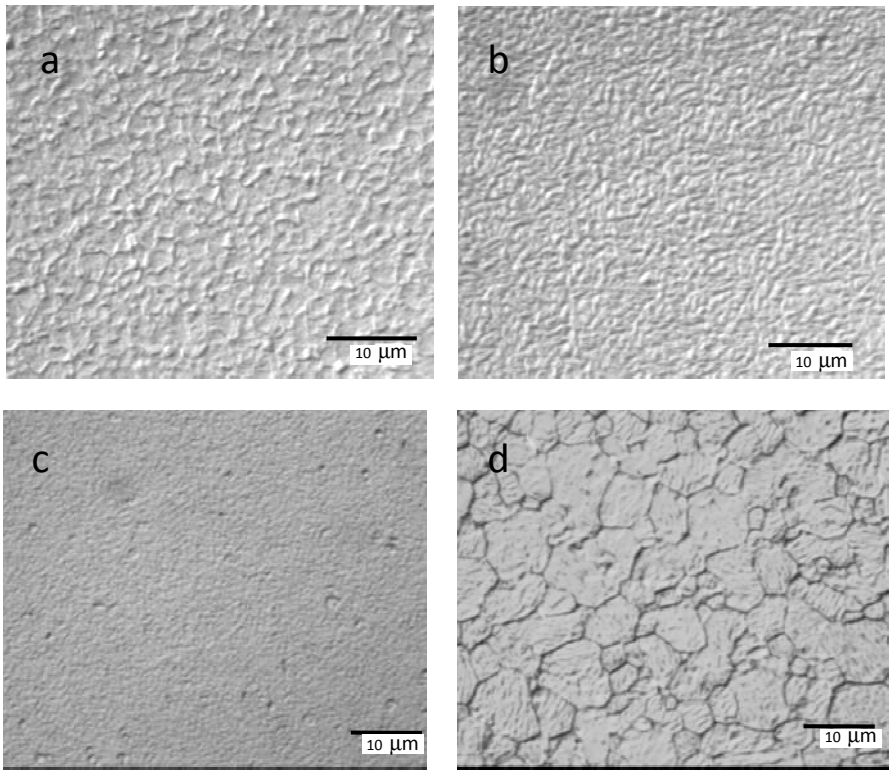

Figure 3.4: microscope images of the various samples: a) DHF treated surface with a room temperature sputter. b) RCA treated surface with room temperature sputter. c) DHF treated surface with 160°C sputter. d) RCA treated surface with 160°C sputter.

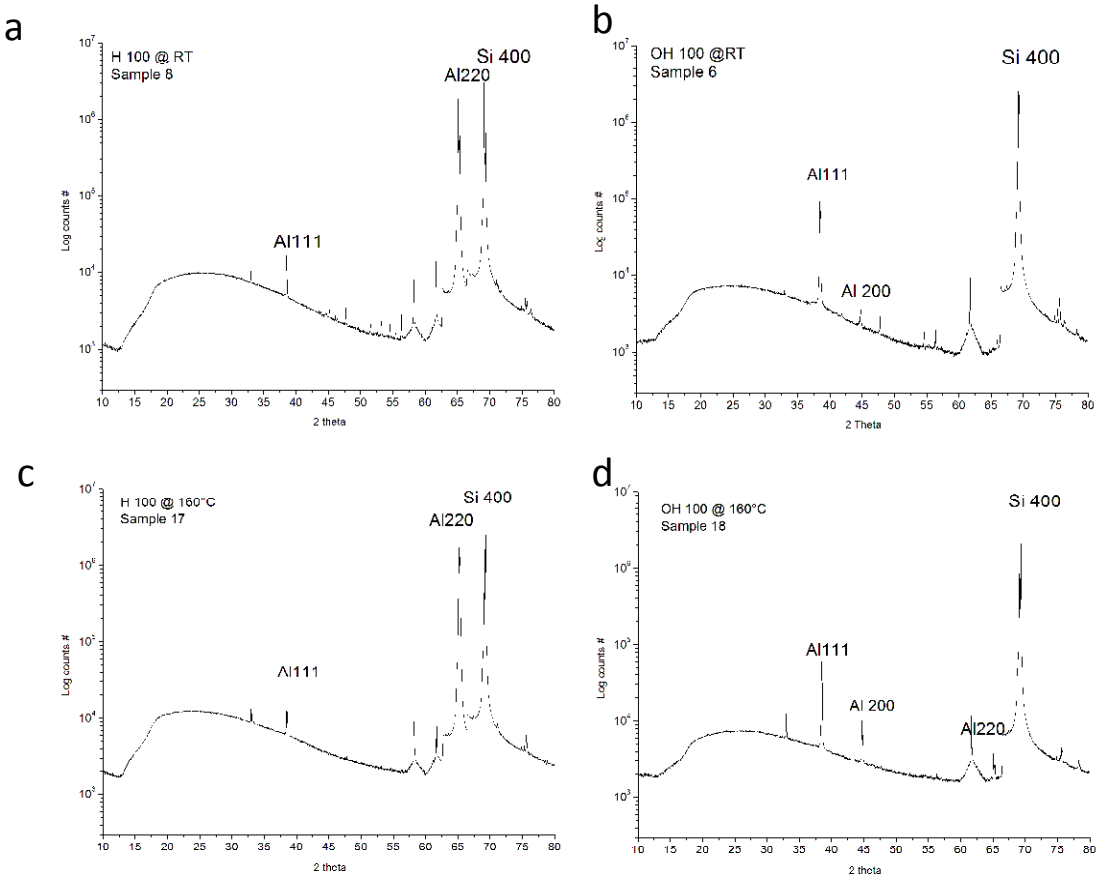

Figure 3.5: DRX diffraction pattern for the for samples. a): DHF treated sample sputtered at room temperature. b) RCA treated sample sputtered at 160°C. c) DHF treated sample sputtered at 160°C. d) RCA treated sample sputtered at 160°C

Due to the importance of the interface, we also made some depth profile spectra with XPS, which are shown in figure 3.6. Since we were only interested in what happens at the interface, in the graphs we will report only the data regarding a few cycles before the interface.

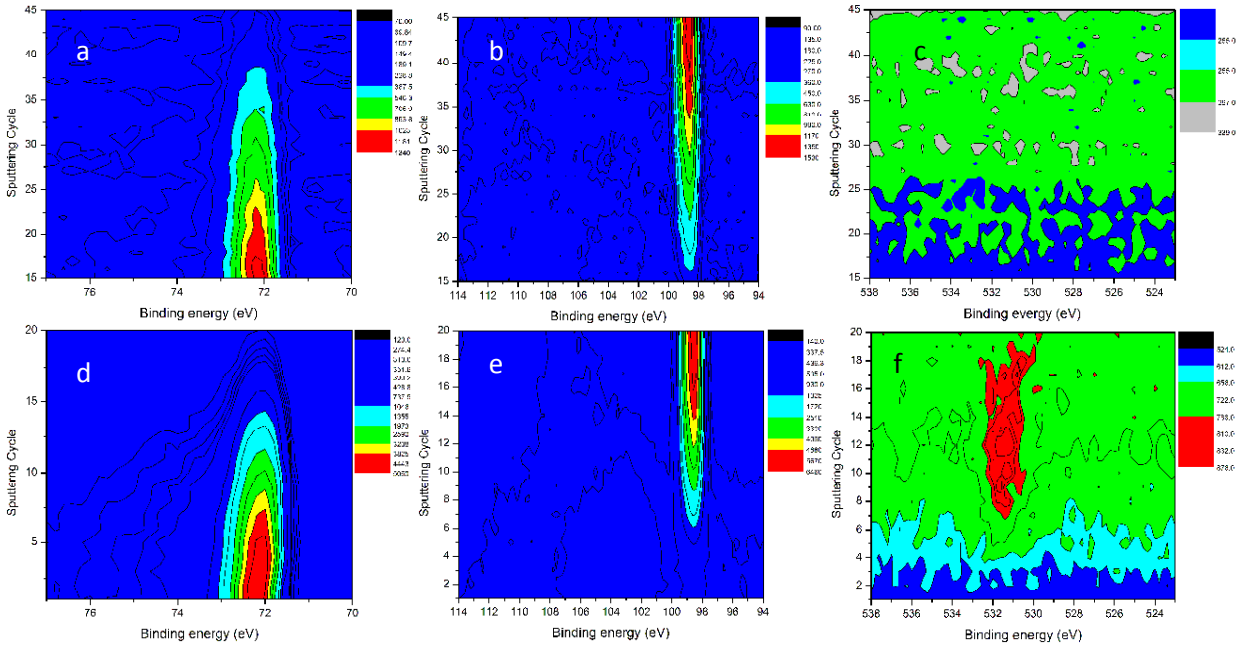

Figure 3.6 . : On the Vertical axis the number of XPS sputtering cycles is reported, each cycle was 15" in argon pressure. On the horizontal Axis the binding energy is reported, with a color scale to represent the counts value. On the first row the sample with DHF preparation is presented with Aluminum peak (a) Silicon Peak (b) and Oxygen peak (c). On the second row the sample with native oxide at the interface is presented with Aluminum peak (d) Silicon Peak (e) and Oxygen peak (f)

As can be seen from picture 3.4a and 3.4c, on samples with H terminated surfaces, even if the roughening of the surface changes, no visible surface feature is generated with a change in the sputter temperature. In picture 3.4b and 3.4d we can see that on OH terminated surface on the other hand, the microstructure changes completely passing from room temperature to 160°C.

3.3.3 Discussion.

The XRD analysis is greatly useful in order to achieve an insight on the effect exerted by the H and OH terminated silicon surface, respectively, on the film microstructure. Indeed, from an analysis of the X-ray diffraction patterns, it appears that the internal structure of the AlSi layers depends on the interface between the metal and the substrate, while there is no evidence of a dependence on the substrate temperature or on the microstructure. In fact, the microstructure changes dramatically with the temperature increase on the OH terminated surfaces. At low temperatures no grain structure is clearly visible, while the grain structure becomes visible starting above 100°C, as the temperature increases. Moreover, starting from this temperature, hillocks and grain boundaries are generated in order to release the thermal stress. From the XRD spectra acquired on the films grown on OH terminated surfaces (fig. 3.5b and 3.5d) it appears that the diffraction patterns are very similar, even if the film morphologies are very different (fig. 3.4b and 3.4d). In fact, on both samples we can see the peaks related to the Al [111] and [200] crystal planes. On the high temperature sample (fig. 3.5d) is possible to

see also the [220] peak, while on the one grown at room temperature (fig. 3.5b), the same peak is present with a much lower intensity.

On the H terminated surface the results are completely different, as shown by the XRD diffraction patterns shown in figure 3.5a and 3.5d. In this case, no [200] peak is visible and the [111] is very small. Moreover, the peak related to [220] crystal planes is predominant, with an intensity similar to the one relative to crystalline Si [100] planes. Its shape furthermore has the characteristics a mono-crystalline layer.

An explanation of this behavior can be found looking at the lattice parameters of the unit cells. In fact, Al crystal has a FCC lattice with a cell parameter of a=4.049 A. Silicon, on the other hand, has a diamond type structure with lattice parameter of 5.43 A. As was schematized in figure 3.7, we can see that if we rotate one lattice with respect to the other of 45°, the two are compatible, with a reticular mismatch of 5.5%.

It is possible to presume that Aluminum, during the initial stages of its grown on a silicon crystal, uses it as a template producing the formation of an almost mono-crystalline layer. It is surprising that the metal can keep such a order, considering that the growth rate is over one micron per minute. However, when a OH termination is present this phenomenon does not happen, as was shown by the XRD analysis.

A possible explanation of this behavior could be proposed suggesting an involvement of the amorphous native oxide layer, which is naturally present on OH-terminated silicon substrates, but not on H-terminated ones. . In fact, during the first steps of Al-Si films growth on OH-terminated surfaces, the Al atoms are adsorbed on the surface of the thin amorphous oxide layer, and cannot take advantage of the long range order of the silicon substrate to guide the formation of a crystal structure. The presence of the oxide layer could thus inhibit the formation of an ordered Al-SI film.

A different explanation could also be proposed, taking into account the great affinity of Aluminum for Oxygen, due to which a chemical bond could be created between Aluminum and Silicon a short time after the aluminum atoms are adsorbed on the Silicon surface. In this way, the surface mobility of the adsorbed Al atoms would be strongly reduced, and the structure could not achieve a long range order, then organizing in small grains with random orientations.

In order to better understand the mechanism we can look at the XPS spectra. Indeed, comparing fig. 3.6c and 3.6f we can see that, as expected, on sample with DHF treatment, no oxygen is present at the interface. On samples with RCA treatment on the other hand, the oxygen signal is present when the depth profile reaches around 6 sputtering cycles. If we look at the corresponding Aluminum peak, we do not see any shoulder on the Al peak that can suggest a bond between Al and O, and this may suggest that there has been no interaction between the two elements.

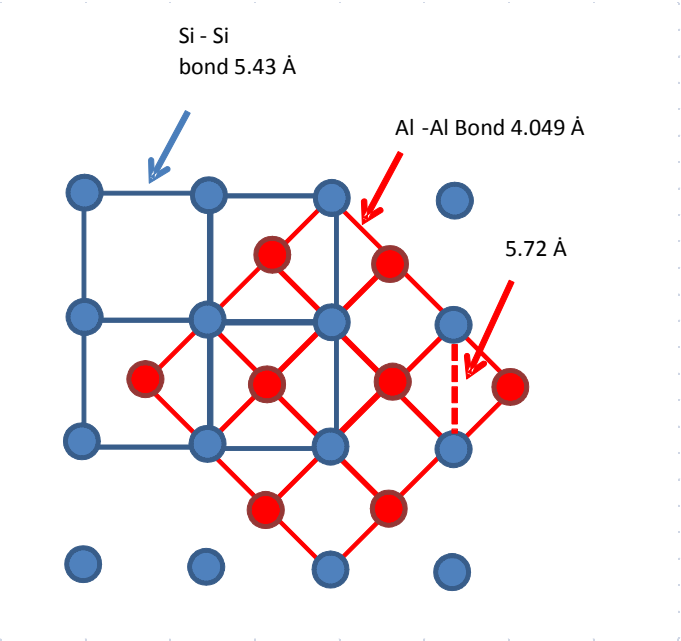

Figure 3.7: Scheme of Silicon and Aluminum lattices. As can be seen the two lattices are compatible if one is rotated of 45° with respect to the other. The mismatch is around 5%

As we have seen, the type of substrate's termination selects the crystal structure of the AlSi film. The microstructure evolution of the film with temperature depends on the type of crystal structure, giving origin to totally different types of features. For this reason the investigation of the evolution of microstructure with temperature will be done considering separately substrates with a native amorphous oxide layer at the interface, and those with H termination. At the end we will see how we can put in correlation the two discussions.

3.4 OH terminated silicon

3.4.1 Experimental

To investigate the microstructure evolution in samples with oxygen at the interface, we deposited three microns thick AlSi film at increasing temperatures (starting from 30°C up to 250°C). The employed substrates were [100] Cz silicon and before the deposition they were all treated with an RCA clean.

After the deposition we inspected all the samples using an optical microscope, and on key features we took images with a SEM. A stress measurement was performed with a Tencor Flexus FLX2320

3.4.2 Results

In figure 3.8 all the images of aluminum surface at different temperatures are collected; SEM images taken on the main features found on the samples are reported in figure 3.9

The stress values using curvature method are plotted in figure 3.10

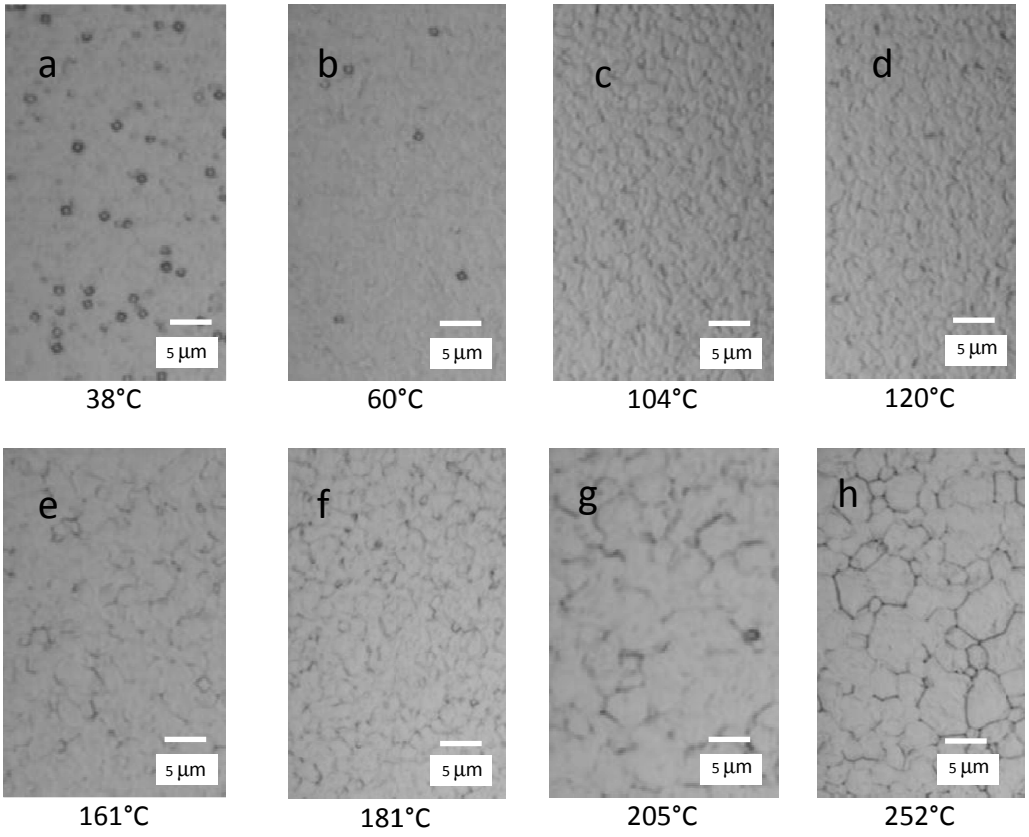

Figure 3.8 a/h. Optical microscope pictures of aluminum film grown on RCA treated sample with sputter temperatures ranging from 38°C to 252°C.

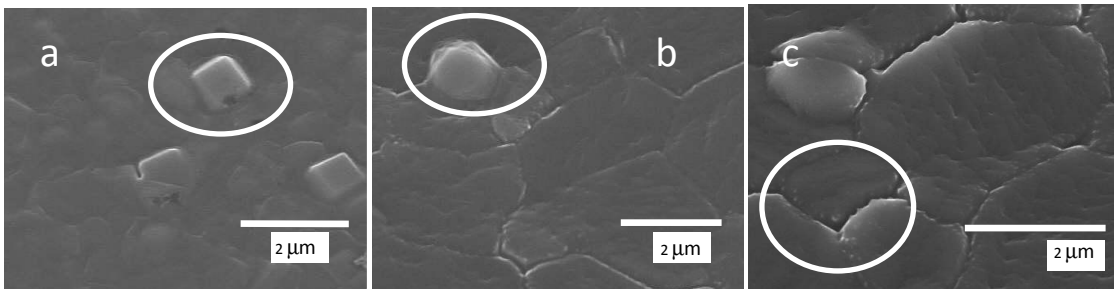

Figure 3.9. SEM images of the main surface features found. a) cubic structures on the surface found until 60°C. b) Hillocks found above 100°C. c) grain boundaries are clearly distinguishable over 120°C

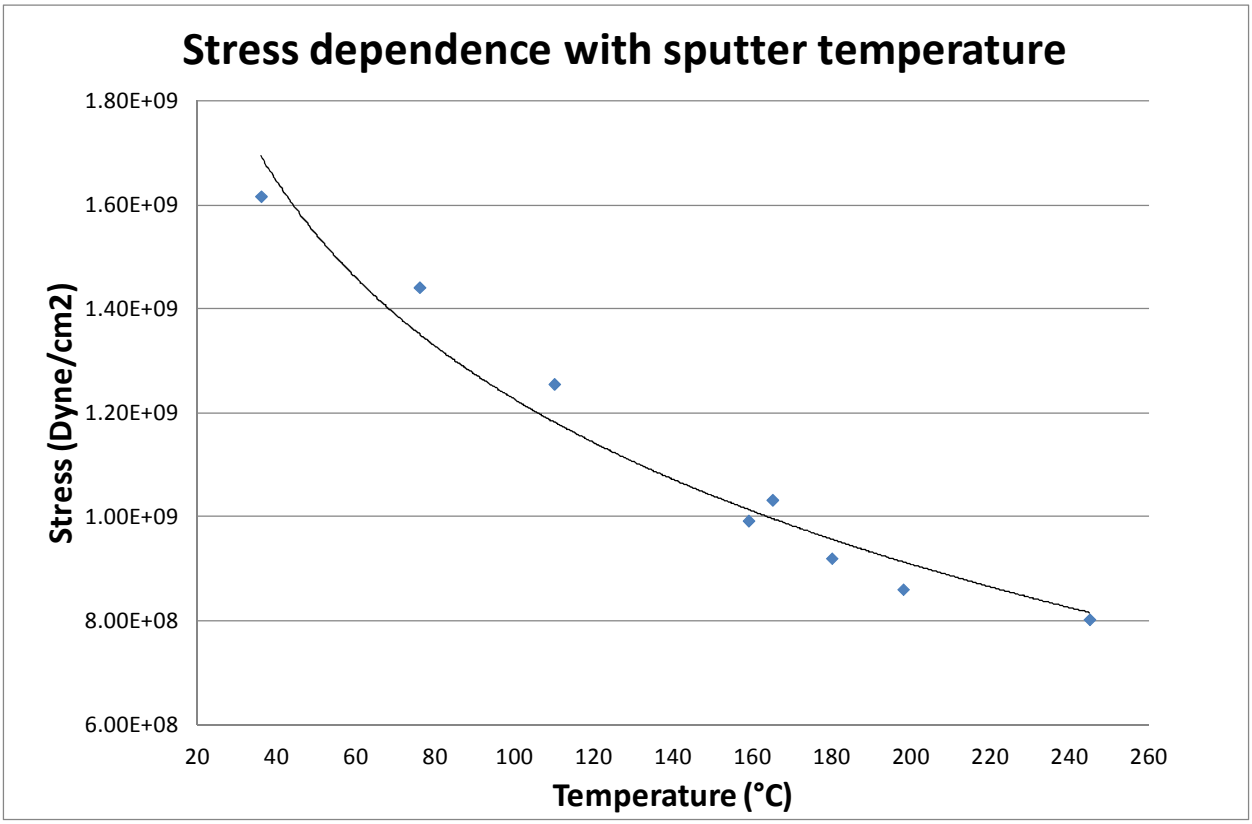

Figure 3.10 Values of stress at various sputtering temperatures using curvature method

The FLX2320 is also capable to make measurements at high temperatures. For this reason we made a stress Vs temperature plot. The data acquired in this way have been used to calculate the Thermal / Intrinsic contributions to total stress.

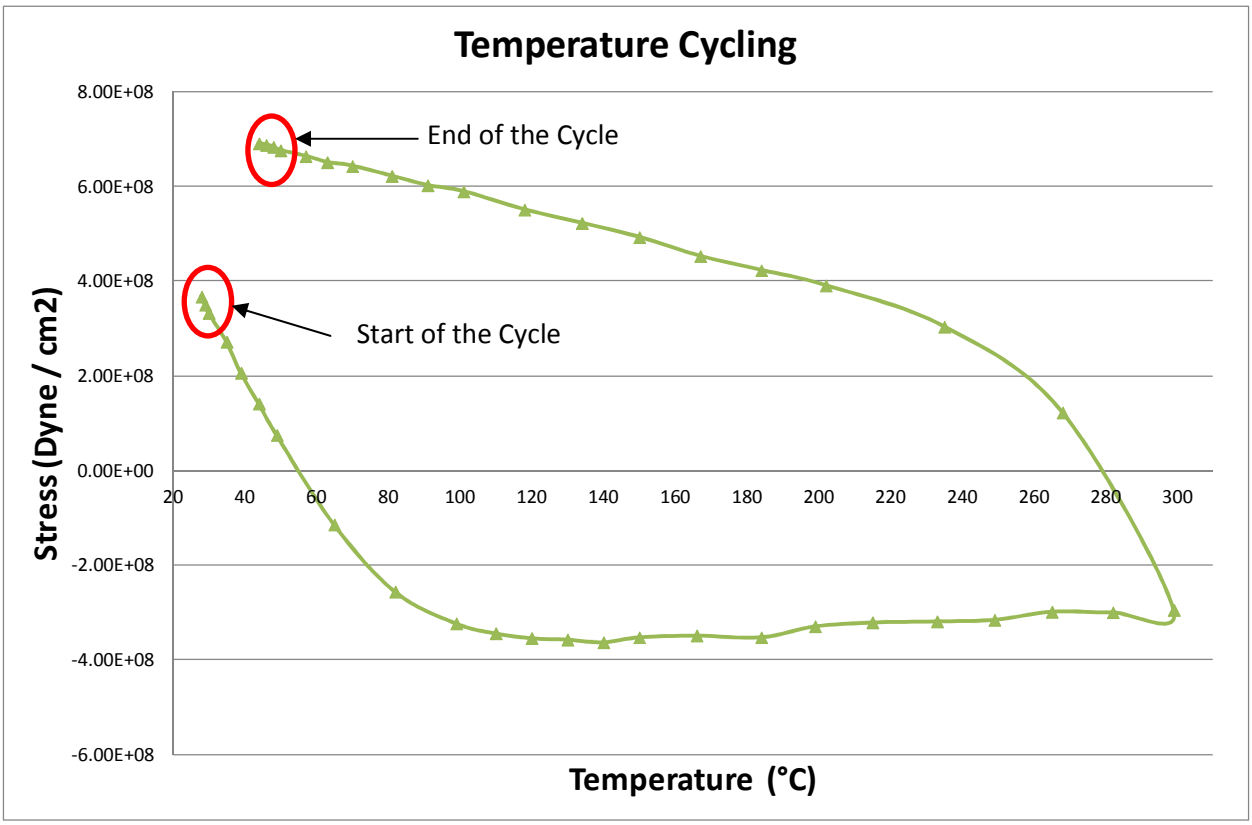

Figure 3.11 data resulting from temperature cycle of a sample grown at 200°C

3.4.3 Discussion and comments

In picture 3.12 we can see the standard zone diagram for a metallic sputtered film. It represents the different types of microstructures generated at various conditions of Argon pressure and Deposition temperatures. The standard zone diagram is a general plot, valid for many metals. For this reason a dimensionless unit, given by the ratio between the deposition temperature and the melting point of the material, is used. All our films have been sputtered using 7mTorr of argon.

Note that the temperature in the SZD refers to the temperature of the wafer. When we talk about temperature in our experiments we will talk about the heater temperature. There are many fixed contributions to the real temperature of the wafer (kinetic energy of incoming material, heat of condensation, electrical heating due to Joule effect) that will not be a source of investigation. This is the reason why we will find heater temperatures lower from what predicted by SZD.

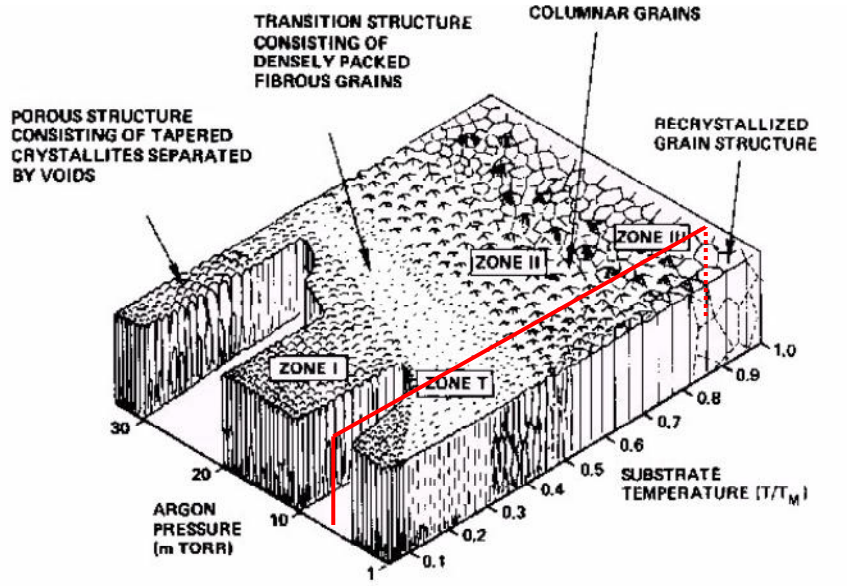

Figure 3.12 Standard Zone diagram

On substrates with oxide at the interface, the evolution of microstructure is quite visible using an optical microscope. At the lowest temperatures (up to 80°C) the surfaces show high reflectivity, and some cubic structures can be seen (figure 3.9a). Between about 80°C and 120°C there is a zone where the grain structure is not visible, and no surface defect is present. This zone can be linked with the "T zone" of the standard zone diagram. For further increasing temperatures the grain structure becomes clearly visible and "hillocks" start to form (zones II and III of the SZD).

We calculated for the different sputtering deposition temperatures the thermal and intrinsic contributions to total stress. To calculate the thermal stress and successively the intrinsic one, two methods can be used. Eq (7) chapter 2, knowing the thermal expansion coefficient and the difference in temperature between deposition and measurement can be employed. Alternatively the slope of the temperature cycle in the first part (figure 3.11) can be employed, because in this region the response is linear and the sample is behaving elastically. The result obtained with the second method are plotted in figure 3.13

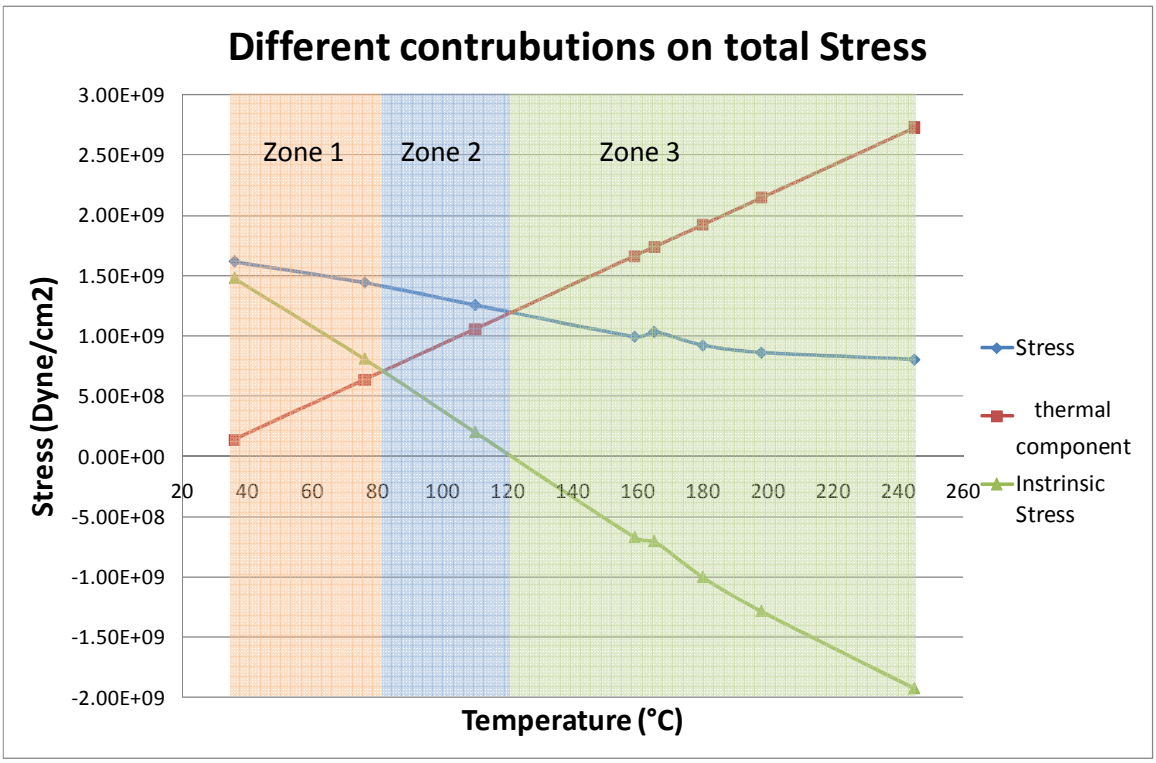

Figure 3.13. The total, thermal and intrinsic stress of the sputtered Al/Si film

We can divide the obtained plot in three main areas. In the first one (room temperature up to 80°C), the intrinsic component dominates, its value is tensile, and is greater than the thermal one. Between 80°C and 120°C the thermal component is greater than the intrinsic one, and intrinsic stress is still tensile. Above 120°C the film is intrinsically compressive.

In table 3.14 a summary of all the characteristics of the films is reported.

Temp (°C)	20	40	60	80	100	120	140	160	180	200	220	240	260	280	300
Stress type	Intrinsically tensile						Intrinsically compressive								
Stress ratio	**Intrinsic > Thermic**				Thermic > Intrinsic										
Structures	Cubic structures						Hillocks and grain boundaries								

Table 3.14. Characterization summary of the AlSi film

When the temperature is low, and the film is intrinsically tensile, with the intrinsic component grater then the thermal one, the structure presents the cubic agglomerates at the surface. In the range of temperatures where the film is still intrinsically tensile, but this component is not the main one, the

layer looks smooth and compact. The grain structure and hillocks appear when the film is intrinsically compressive.

3.5 H terminated samples.

On samples deposited on H terminated substrates, grain boundaries are never present. With those type of samples the analysis is harder, since the system is less stable and shows great variability even without changing the deposition conditions. In figure 3.15 it is possible to see a plot of the stress variability of 25 wafers, with the same sputtering conditions (7 mTorrs argon pressure, 160°C heater temp). As can be seen the average value of stress is less tensile with H termination at the interface, compared to samples with native oxide, but the standard deviation is much higher.

The most peculiar visual difference between this types of wafers is the so called “marble effect”. Marble effect is caused by the presence of some sort of “flakes” inside the aluminum structure. Those flakes reflect the light in a different way compared to the surrounding material and the effect can be seen with naked eye inspection . This kind of effect is visible in figure 3.16 on plain silicon wafers(3.16a), and on a substrate were actual devices have been fabricated(3.16b). In figures 3.17 magnifications are presented. Notice that in many cases the boundaries of the flakes are 45° rotated with respect to the wafer flat. In the next experiment we will study how this effect is generated. In order to give a quantification of the phenomenon, during experiments we will give the % of the wafer surface covered with the flakes (see pictures 3.16 c and 3.16 d).

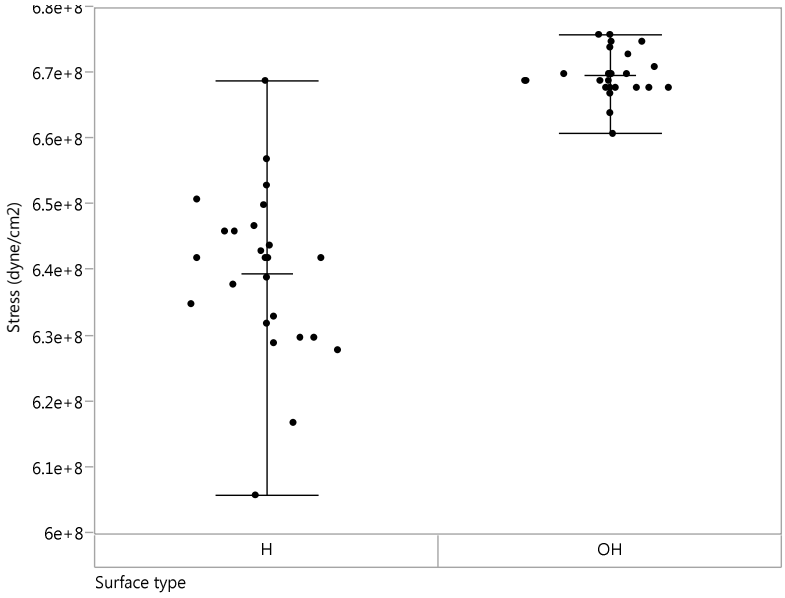

Figure 3.15. Variability of stress on 25 wafers processed with the same recipe on H and OH terminated substrate

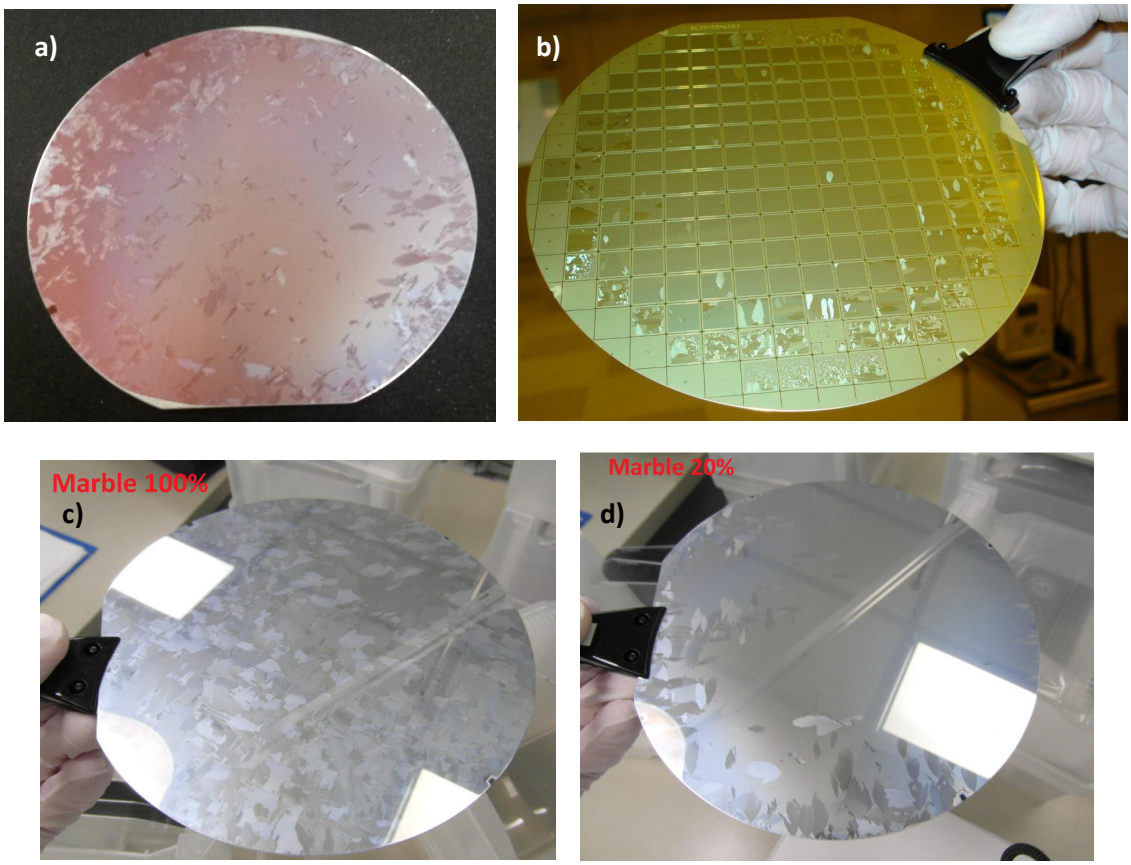

Figure 3.16 wafers with marble effect. a) Plain silicon wafer b) production wafer c) a wafer with 100% of the surface covered by marble effect d) a wafer affected by marble effect at 20%

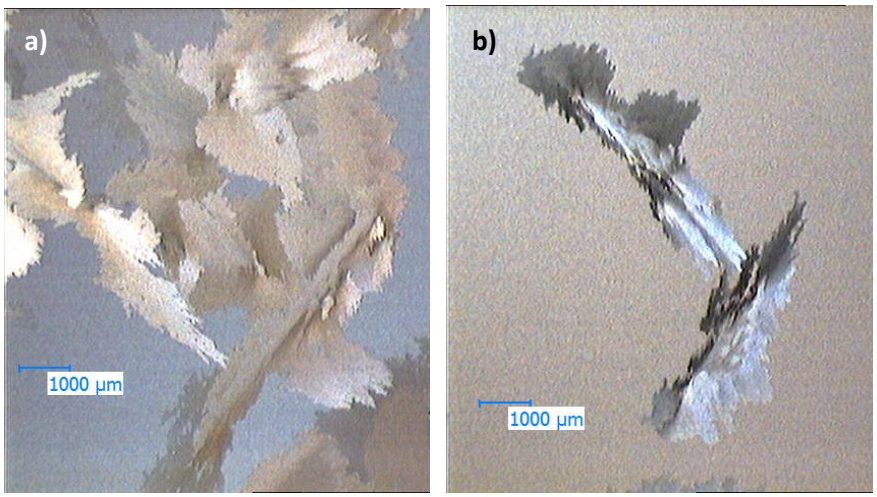

Figure 3.17 magnification of the marble effect

3.5.1 H terminated samples, experiment 1.

3.5.1.1 Introduction

We did some preliminary experiment in order to see if we could correlate this effect with temperature or with the surface preparation, since we have demonstrated that those parameters have a great influence in the generation of different microstructures.

3.5.1.2 Experimental details

On the first experiment, we used as factors the sputtering temperature, and the type of surface preparation. The temperature ranged between 60°C and 160°C. The surface preparation was always done in diluted HF, but we changed the time of the bench dip between 30" and 90".

As substrates we used [100] Cz silicon. The main output of this preliminary experiment was the presence of marble effect

3.5.1.3 Results and comments

In the table 3.18 the results of this first preliminary experiment is reported

Temperature °C	HF time (sec)	% of marble effect coverage
160	90	30
160	90	10
160	30	40
160	30	40
60	90	0
60	90	5
60	30	0
60	30	0

Table 3.18. Summary of the preliminary DOE

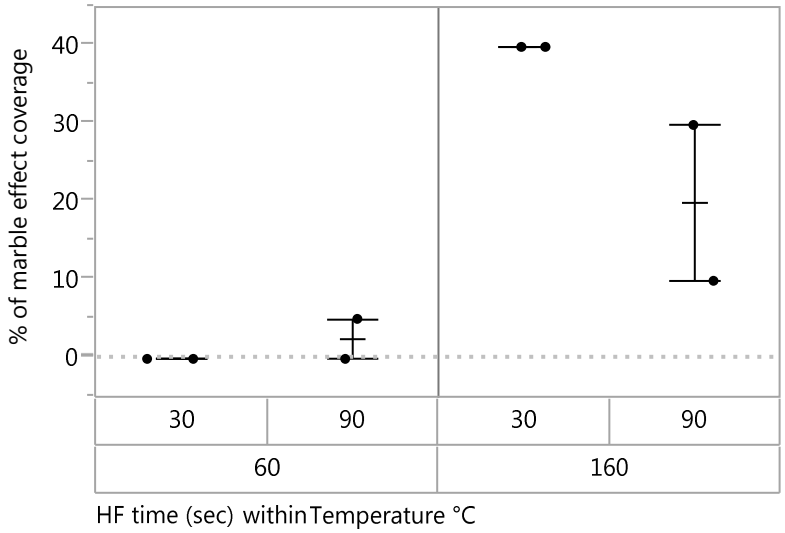

Figure 3.19. Plot of the results for preliminary experiment

From this preliminary data we can see that there is a clear impact of the temperature: all the samples at 160°C show marble effect, while at lower temperature only one sample showed a low marble effect. The surface preparation on the other hand do not show any significant impact.

3.5.2 Production data collection

As we have seen in the introduction on H terminated substrates, the variability of this type of system is larger than for OH one. This generates a lot of issues since in experiments this great variability can hide significant effects of the factors. Since AlSi layer is also applied in the production line, we collected a lot of data coming from actual devices production. This type of data is very useful, since it incorporates all the sources of variability, much larger from the ones present in a typical experiment, and can be used to take a complete picture of the phenomenon we are trying to explain.

All the data can be seen in table 3.20.

Note to the table: In production environment the main deposition temperature is 160°C, even if some devices use 200°C. In the table data from both temperatures are presented

Temperature °C	Stress Dyne/cm2	marble (%)
160	7.28E+08	95
160	5.47E+08	90
160	5.59E+08	90
160	5.53E+08	90
160	5.33E+08	90
160	1.54E+09	10
160	8.15E+08	70
160	1.44E+09	15
160	1.27E+09	40
160	6.92E+08	90
200	4.73E+08	90
200	5.01E+08	90
200	4.75E+08	90
200	4.75E+08	90
200	5.33E+08	90
160	1.18E+09	40
160	1.10E+09	60
160	1.29E+09	50
160	1.32E+09	50
160	1.25E+09	50
160	1.44E+09	5
160	1.00E+09	60
160	1.26E+09	30
160	1.37E+09	5
160	1.12E+09	50
160	1.49E+09	10
160	1.42E+09	10
160	1.47E+09	10

Table 4.20. Production data.

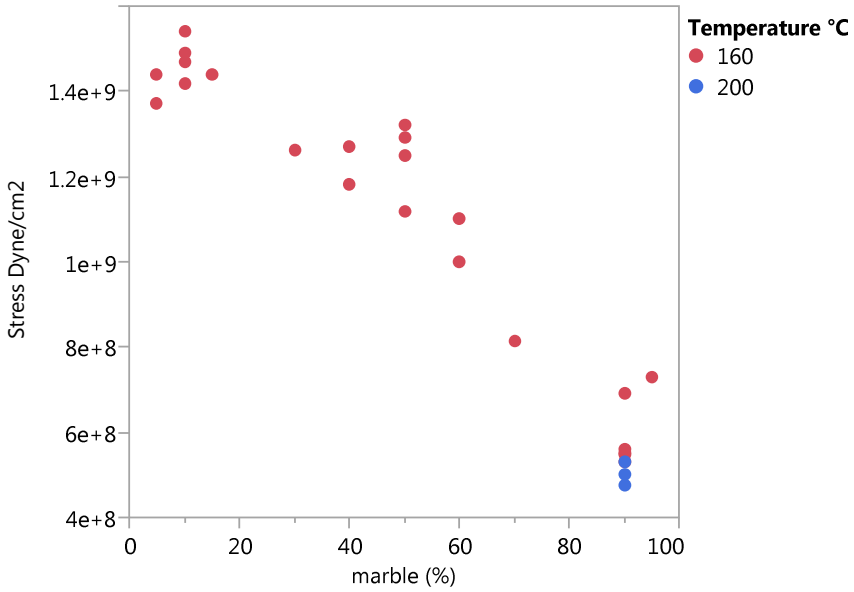

Graph 3.21. stress vs marble plot for production data

From production data, we can clearly notice a correlation between stress and marble level. The lower is the stress, the larger is the impact of the marble effect. Even if less samples coming from higher temperatures (200°C) are available, we can see that all are located at lower stress level, with the corresponding coverage of marble near 100%.

It is important to notice that XRD analysis has been done on samples with this marble like effect, and the results were comparable with what we have seen in figure 3.4. We can state that marble effect is the method the system uses to release the stress, and inside the flakes the crystalline structure is still that of an ordered film with [110] orientation. If enough energy is available, since the reticular mismatch between Al and Si adverses the formation of a single crystal, the system generates crystal domains and in this way relaxes the stress. If we carefully look at the shape and orientation of this "flakes creating the marble effect", we can see that many of them show a 45° orientation with respect to the flat on [100] material, according to the [110] orientation of the film.

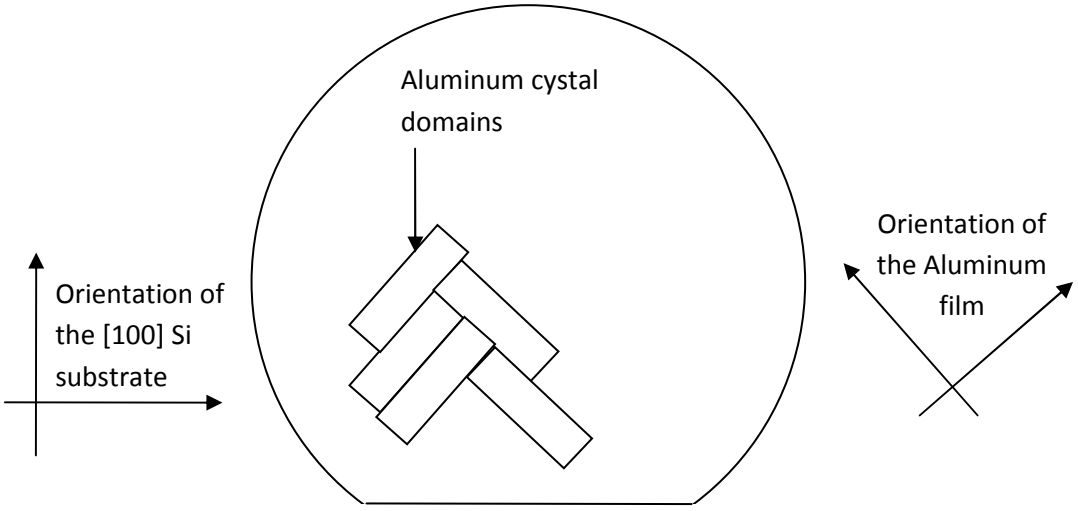

Figure 3.22: scheme of marble effect

3.6 Conclusions.

We have analyzed the microstructure and crystal structure of AlSi deposited on [100] Silicon substrate. The result is that the first variable influencing the film crystal structure is the type of termination of the substrate. If an amorphous silicon oxide layer is present, the film does not tend to generate a preferential orientation. On the other hand if the wafer is treated with HF and the surface is passivated with H, the aluminum film uses the substrate as a template in order to generate a film that is almost monocrystalline with a 45° tilt.

This two types of different crystal structures release the stress caused by temperature in different ways. On non orientated material, coming from OH terminated substrates, the stress is released creating grains and a microstructure that follows the Standard Zone Diagram. On H terminated samples on the other hand, since the resulting film appears to have large crystals, with an XRD pattern near to a monocrystalline material, grain and grain boundaries are not generated. The system relaxes the stress, generating crystal domains and the marble effect.

4 Silicon substrate / AlSi interaction

4.1 Introduction

In order to create a good and stable schottky junction between aluminum and silicon, a lot of process parameters must be taken into account. Depending on the thermal treatments, surface preparation, aging time before metal deposition, the system behavior may change. We have seen in the previous chapter that surface preparation may have dramatic effect on the selection of crystal structure, and that the sputtering temperature can change the stress of the sputtered film. In this chapter we will analyze how those changes will impact the metal/semiconductor junction. In the first part we will summarize literature results (ref. 5), based on pure Al samples. We then will focus on our experiments on AlSi (1% Si) films

4.2 Schottky barrier with pure aluminum

Nominally Aluminum has a Φ_{bn} (schottky barrier on n type silicon) of 0.7 eV. The corresponding Φ_{bp} (schottky barrier on p type substrates) is 1.15eV -0.7eV = 0.45eV (bandgap of silicon- Φ_{bn}= Φ_{bp}) .

4.2.1 Schottky barrier with oxide at the interface.

The presence of silicon dioxide at the interface can modify the barrier height. This type of layer is always present on top of silicon and its thickness is around 12/20 Angstroms. The dependence of SBH to the thickness of oxide at the interface can be seen in figure 4.1.

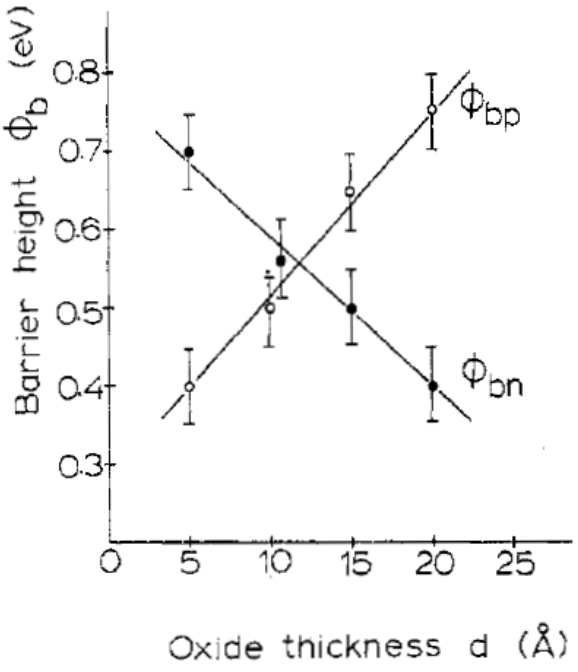

Figure 4.1: Schottky barrier variation with thickness of native oxide

It looks like that oxygen reduces the SBH on n-type silicon substrates, and rises the SBH on p-type silicon. This is due to the presence of positive charges inside the oxide layer. This changes in SBH can be recovered either with aging of the sample or with a low temperature furnace anneal as can be seen in figures 4.2

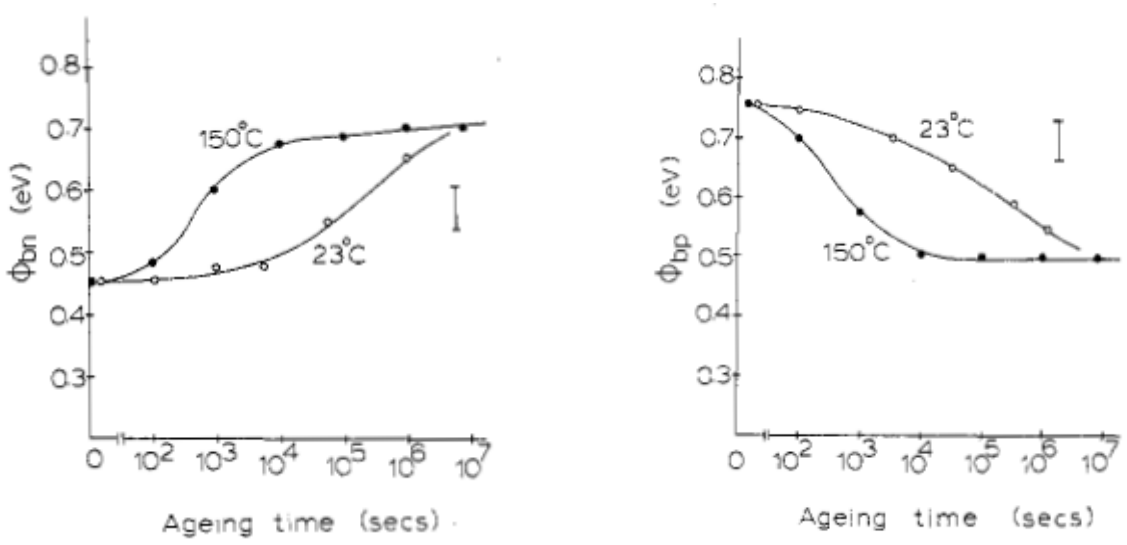

Figure 4.2 effect of time or light furnace anneal on SBH of a sample with oxide at the interface for a)n-type and b) p-type silicon

4.2.2 Thermal treatments

Another major effect on SBH is given by high temperature anneals. In our experiments we will use 420°C. This temperature produces very good ohmic contacts, and is high enough to stabilize the system for the last part of the fabrication process (including back end and assembly). Those types of thermal treatments can also change the schottky barrier, and in particular it rises it on n-type substrates and it lowers it on p-type substrates

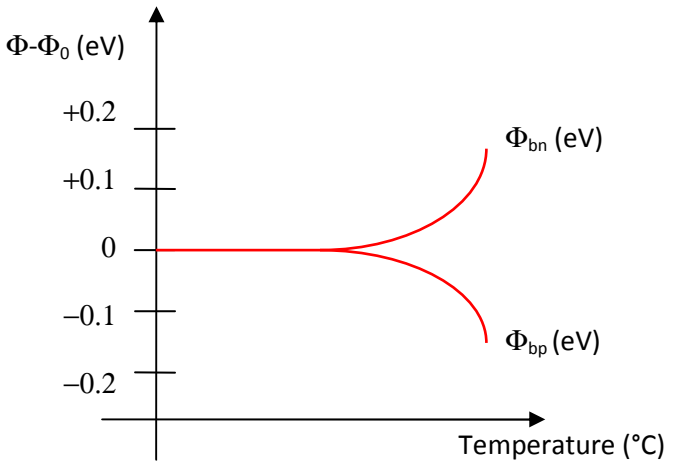

Figure 4.3 annealing temperature effect on SBH

For n type silicon we can see in figure 4.4 some measurements with different types of annealing temperatures

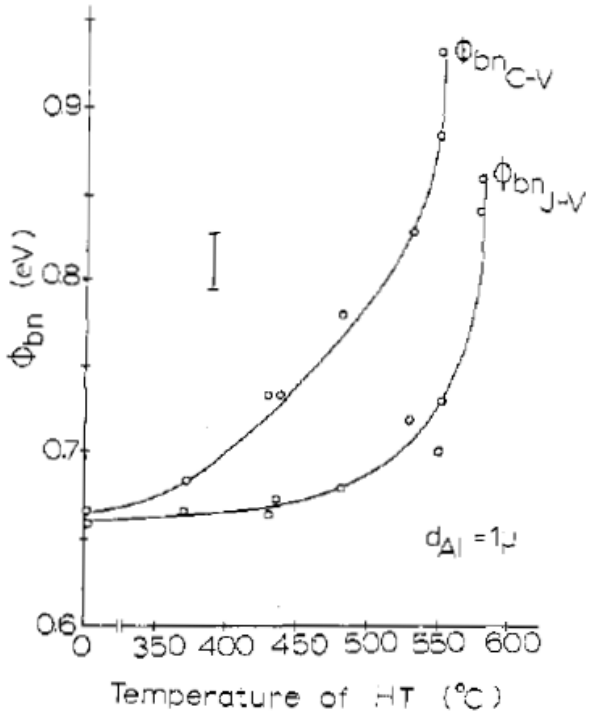

Figure 4.4 effect of temperature on n-type silicon on SBH measured with both CV and JV methods

This increase of SBH on n-type substrates (and the corresponding decrease on p-type) is due to the interaction between Aluminum and Silicon at temperatures above 400°C.

When temperature rises, silicon is dissolved inside aluminum according to the phase diagram. Then when cooling happens, the excess of silicon re-crystallizes at the interface. This type of crystallization happens all in solid phase, and the result is a sort of epitaxial layer at the interface. This re-crystallized layer is heavily p-doped since aluminum is a p-dopant for Silicon. The resulting p-n junction rises the apparent SBH on n-type silicon

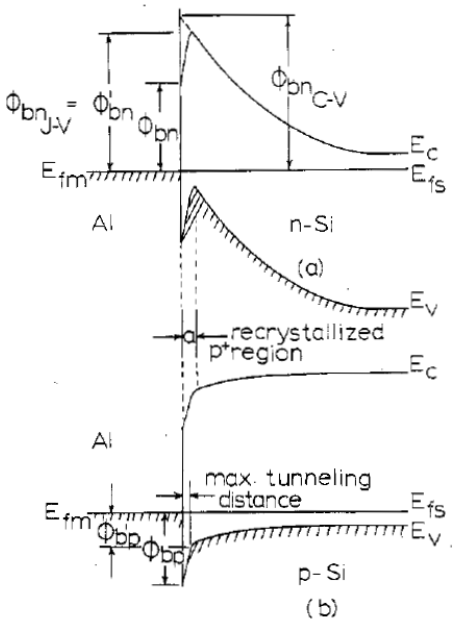

Figure 4.5 Recrystallized material at the interface effect on apparent SBH on a) n-type and b) p-type silicon

4.3 Experimental.

In order to test the SBH of different types of Al/Si interfaces, we generated simple devices. In figure 4.6 is possible to see the process flow. Since there is no need that the devices can sustain reverse bias, the termination is not necessary. In any case on the outer part of the die, we designed an oxide guard ring. The reason why we applied the oxide is to avoid undesired contact between adjacent devices: when aluminum is removed from silicon, a surface contamination persists, and this don't allow a good electrical insulation. The removal from oxide on the other hand is very effective (see figure 4.7) and each die can be tested separately. As substrates we used Cz Silicon with a [100] orientation with on top a low doped n epitaxial layer of 30 microns.

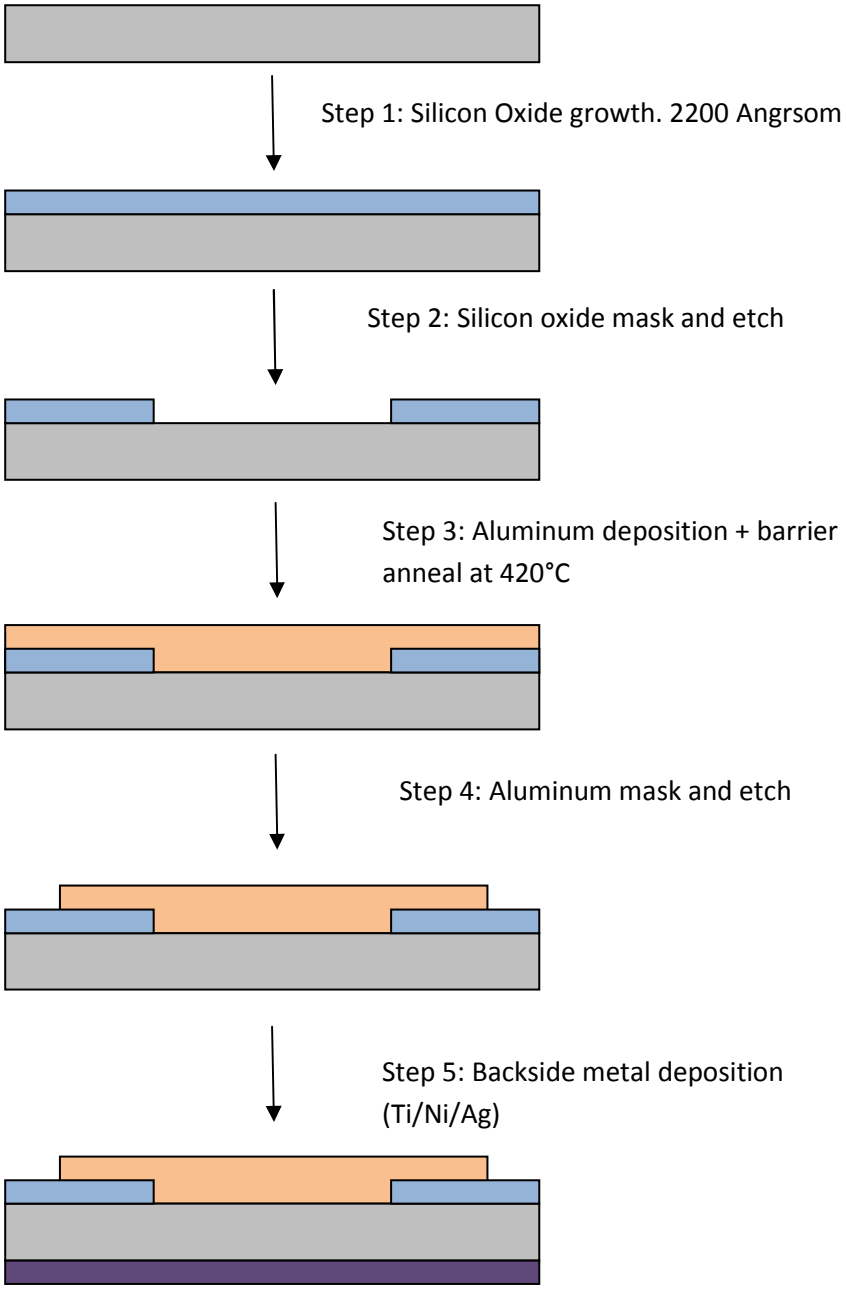

Figure 4.6. Process flow for simple devices to test SBH

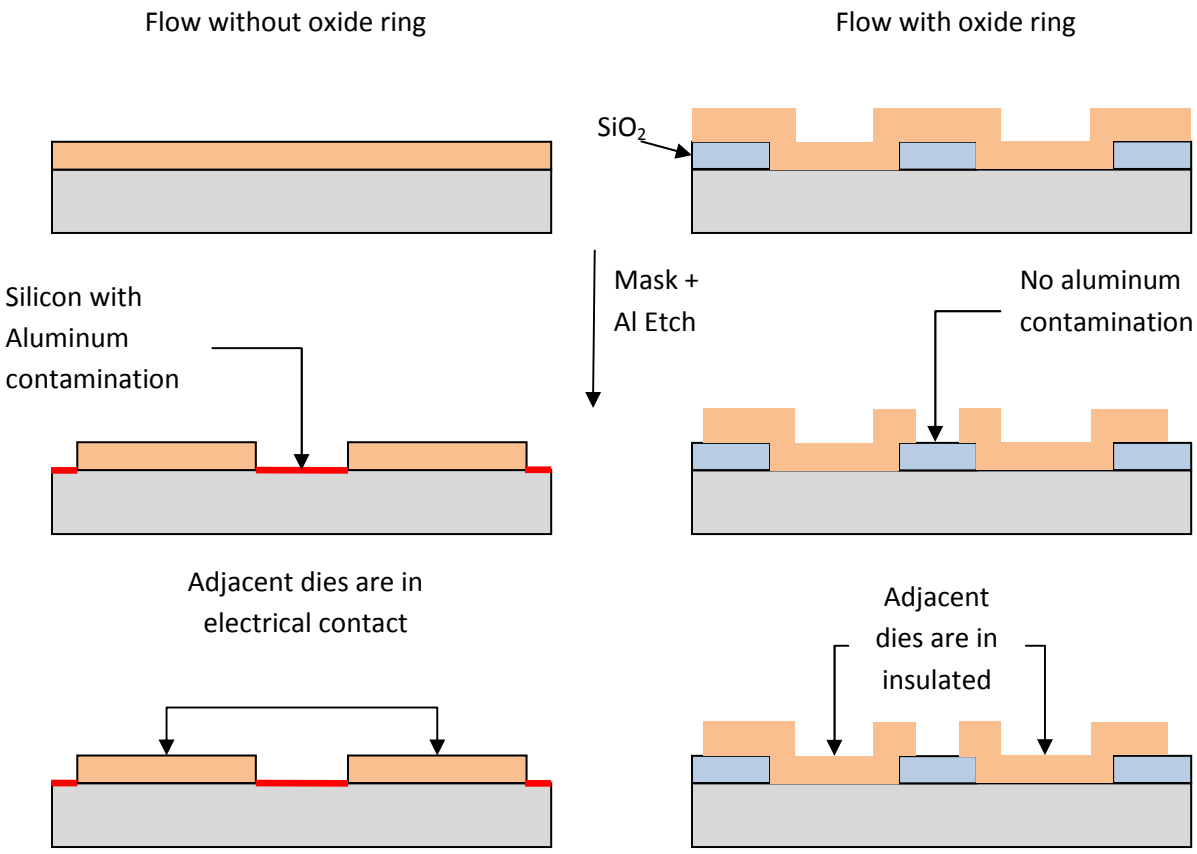

Figure 4.7 electrical insulation between adjacent dies

4.3.1 Experiment 1: Surface preparation and metal type influence

4.3.1.1 Introduction

The purpose of the first experiment is to test two factors: The type of surface preparation and the type of metal. We used three different types of surface conditioning: a diluted HF solution (1:50 HF:H2O at room temperature with 30" of bath time), a sulphuric peroxide mix (SPM, 20:1 H2SO4:H_2O_2 at 140°C) and an RCA cleaning (standard cleaning 1 + standard cleaning 2. For details see §3.3.1). We applied the different surface preparations between step 2 and 3 of the flow in figure 4.6. In the successive process step we deposited two different materials: a pure aluminum layer using an e-beam evaporator, and a AlSi alloy (1% Si content) using DC magnetron sputtering.

After samples preparation we measured the SBH and ideality factor for each sample using the JV method

4.3.1.2 Results

In table 4.8 the experimental results are listed. In graphs 4.9 and 4.10 the SBH and ideality factors are plotted.

Deposition method	Surface Preparation	SBH (eV)	n
Sputter (AlSi)	RCA	0.927	1.021
Sputter (AlSi)	RCA	0.905	1.04
Sputter (AlSi)	HF	0.989	1.009
Sputter (AlSi)	HF	0.967	1.034
Sputter (AlSi)	SPM	0.857	1.054
Sputter (AlSi)	SPM	0.817	1.08
evap (Al)	RCA	0.807	1.135
evap (Al)	RCA	0.811	1.099
evap (Al)	HF	0.837	1.092
evap (Al)	HF	0.831	1.095

Table 4.8. Preliminary experiment data

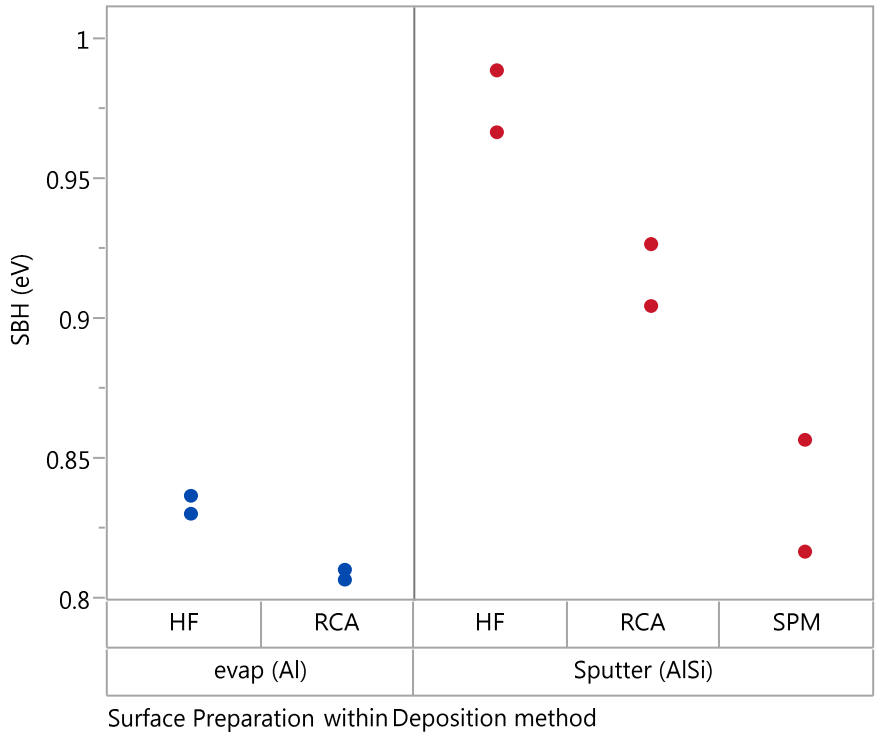

Figure 4.9: SBH measurements for experiment 1

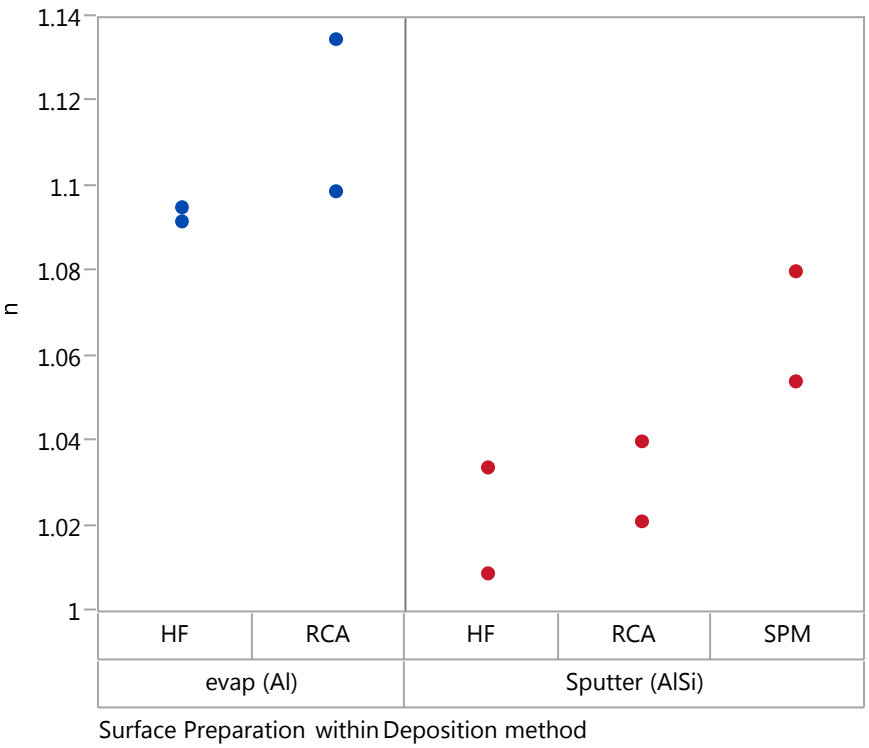

Figure 4.10: ideality factor for experiment 1

4.3.1.3 Comments

The values we obtained are consistent with the trends found in literature: after a thermal treatment on n-type silicon we have SBH values exceeding 0.7 eV, and an oxide interface lowers the SBH. This fact can be observed both for pure aluminum (RCA sample has a lower SBH compared to HF treated sample) and for the AlSi Alloy (RCA and SPM generate oxide at the interface and their SBH values are lower compared to the HF treated sample). If we consider only samples with oxide at the interface, since SPM is a very strong oxidizing treatment (much stronger compared to RCA) the SBH values for samples treated with this solution are lower compared to the ones treated with RCA.

It is also interesting to look at the comparison between the two types of metallization. Values calculated from devices using pure aluminum metallization are lower, while AlSi alloy has SBH reaching almost 1 eV, a value that is higher compared to what we have found in literature for this type of junction at this temperature of furnace anneal.

4.3.2 Experiment two: temperature effect

4.3.2.1 Introduction

We decided to explore in greater detail the sputtered AlSi alloy, since less data is available and is of great interest in production flows. We focused on the HF surface preparation. This is due to the fact that, if we produces devices using a barrier with oxide at the interface, the leakage current in reverse bias is very high. If no oxide is present on the other hand, we can keep control of this parameter. For this reason the junction with oxide is less interesting from an applicative point of view.

In the design of the second experiment, we used the information gathered during the microstructure exploration (chapter 3). We wanted to explore the complete range of microstructures of aluminum on H terminated substrates. As variables we have chosen the sputter temperature, in order to generate different stress levels. We did two series of experiments in different days for each temperature, in order to include the run to run variability (as we have seen in the previous chapter, with H termination the system produces very variable results). The first two samples for the lower temperatures are the same generated in experiment 1

As responses we measured the stress level, the SBH and ideality factor, and we gave a % of the wafer coverage of the marble effect, with the same criteria used in chapter 4.5.

4.3.2.2 Results

On table 4.11 is possible to see the values obtained for the experiment, and on figure 4.12 is shown the corresponding scatterplot matrix

Sputtering temperature (°C)	Marble	Stress Dyne/cm2	SbH (eV)	n
160	5%	1.54E+09	0.99	1.01
160	7%	1.44E+09	0.97	1.03
160	10%	1.21E+09	0.91	1.02
160	30%	1.18E+09	0.90	1.03
200	35%	9.49E+08	0.90	1.05
200	60%	8.15E+08	0.89	1.04
200	90%	7.28E+08	0.89	1.02
200	90%	6.92E+08	0.88	1.05

Table 4.11: data for experiment 2 on schottky barrier of AlSi/Si contacts

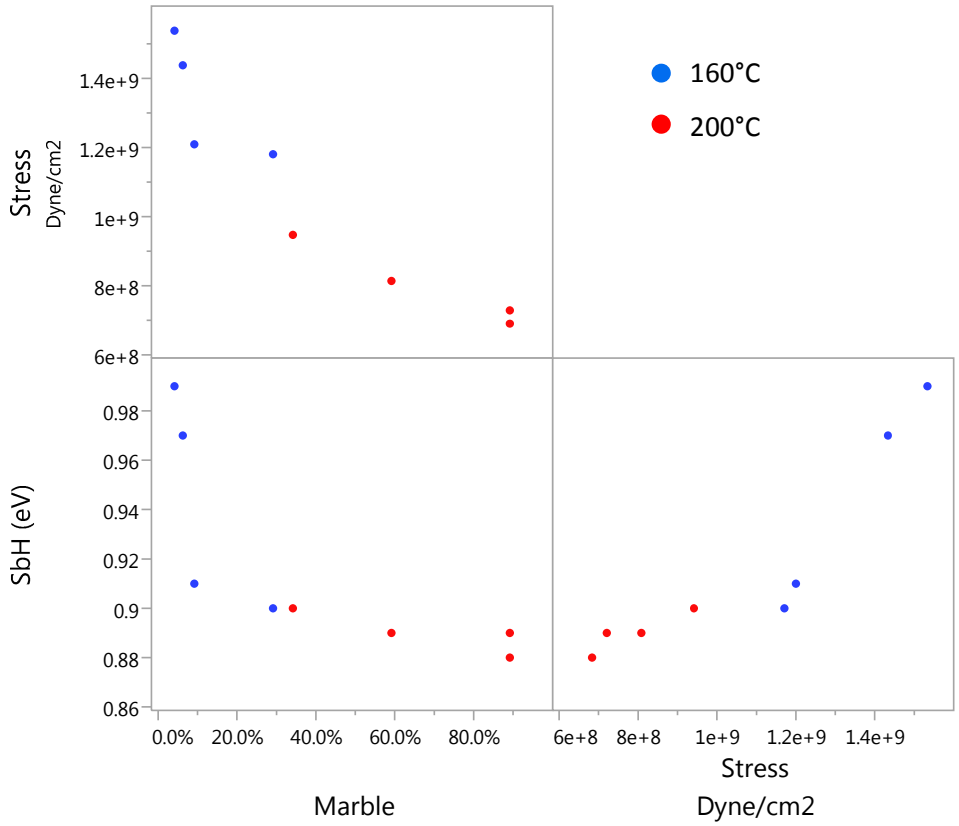

Figure 4.12 Scatterplot matrix for experiment 2

4.3.2.3 Comments

The first thing that is possible to notice looking at the results is the great variability of SBH. It ranges from almost 1 eV to 0.88 eV. As we have seen on the previous chapter there is a link between the quantity of the effect that we called “marble” and the stress. The lower is the stress the higher is the marble effect. The formation of those 45° oriented flakes, helps the system to relax the stress. With this experiment we found another important link between the stress, the microstructure and the SBH: the higher is the stress, the higher results the SBH. This is especially true for high values of stress. When this parameter is high, and the marble effect is almost non visible (the resulting wafers are bright and uniform) , the SBH rises, reaching values near to 1eV. Since this increase is so steep, it is very hard to control the resulting characteristics of the devices. In the range between 1.4E+09 and 1.2E+09 dyne/cm2 the SBH ranges from 0.9 to 0.99 eV. This can be very dangerous, since in production conditions the perfect control of all the parameters is crucial to achieve stable yields.

4.3.3 Inspection of the interface

4.3.3.1 Introduction

In order to further investigate what may cause the increase of schottky barrier in AlSi, we took two samples with different stress and microstructure, and we removed the metallic layer. Then we inspected the interface using SEM and AFM. Figures 4.13 and 4.14 show the results.

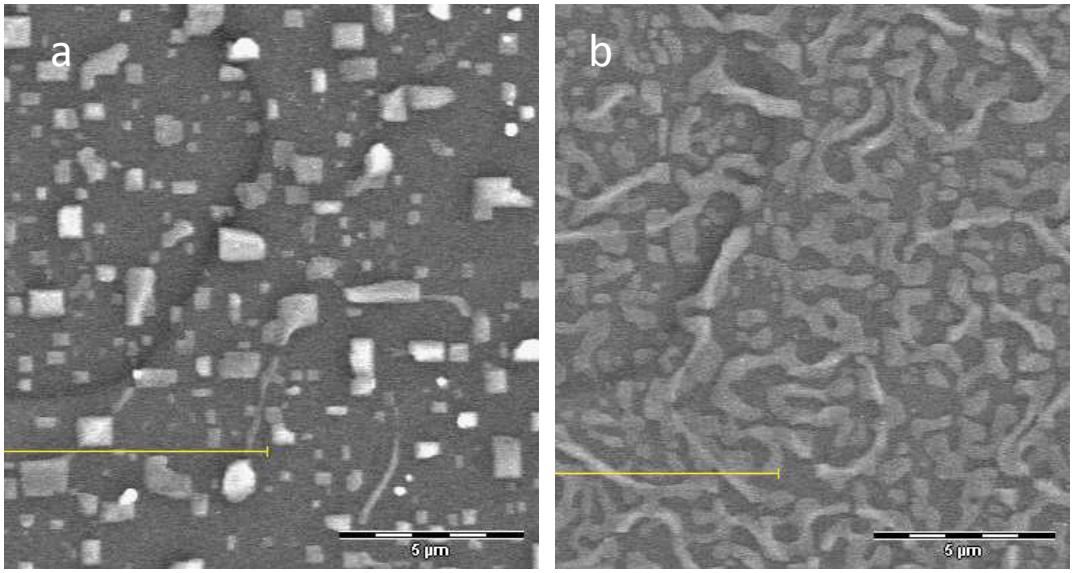

Figure 4.13: **a)** Interface on a sample showing marble and a stress level of 8E+08 dyne/cm^2 **b)** interface on a sample without marble effect and a stress level of 1.5E+09 Dyne/cm^2

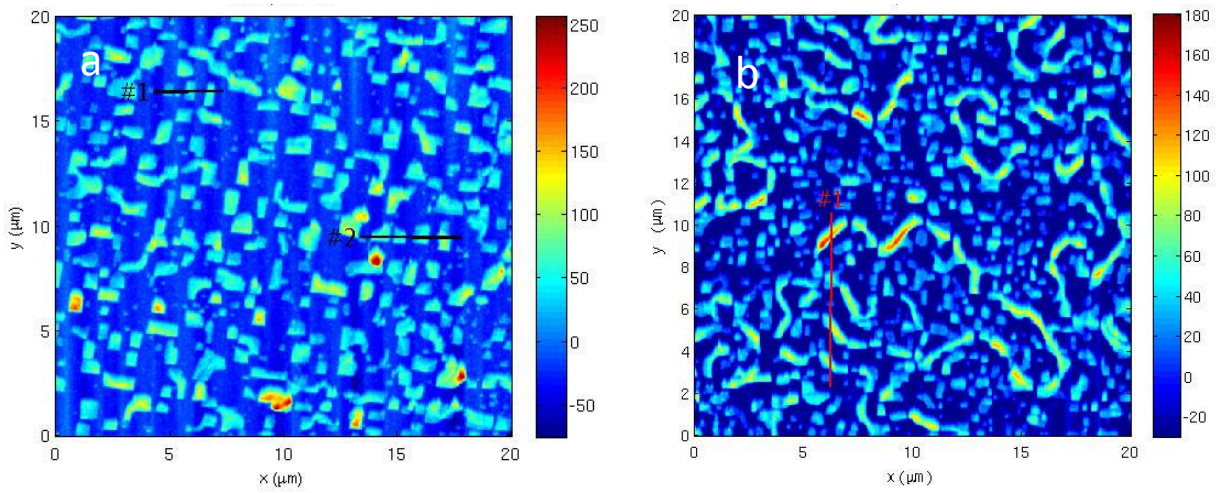

Figure 4.14: AFM images on **a)** sample showing marble and a stress level of 8E+08 dyne/cm^2 **b)** sample without marble effect and a stress level of 1.5E+09 Dyne/cm^2

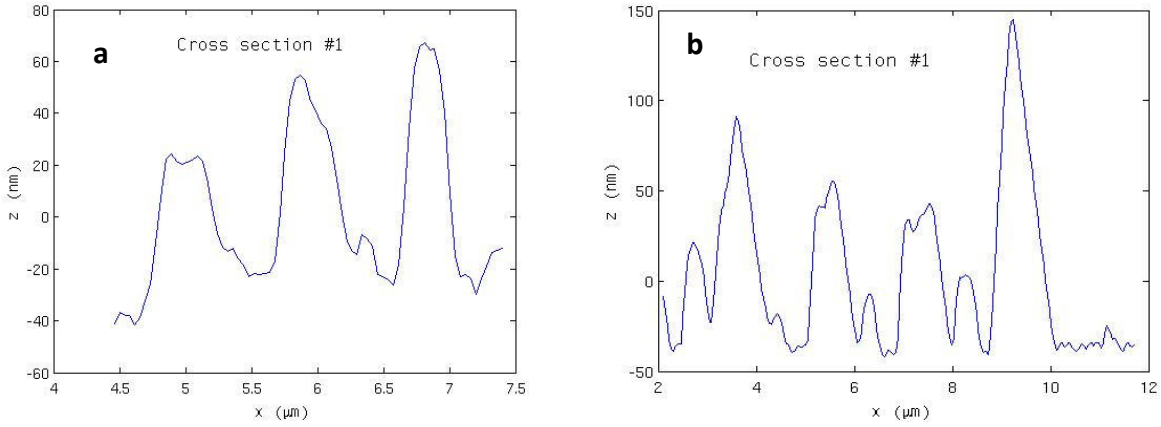

Figure 4.15: Profiles taken from AFM **a)** sample showing marble and a stress level of 8E+08 dyne/cm^2 **b)** sample without marble effect and a stress level of 1.5E+09 Dyne/cm^2

4.3.3.2 Comments

After the metal removal, we found on the interface between aluminum and silicon cubic structures with the side parallel to the flat (see figure 4.16)

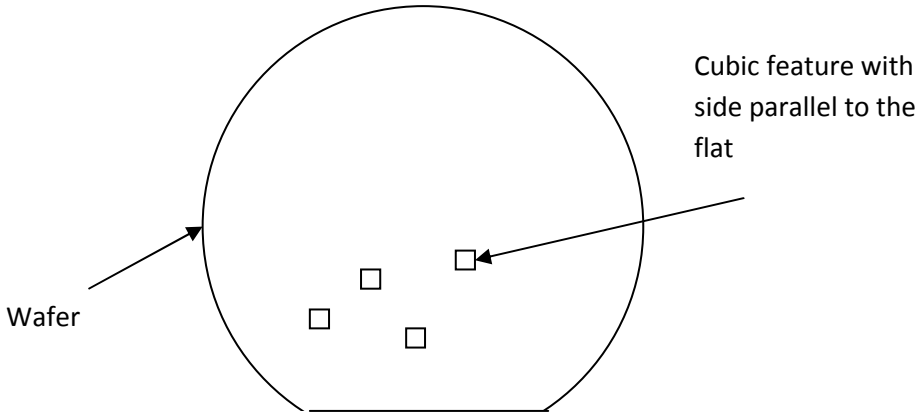

Figure 4.16: schematic representation of the cubic silicon precipitates and their orientation with respect to the flat on a [100] monocrystalline silicon wafer

Those cubic islands are silicon re-crystallizations coming either from the reaction between the silicon substrate and the aluminum film and precipitates coming from the AlSi alloy. This contribution coming from precipitates during cooling of the AlSi alloy, explain the greater SBH of sputtered material compared to pure aluminum obtained with e-beam evaporation.

If we look at the XRD data acquired from AlSi film, we can see that both at high and low temperatures, the almost monocrystalline [220] peak already discussed in chapter 4.5, is located exactly at the expected angle as for pure aluminum (2θ= 65.14° and 65.13°, the expected value is 65.16 for a d=1.43). This can imply that the aluminum cell is not distorted by silicon inclusion. Since in this condition no grain boundaries where silicon can migrate were found, we can suppose that all the Silicon that was present inside the film , precipitated at the interface. If we calculate the average height of the silicon precipitates from AFM data, we find that on less stressed sample (with marble effect) the average is 830 Angstroms, while on the bright with high stress the average is 700 Angstroms. Since we started from a 30000 Angstroms layer with 1% Silicon inside, and even considering the different density of Aluminum and Silicon (Aluminum : 2.7 g/cm^3 Silicon 2.3 g/cm^3) we can conclude that the silicon present inside the AlSi film cannot explain alone all the cubic material at the interface. This means that the cubic precipitates are generated by the sum of silicon coming from the AlSi film and from the interaction between the first layer of the interface between silicon substrate and AlSi film. In figure 4.17 a complete diagram of the precipitates formation is shown.

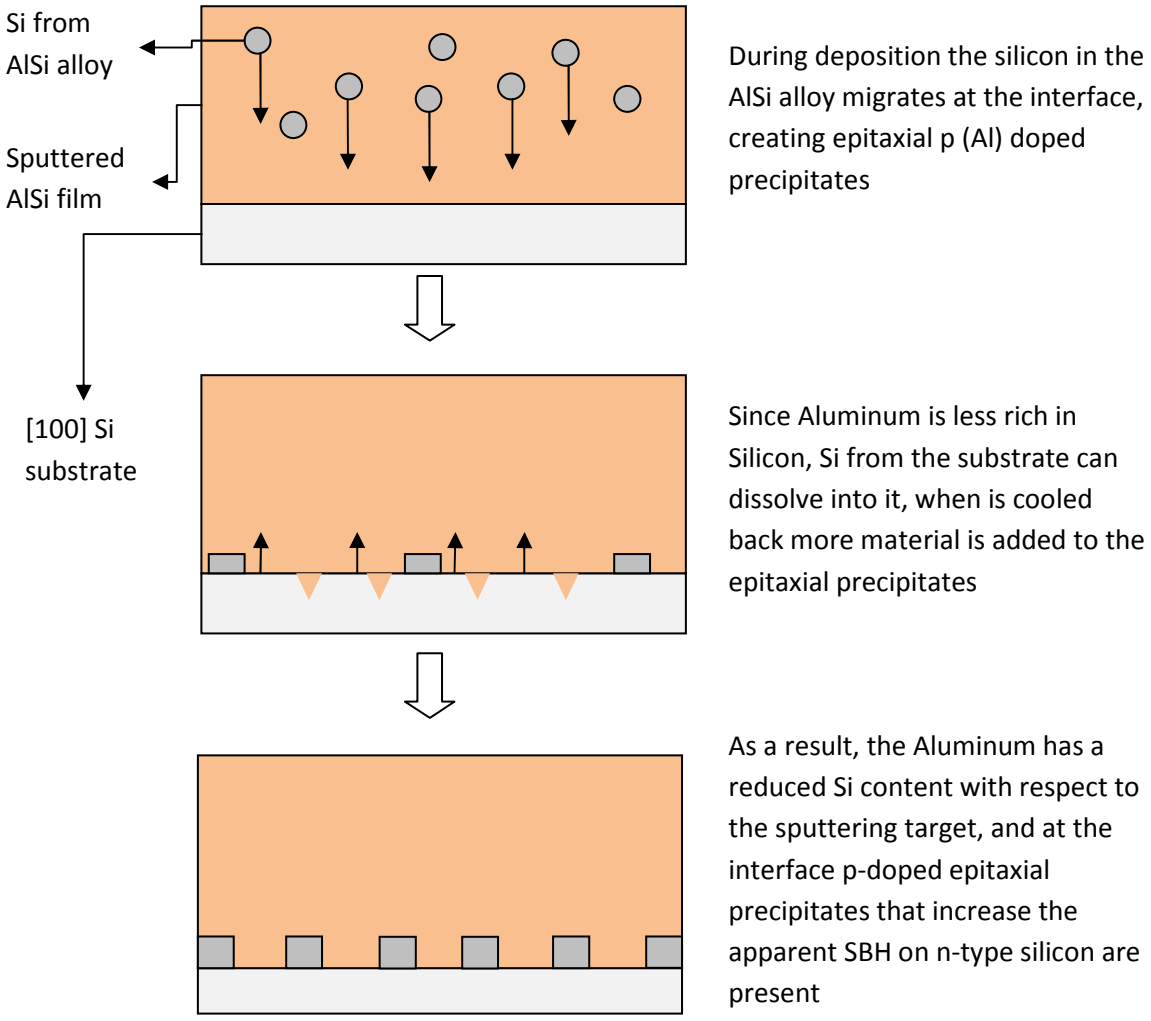

Figure 5.17. Scheme of the interface precipitates formation

4.3 Conclusions

We investigated the junction between monocrystalline [100] silicon and a sputtered AlSi (1% Si content) film with a 420°C furnace anneal. We found that native oxide at the interface lowers the SBH, and with oxide at the interface the leakage current of devices is high. We also made a comparison between pure aluminum and AlSi alloy film, demonstrating that AlSi film results in higher SBH, and the values are above what we found in literature. This depends from the Silicon present inside the film that precipitates at the interface, building epitaxial p-doped (rich in aluminum) islands. We also found a correlation between stress, the SBH and the marble effect. The lower is the stress values, the lower is the Schottky barrier and the higher is the % of the wafer covered with marble effect. We have also seen that, for high stress values, the control of schottky barrier is critical: the SBH varies rapidly from 0.9eV to 1eV . This condition is not good for production devices, since this non predictable variation of the SBH leads to a high variability of the devices electrical parameters.

5 a-Si film deposition

5.1 Introduction

In this chapter we will introduce the amorphous silicon layer. This film is employed in the termination of power devices in order to obtain high efficiencies as we have seen in chapter 2.

The introduction of this material in the device's structure adds complexity to the system, since amorphous silicon characteristics should be tuned carefully in order to achieve the correct impact on electrical parameters. Furthermore, the interaction between the new layer and aluminum can trigger different types of phenomena, as we will see in chapter 6.

We can use different types of techniques in order to deposit amorphous s silicon. We will focus on PVD, and in particular on e-beam evaporation and DC magnetron sputtering. As we have seen also for the contact metal deposition, the preferred method in production is sputtering. Sputtering is a convenient technique since it can be easily automatized, and has short process times. E-beam evaporation on the other hand requires a lot of operator-time, and has a lower throughput. Films obtained by e-beam usually have lower stress and are less subject to contaminations. E-beam tools has usually a lower base pressure compared to sputtering and on sputtering films there is always the possibility of contamination by the carrier gas.

5.2 Refractive index validation

5.2.1 Introduction

The amorphous silicon film has an important electrical role in the termination of the device. One of the first things that needed to be addressed was to find an easy, effective and fast method characterization method, able to evidence the differences between various samples before applying them on actual devices.

One of the most used techniques in production to evaluate thin films is to measure their thickness using a reflectance spectrophotometer. We have used two spectrophotometers in our work: a Nanospec and an n&k 1500. We have described the differences between those tools in chapter 2.

The main difference between Nanospec AFT210 and n&k 1500 is the ability of the "n&k 1500" analyzer not to give a spectral dependence of the optical characteristics of the films. The Nanospec AFT210, assumes that the refractive index is constant with wavelength, and then calculates the thickness of a film according to the number of interference fringes found in a range of wavelengths.

5.2.2 Experimental.

In order to choose the best method to characterize the film's thickness, we generated two samples with a DC magnetron sputtering with different process parameters. Then we measured them with three systems: a Nanospec AFT210, a n&k 1500 and a profilometer (Tencor P10).

The profilometer uses a completely different evaluation method with respect to the optical one, since it uses a stylus touching the sample that, with a piezoelectric tip, can detect mechanically steps and heights. See figure 5.1 for a schematic representation of the system. We will use these data to compare the accuracy of reflectance evaluation results.

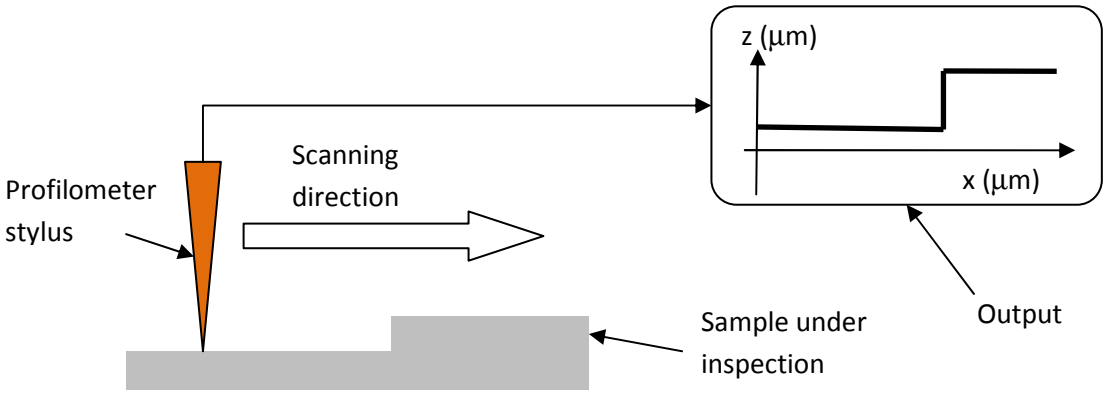

Figure 5.1 diagram of a stylus profilometer

5.2.3 Results and discussion

In table 5.2 the thicknesses values obtained on two different films (sputtered in different chamber conditions and exhibiting different n values as obtained from n&k) are reported

	n@633 nm =4.73	n@633 nm = 4.59
n&k	1410	1130
nanospec	1663	1278
profilometer	1564	1264
Nk/prof.	90%	89%
Nano/prof.	94%	99%

Table 5.2: Data result

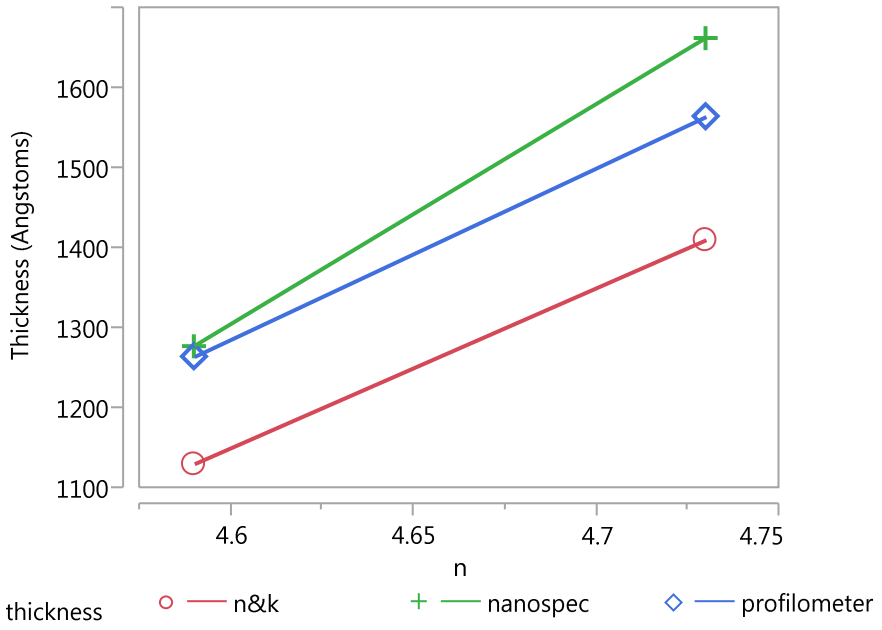

Figure 5.3: Comparison between different measurement types. As can be seen n&k and the profilometer has the same pendency, this means that the two systems are able to follow in the same way the change in refractive index of the material

The result shows that the thicknesses measured with the n&k analyzer have a constant difference of about 10% with respect to the profilometer ones, even for very different samples. The nanospec instrument otherwise shows a measure that is very close to the one measured with the Tencor p10, for the film with the smaller refractive index. The situation changes for the film with a different refractive index. For this reason, using the nanospec to measure sputtered amorphous silicon samples, can take to misleading results in the case of a variation of the film's optical characteristics. This variations are common in sputtered materials since the deposition conditions can produce layers with different densities, and this fact has an immediate impact on the refractive index. In the following paragraphs, we will use the n&k data directly, without adding a 10% of thickness variation in order to have the same type of values as per a profilometer.

5.3 Amorphous silicon influence on leakage

The type of amorphous layer present on the surface directly impacts the leakage current of the devices. Any contamination, difference in structure or surface charge, has a direct impact on conductivity of the material. For this reason in a device's termination such as the one proposed in figure 5.4a. a leakage current may flow in the way schematized in figure 5.4b when the device is reversely biased.

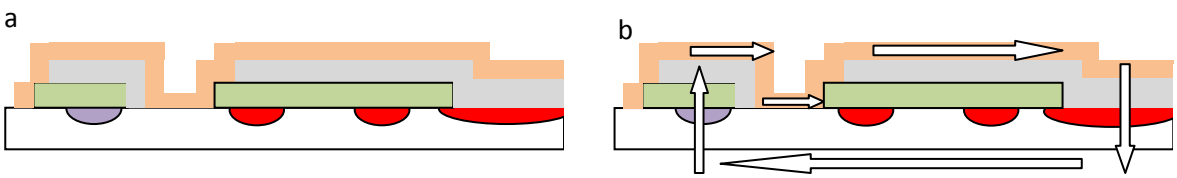

Figure 5.4 a) scheme of the device's termination b) Leakage current flow inside the device in reverse bias using amorphous silicon to conduce current

This type of leakage current is especially visible on low loss devices such as p-n diodes, where the leakage current at nominal tension can be of the order of nA.

A low leakage (in the order of nA) current and a good efficiency of the termination has been obtained using an amorphous layer deposited with an e-beam equipment. In the next chapters we will see the characterization of a sputtered a-Si film, and we will try to tune its properties on order to match the e-beam evaporated one.

5.4 Sputtered a-Si characterization

5.4.1 Introduction

In this series of tests, we will describe an experimental matrix used to explore the sputtered a-Si film, with respect to the main process parameters. We will make a comparison between the obtained results and the reference e-beam material. We will then test the obtained layer on actual devices in order to monitor the performances. Note: in all the experiments the sputtering time is 60"

5.4.2 Experimental

We have selected three factors to test:

- Sputtering power
- Pressure
- Temperature

We will make a simple design with a center point and no repetitions. The responses of the experiment will be:

- Energy gap
- n
- k
- Stress

The energy gap and the real and imaginary part of the refractive index will be calculated using a n&k 1500 reflectance spectrophotometer, the stress will be measured using a Tencor Flexus FLX2320

The Amorphous silicon film will be deposited on a Cz Silicon [100] substrate

5.4.3 Results and discussion

In table 5.5 we can see the experimental results, the data on the first row refers to a e-beam evaportated sample.

Deposition tool	Temp	Pressure	pow (% of 5 KW)	Eg (eV)	n @633 nm	k @633 nm	Stress E9 Dyne/cm2
e-beam	NA	NA	NA	1.670	4.110	0.260	
sputter	40	9	32	1.512	4.560	0.410	-6.54
sputter	40	9	26	1.598	4.530	0.426	-6.14
sputter	40	5.8	26	1.551	4.660	0.426	-9.52
sputter	40	5.7	32	1.486	4.633	0.407	-9.52
sputter	80	7.5	29	1.558	4.710	0.396	-8.71
sputter	120	9	32	1.554	4.660	0.390	-7.04
sputter	120	9	26	1.616	4.645	0.405	-6.83
sputter	120	5.8	26	1.569	4.806	0.419	-9.3
sputter	120	5.6	32	1.536	4.775	0.393	-9.63

Table 5.5 Experimental data table for sputtering conditions experimental matrix

In the next paragraphs, the data analysis for each response is presented. A stepwise regression was performed in order to select the most significant factors and interactions for each parameter, then the linear regression for each significant parameter has been done. For each factor the coefficient for the regression and the all the t tests will be presented in a separate table. This will help us to build a simple scheme that can be useful to understand the system reaction to the variation of each factor.

5.4.3.1 *Energy gap*

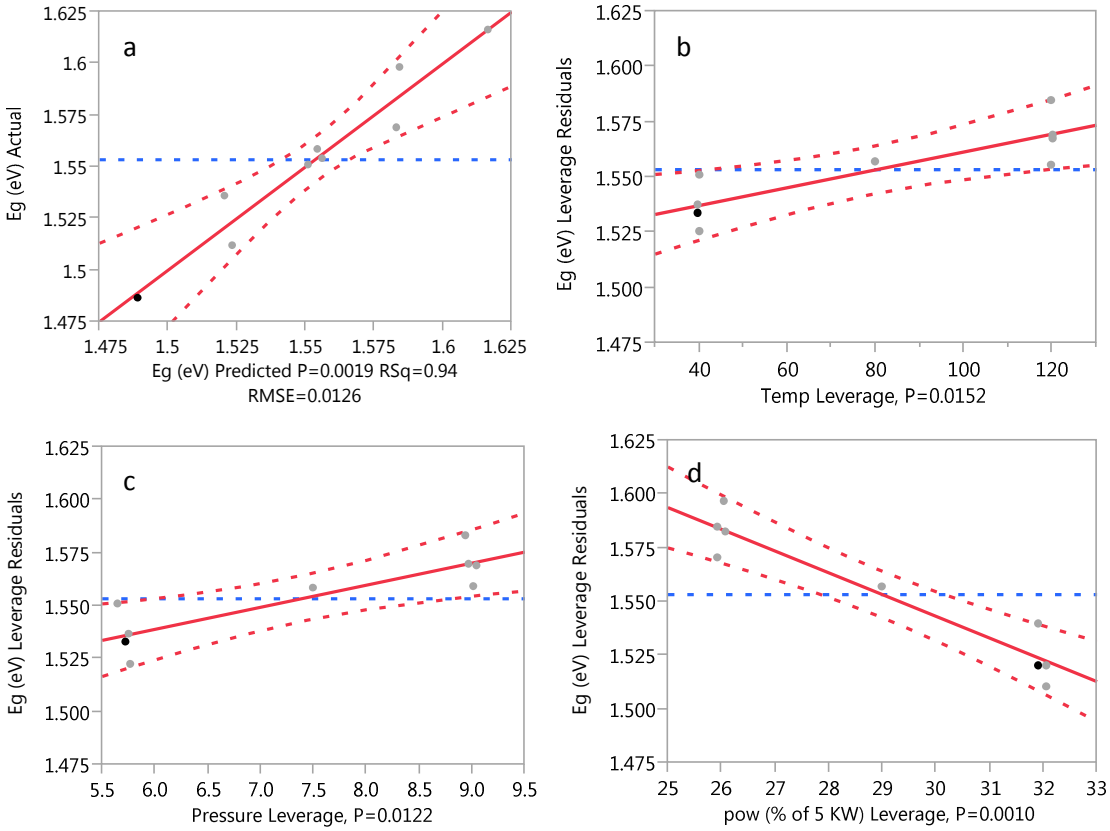

Figure 5.6. Energy gap: a) actual vs predicted by the model b) leverage plot for temperature c) leverage plot for pressure d) leverage plot for power

Term	Estimate	Std Error	t Ratio	Prob>|t|
Intercept	1.74E+00	4.89E-02	35.510	<.0001
Temp	4.03E-04	1.11E-04	3.620	0.015
Pressure	1.04E-02	2.72E-03	3.830	0.012
pow (% of 5 KW)	-1.01E-02	1.49E-03	-6.820	0.001

Table 5.7: t test and estimates for Energy gap

5.4.3.2 n

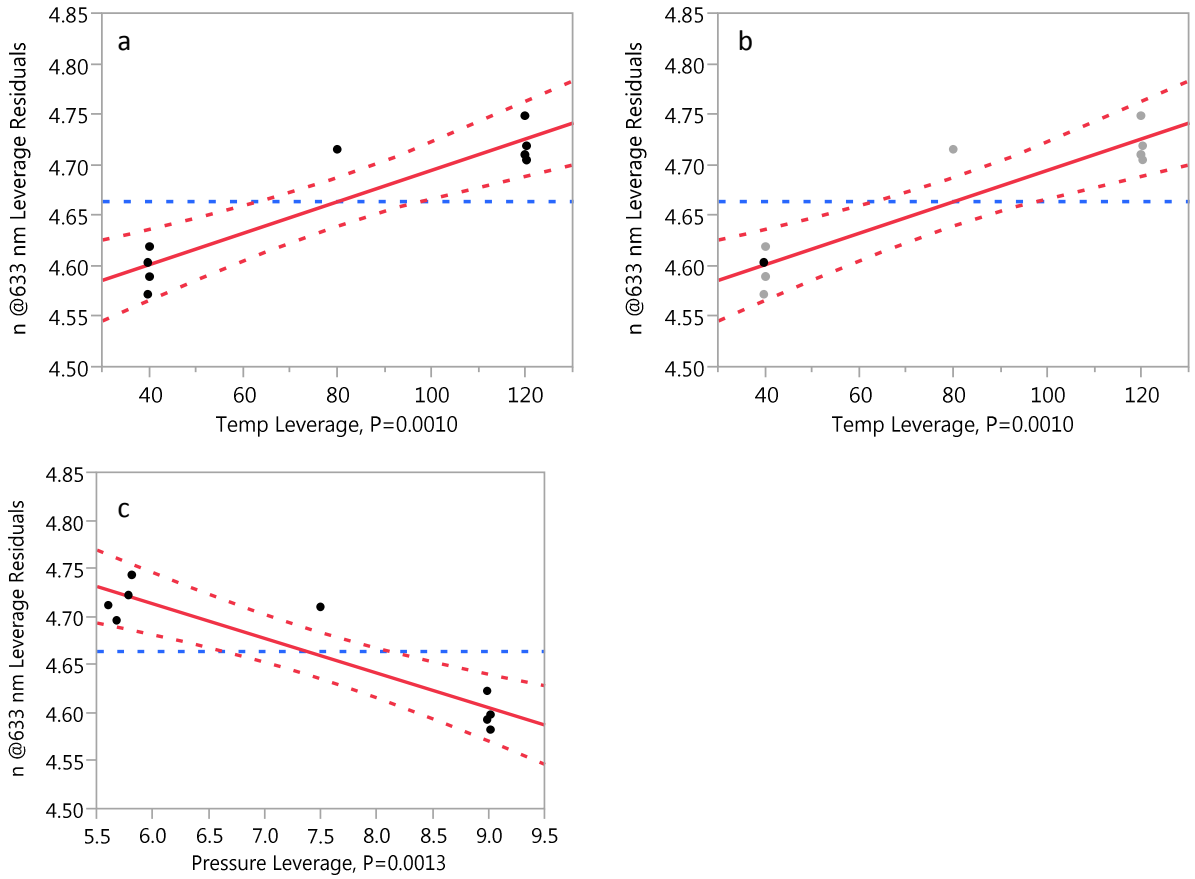

Figure 5.8. n: a) actual vs predicted by the model b) leverage plot for temperature c) leverage plot for pressure

Term	Estimate	Std Error	t Ratio	Prob>|t|
Intercept	4.81E+00	5.23E-02	91.910	<.0001
Temp	1.56E-03	2.60E-04	6.000	0.001
Pressure	-3.60E-02	6.34E-03	-5.680	0.001

Table 5.9: t test and estimates for n

5.4.3.3 k

The modeling of the extinction coefficient was impossible without removing the center point. This can be due to a curvature in the response (in this screening design we are assuming linear responses)

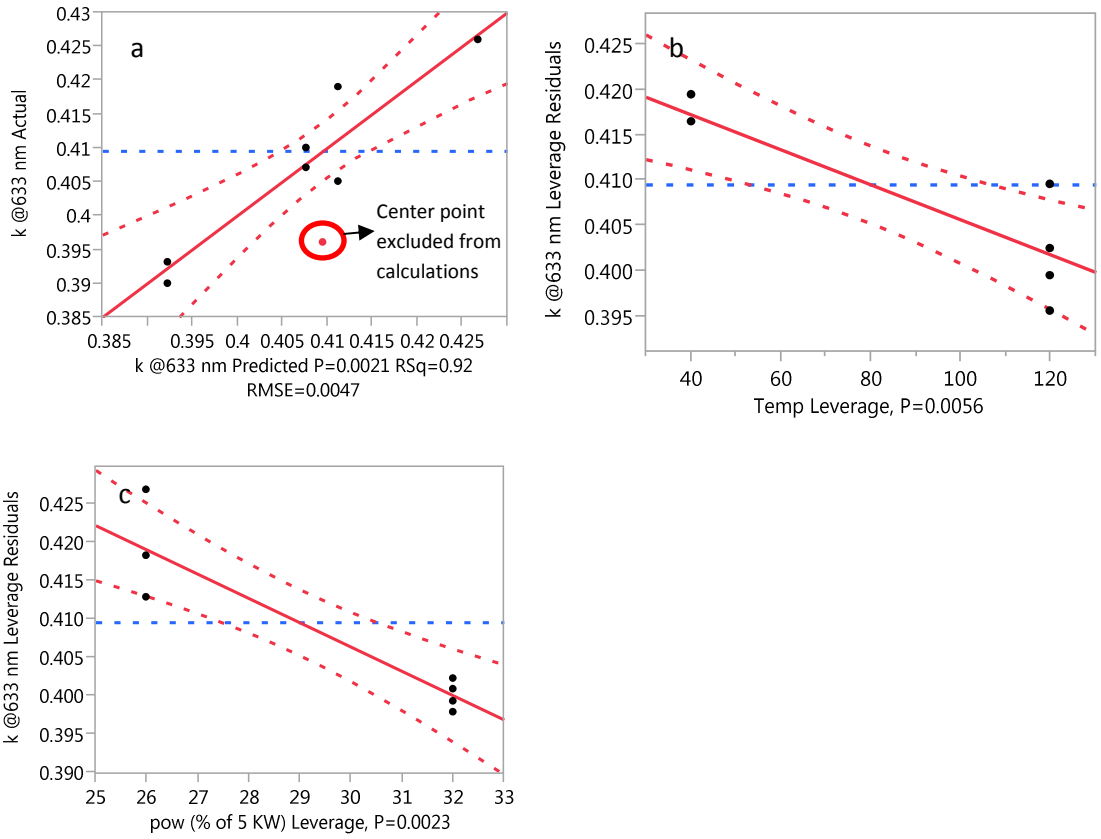

Figure 5.10. k: a) actual vs predicted by the model b) leverage plot for temperature c) leverage plot for power

Term	Estimate	Std Error	t Ratio	Prob>|t|
Intercept	5.17E-01	1.66E-02	31.200	<.0001
Temp	-1.94E-04	4.17E-05	-4.640	0.006
pow (% of 5 KW)	-3.17E-03	5.57E-04	-5.690	0.002

Table 5.11: t test and estimates for n

5.4.3.4 Stress

On the stress the variable that dominates the effect on the response is the chamber pressure

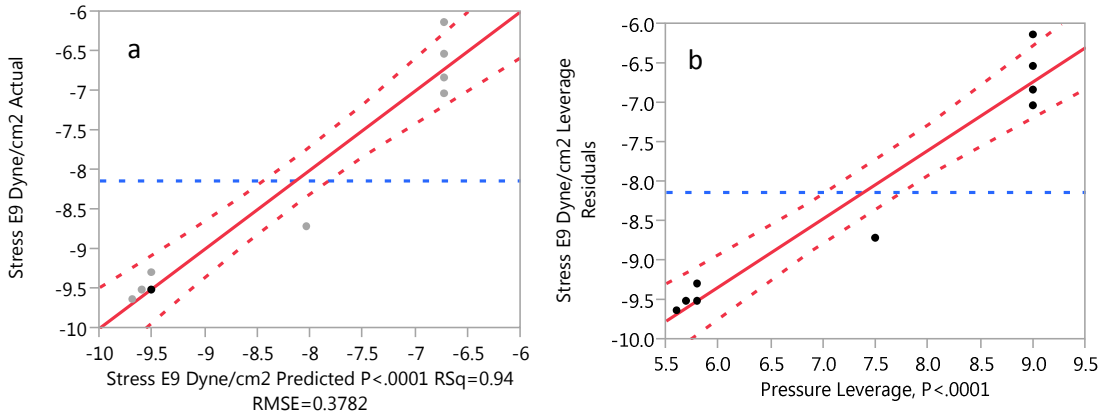

Figure 5.12: Stress a) actual vs predicted b) Leverage plot for pressure

Term	Estimate	Std Error	t Ratio	Prob>|t|
Intercept	-1.45E+01	6.15E-01	-23.640	<.0001
Pressure	8.68E-01	8.16E-02	10.640	<.0001

Figure 5.13: t test and estimates for stress

5.4.4 Results summary.

In table 5.14, we have summarized all the results obtained

Effect of increasing	Film Characteristics			
	Eg	n@633nm	k @ 633 nm	Stress
Power	↓↓	=	↓	=
Argon	↑	↓	=	↑↑
Temperature	↑	↑	↓	=

↑ Increase of the value, the film becomes less compressive

↓ Decrease of the value, the film becomes more compressive

= The variable has no influence on the response

Table 5.14: Summary table for process parameter impact on a-Si sputtered film

5.4.5 Test on production samples

5.4.5.1 Results

We have produced one lot (50 wafers) using three different types of amorphous silicon, in order to check if the measured characteristics may correlate with electrical data

A summary of the characteristics of the three layers used is available in table 5.15

Sample ID	Temp	Pressure	pow (% of 5 KW)	Eg (eV)	n @633 nm	k @633 nm	Stress E9 Dyne/cm2
e-beam	NA	NA	NA	1.670	4.110	0.260	
Sputter low Eg	40	5.7	32	1.486	4.633	0.407	-9.52
Sputter High Eg	120	9	26	1.616	4.645	0.405	-6.83

Table 5.15: characterization of the different films used on production lots

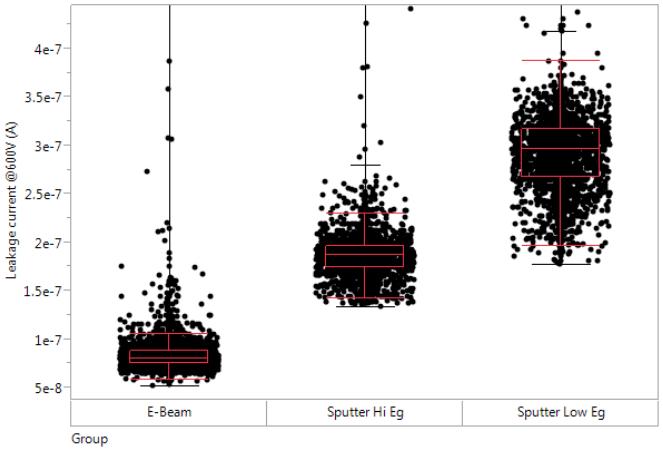

Figure 5.16: comparison of leakage on actual devices with different films

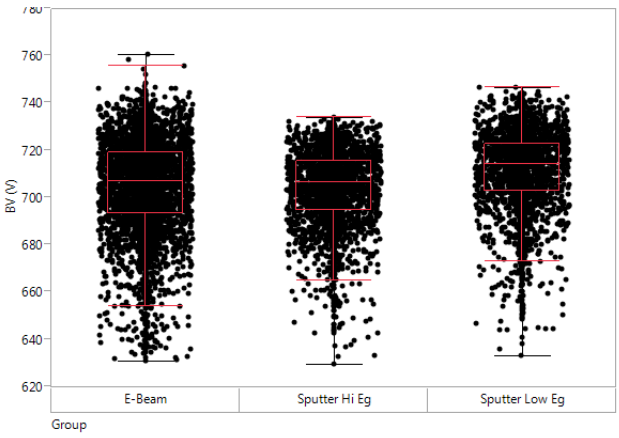

Figure 5.17: comparison of breakdown voltage on actual devices with different films

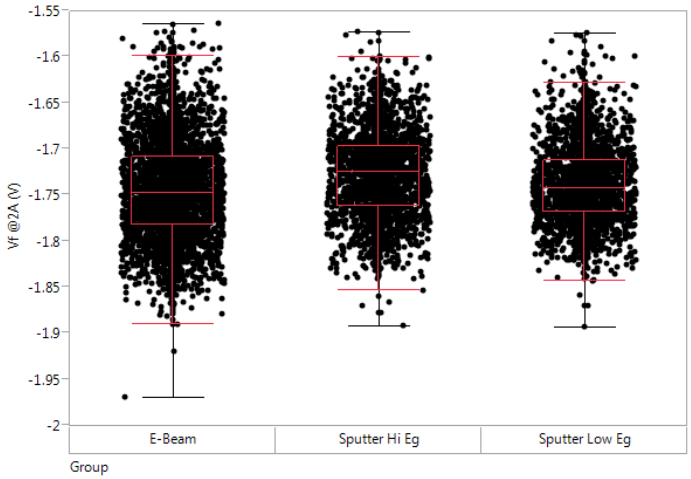

Figure 5.18: comparison of forward voltage drop on actual devices with different films

5.4.5.2 Comments

As we expected variations on a-Si had an impact on the leakage current of devices. Higher Eg films produced devices with lower leakage and more similar from what we obtained with e-beam evaporator, even without reaching the same performances. A lower Eg film, on the other hand, gives a film with higher leakage current. The other parameters: breakdown voltage and forward voltage drop, did not suffer the change of film type on the termination. This means that the film is not active during direct bias conditions and that, in the considered range, the efficiency of the termination is not affected by the changes of amorphous silicon.

5.5 Hydrogen addition on amorphous matrix structure.

5.5.1 Introduction

As we have seen in the previous paragraphs, the quality of sputtered material cannot match the one coming from e-beam evaporation. Sputtered material grows at lower vacuum levels in presence of a carrier gas. The speed of growth is faster, and the atoms carry a high kinetic energy due to the sputtering process. For all this reasons this material results in higher coordination defects level generating localized states in the bandgap. Measuring optically the Energy gap we have seen that apparently the calculated bandgap is lower for sputtered amorphous silicon while is higher on evaporated material and that, even with a change of sputtering condition, we never reach the same values as per e-beam material.

In order to try to produce a film with DC sputtering that can match the e-beam one, we decided to add to the carrier gas a small percentage of Hydrogen (2.5%). We have chosen such a small amount in order to have the hydrogen under the explosive limit. In this way the resulting gas mixture is inert and can be used also in tools not specify designed to handle explosive gases. As we have seen in chapter 2 hydrogen

is capable to saturate dangling bonds, and to reduce the film's stress. In figure 5.19 the sputtering scheme is presented.

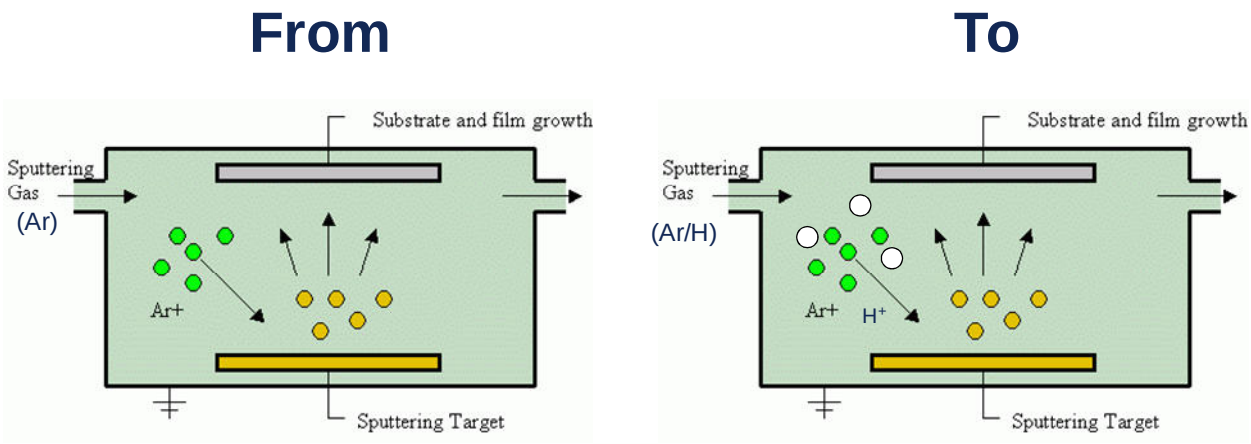

Figure 5.19: Hydrogen addition to carrier gas

We needed to validate that such diluted gas was still able to be incorporated in the silicon matrix changing its characteristics.

5.5.2 Experimental

We sputtered 5 wafers with the same deposition conditions (120°C heater temp, 7mTorr Argon, 50% power on a 3 kW power generator) for both a-Si and a-Si:H

In Table 5.20 is possible to find all the values relative to e-Beam evaportated, sputtered, and sputtered with hydrogen films. In figure 5.21 the corresponding scatterplot matrix is visible

Layer	Eg (eV)	n	k	STRESS e9 DYNE CM2
Sputter H	1.66	4.50	0.31	-4.29
Sputter H	1.65	4.49	0.31	-4.22
Sputter H	1.67	4.49	0.30	-4.32
Sputter H	1.65	4.50	0.31	-4.33
Sputter H	1.63	4.50	0.31	-4.35
Sputter	1.52	4.57	0.45	-6.43
Sputter	1.52	4.56	0.45	-6.36
Sputter	1.51	4.56	0.46	-6.4
Sputter	1.52	4.56	0.45	-6.31
Sputter	1.51	4.62	0.44	-6.65
e-beam	1.67	4.11	0.26	

Table 5.20: a-Si a-Si:H data comparison

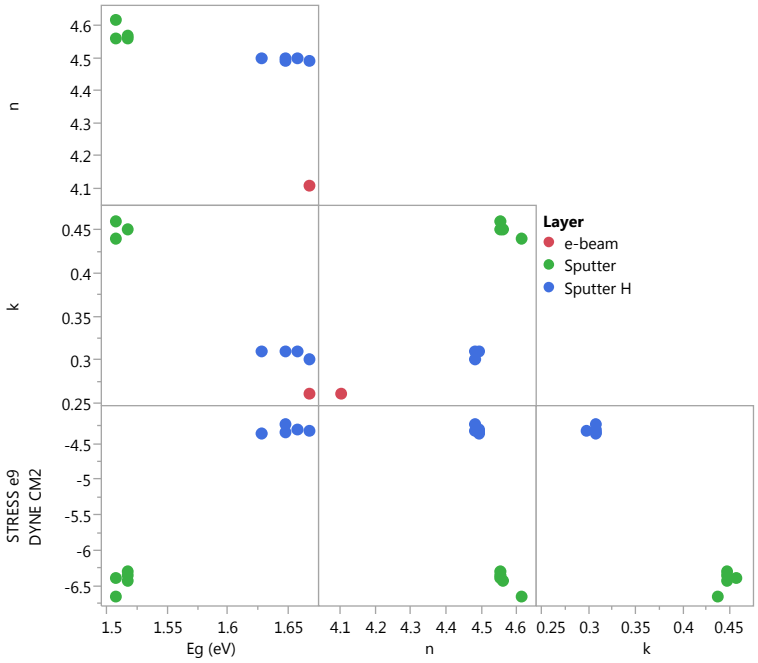

Figure 5.21: Scatterplot matrix

5.5.3 Comments

The results in the sputtered a-Si show that both the energy gap and extinction coefficient of a-Si:H went in the right direction to match those of e-beam evaporated a-Si. The real part of the refractive index is still higher, even if is lower than for pure sputtered a-Si. Also the stress is less compressive on a-Si:H. Those values means that the a-Si:H compared with pure a-Si is less dense and, due to the higher Eg presents less dangling bonds and coordination errors.

5.5.4 Test on Production samples

We tested the new a-Si:H film on a production lot as we did with the sputtered a-SI without Hydrogen. In figure 5.22 is shown the result.

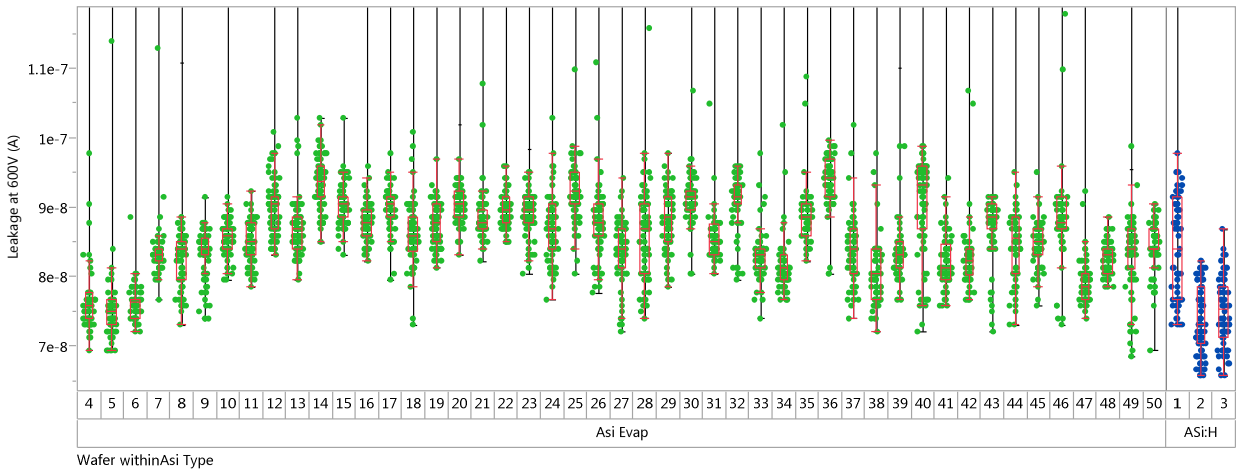

Figure 5.22: comparison of leakage current between a-Si:H obtained with sputtering and e-beam evaporated a-Si

As can be seen the film with hydrogen addition has the same leakage current compared with the one obtained with e-beam evaporation.

5.6 Conclusions

We developed a-Si:H film that can be used in a SIPOS termination with the same performances of a e-beam evaporated one. We have demonstrated that, if a small percentage of H is injected together with the carrier gas during the sputtering phase, the optical response as well as the structure of the material change with respect to a non hydrogenated a-Si film.

6 Amorphous Silicon and Aluminum interface interactions

6.1 Introduction

In chapters 3 and 4 we have analyzed the reactions between crystalline silicon and a sputtered aluminum film, and in particular we focused on the formation of the microstructure, the crystal structure (chapter 3) and the metal-semiconductor junction (chapter 4). In both cases oxygen plays a major role selecting the type of crystalline structure and, in this way, influencing the evolution of microstructure with temperature. The presence of oxygen at the interface may interfere with the formation of the schottky barrier. Introducing amorphous silicon on termination, we have to consider another type of interaction: in this case, the substrate is aluminum, with its native oxide on top, and the grown film is amorphous silicon. We will see that also for this system oxygen (this time initially bonded to aluminum) is an important player, that can change the way the two materials interact.

6.2 ALILE: characterization and stress

In this paragraph, we will talk about a phenomenon that is important to consider in order to explain amorphous silicon's behavior in the termination area during thermal treatments: the Metal Induced Crystallization (MIC).

In metal induced crystallization, an amorphous layer crystallizes at low temperatures in presence of a metallic film. This crystallization takes place in solid phase at temperatures way below the fusion point. It is a very interesting effect, since in this way is possible to obtain a low cost polycrystalline material starting from cheap amorphous films. Polycrystalline films are attractive for the industry since they may be employed for example in thin film transistors, in sensors, in solar cells. In order to trigger the amorphous -> polycrystalline transition a thermal treatment must be applied. This treatment is usually at low temperatures compared to the eutectic or fusion temperatures, and for this reason may be used when the system cannot handle high temperatures.

We will describe in detail the solid crystallization of amorphous silicon and in particular the crystallization induced by aluminum (aluminum induced crystallization AIC). In combination with the AIC the so-called aluminum induced layer exchange (ALILE) takes place: after the deposition of a-Si, if a successive sintering treatment above 405°C is applied, the aluminum and silicon layers change their reciprocal position and during the process a reorganization of the silicon internal structure happens

A scheme of the process can be seen in figure 6.1

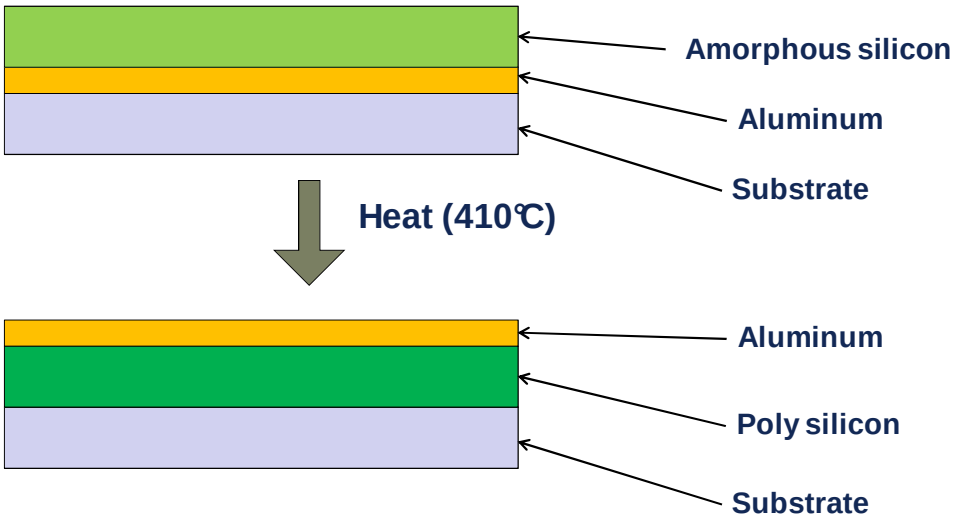

Figure 6.1 Aluminum induced layer exchange

We used three techniques in order to characterize the ALILE phenomenon: Optical microscope analysis, stress measurements and UV reflectance.

Microscope analysis is a valuable method, since amorphous silicon surface changes color near the points where the exchange and crystallization takes place. During the ALILE and AIC processes, the value of the amorphous silicon stress changes. The typical stress of sputtered amorphous silicon is compressive, while in presence of ALILE the layer's stress turns tensile. For this reason, studying the changes of the material's stress, can help to understand what factors plays a major role in ALILE. Finally UV reflectance can help to verify the AIC: due to the creation of a long range order, the two peaks at 276 and 365 nm become visible in the UV reflectance spectra.

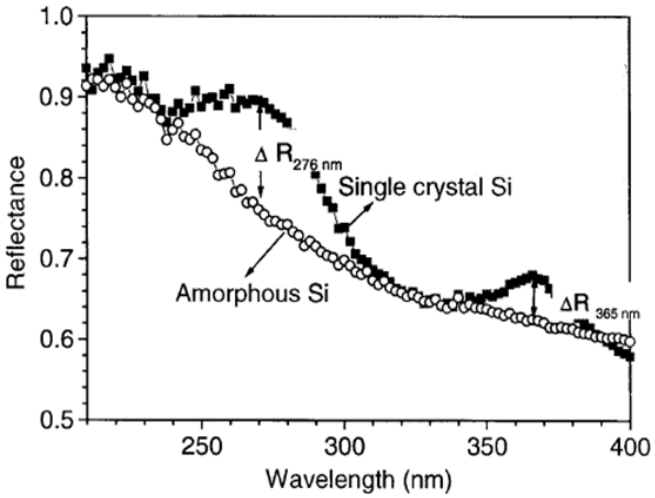

Figure 6.2 the UV reflectance spectra differences between amorphous and crystalline silicon

6.3 Experiments on aluminum / amorphous silicon interaction

As we have already seen in the previous chapters, stress is an important characteristic of thin films. Its control can be a key of success in many aspects of the manufacturing of electronic devices such as: process definition and control, film characterization, evaluation of structural changes. We have used stress to understand the causes of microstructure evolution, to predict the SBH in Aluminum/Silicon junctions and to tune the properties of the amorphous silicon film. Monitoring the stress can also be important in order to avoid wafer breakage due to excessive stress values.

For all this reasons we focused on stress analysis, and we verified how, all the phenomena occurring at the interface between the amorphous silicon film and the aluminum substrate, modified the stress accumulation.

6.3.1 Experiments summary

We did a series of experiments in order to identify all the variables involved

- Experiment 1:
  - Purpose: identify substrate influence on the stress of amorphous silicon sputtered material.
  - Factors: Substrate type
  - Response: stress value
- Experiment 2:
  - Purpose: identify the range of temperatures where ALILE is triggered
  - Factors: Substrate type, temperatures
  - Response: Stress, UV reflectance
- Experiments 3 and 4:
  - Purpose: characterize the variability of AmSi stress, taking into account the role of ALILE
  - Factors: Type of interface
  - Response: Stress

6.3.2 Experiment 1: Identify substrate influence

6.3.2.1 Introduction

The system exploration begun with a fist experiment whose goal was to indentify sources of interaction between amorphous silicon and its substrate. As we have seen in chapter 5, if no interaction is present with the substrate, sputtered amorphous silicon tends to generate compressive stress.

In this experiment we used different types of substrates in order to verify which one has the major impact on Amorphous silicon stress. In particular we focused on the presence of aluminum, either in the form of a surface contamination, or as film acting as substrate.

6.3.2.2 Experimental Flow

Here are presented the four substrates we tested with the corresponding experimental flows.

- [111] Monocristalline silicon: A monocristalline Cz silicon substrate with [111] orientation was used. Before Amorphous silicon deposition an RCA clean was performed.
- Silicon Oxide: a thin layer (2000 angstrom) grown at 1050°C in an horizontal furnace using a H_2O_2 gas mix was used. Since inside an horizontal furnace the film grows on both sides, in order to measure the stress correctly, we decided to remove the oxide from the back of the wafer using a BOE 6:1 solution. the flow can be seen in figure 6.3

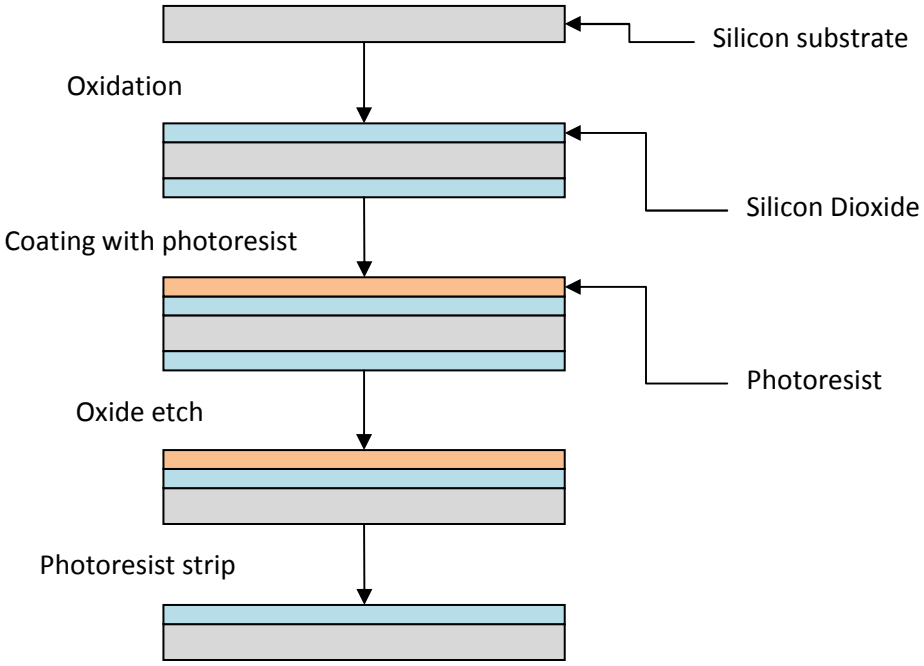

Figure 6.3: Experimental flow for silicon oxide substrates

- Al/Si alloy (1% Si wt). A very thin film (around 200 angstroms, thin enough not to change the substrate bowing) was deposited using a DC magnetron sputtering.
- Crystalline silicon with aluminum contamination. We decided to verify if, even after an aluminum layer was removed from a silicon substrate, the aluminum contamination that may still be present can influence the successive growth of amorphous silicon. For this purpose we sputtered a thin film of AlSi alloy on a [111] Silicon substrate. Then we removed it using a combination of two chemicals: E6 from Fujifilm and a Defreckle etch whose purpose is to remove the Silicon present on the AlSi matrix and that is not etched in the E6 bath.

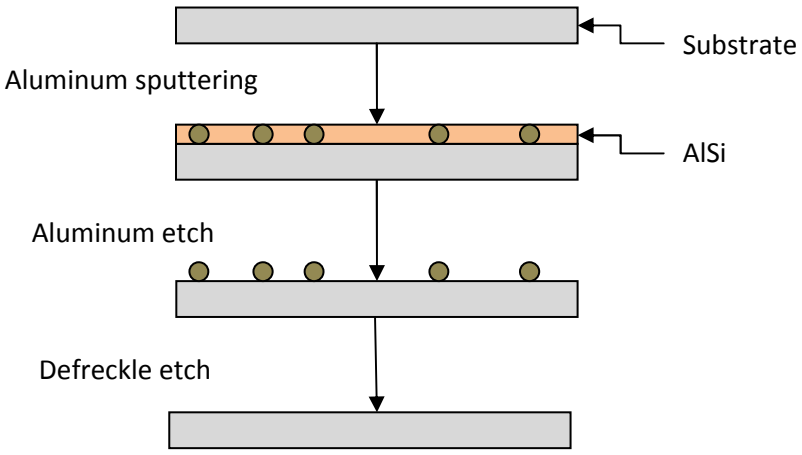

Figure 6.4: Flow for Al contaminated substrate

After the generation of those substrates, we deposited on each one a film of 1400 Angstrom of amorphous silicon

6.3.2.3 Results

In table 6.5 the resulting values of stress for different types of substrates is presented.

Substrate	Stress (Dyne/cm2)	Stress Vs Silicon reference
Bare Silicon	-5.87E+09	101%
Bare Silicon	-5.70E+09	99%
Oxide	-5.90E+09	102%
Oxide	-6.06E+09	105%
Aluminum	-5.00E+09	86%
Aluminum	-3.83E+09	66%
Si + Al contamination	-1.77E+09	31%
Si + Al contamination	-1.42E+09	25%

Table 6.5. Results for experiment 1

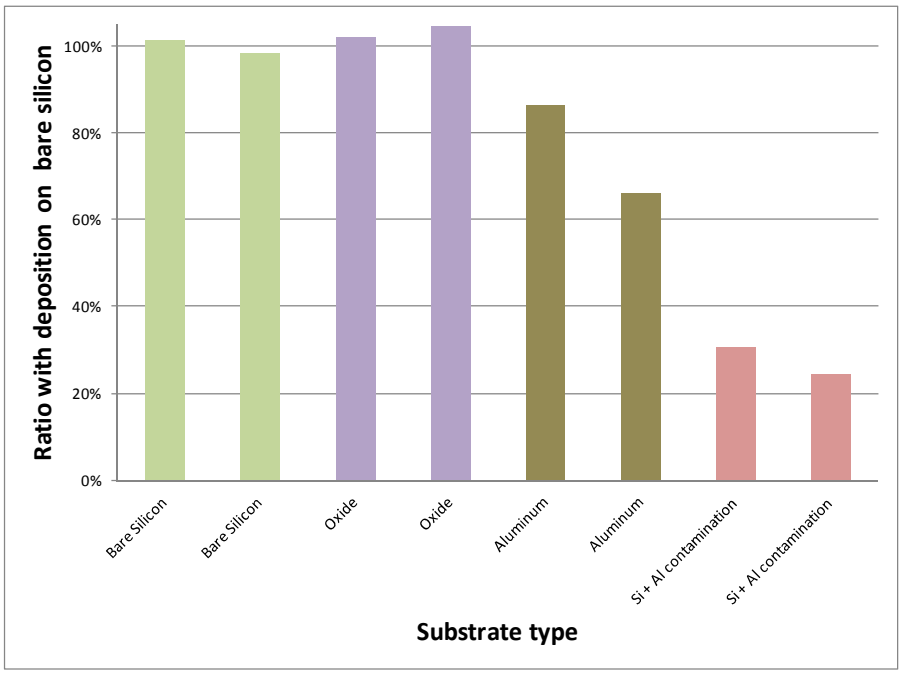

Figure 6.6: data plot for experiment 1

6.3.2.4 Results and comments

- **Bare Silicon sample**. On bare silicon the two runs have a slightly different stress level. the difference is due to normal process fluctuation. We used this stress value as a reference for the other samples.
- **Silicon Oxide Substrate**. It is interesting to notice that this sample behaves in the same way compared to the Bare silicon. We could expect that, since silicon oxide has a different expansion coefficient compared to silicon and aluminum this fact could interfere somehow during the growth.
- **Aluminum**. Stress level on thin silicon samples was less compressive compared to Bare silicon. This difference can be a proof a proof of the formation of a micro crystalline Layer in the interface between Amorphous silicon and the Al substrate. As we have seen on chapter 2 the transition between a disordered system (amorphous) to a much more ordered one shows a tensile component.
- **Al Contaminated interface**. The most interesting result on this samples comes from the aluminum contaminated interface samples. The stress level on this samples is very low, even lower than the Al ones. This Means that After the Al etch + Defreckle the Aluminum is still present on the silicon interface, and its efficiency in the a-Si µcrystallization at the interface is even higher than with pure aluminum.

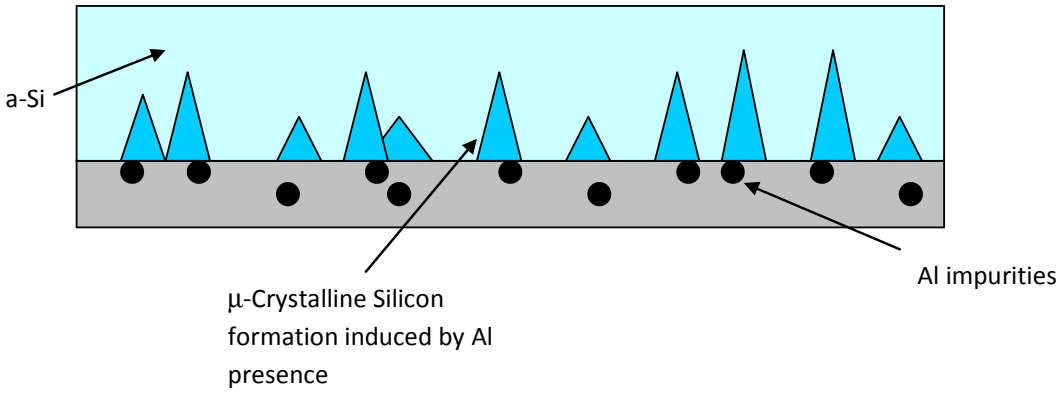

Figure 6.7. A possible scheme for micro crystallization in amorphous silicon film

6.3.3 Experiment 2: Furnace response.

6.3.3.1 Introduction

Since in production flows is common to have thermal treatments even in the final step of the process flow, we verified the influence of a furnace annealing on the samples generated in the previous experiment.

Since from literature for the AlSi system a critical temperature is around 405°C (this is the range of temperature to trigger the ALILE phenomenon), we processed the wafers around this temperature.

In particular we have taken the wafers from experiment 1 and we processed them in an horizontal furnace in nitrogen atmosphere at two different temperatures: 420°C and 380°C.

6.3.3.2 Results

In table number 6.8. for each substrate the ratio between of amorphous silicon's stress after the annealing process and its value after the sputtering of the film is presented.

Substrate	s/s0= @380°C	s/s0= @420°C
Bare Silicon	42%	32%
Oxide	41%	32%
Si + Al contamination	40%	31%
Aluminum	19%	-36%

Table 6.8: a-Si furnace response on different substrates

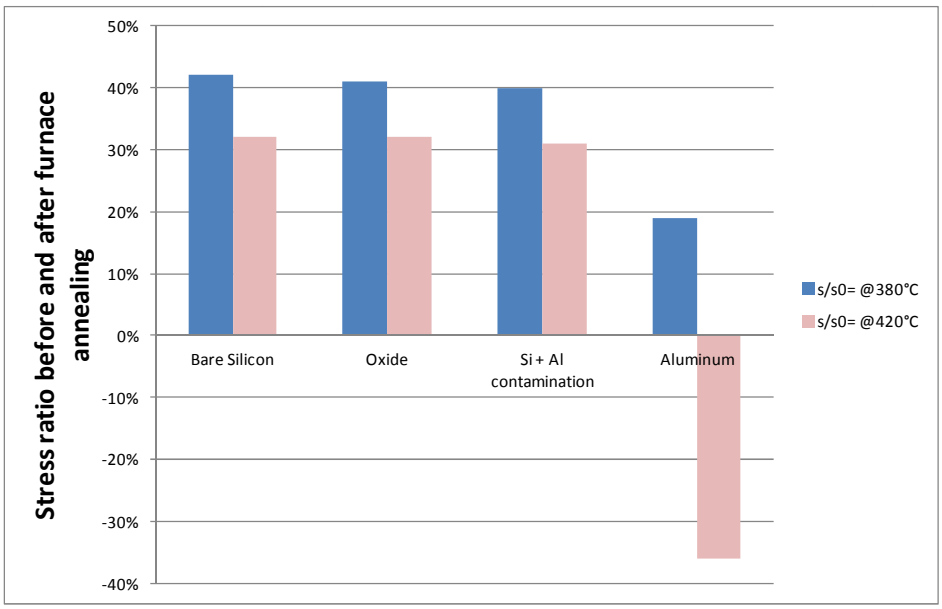

Figure 6.9 plot for a-Si furnace response on different substrates

On the two samples where the major changes of stress occurred (the ones with aluminum substrate), we took the UV reflectance spectra, that can be seen on figure 6.10

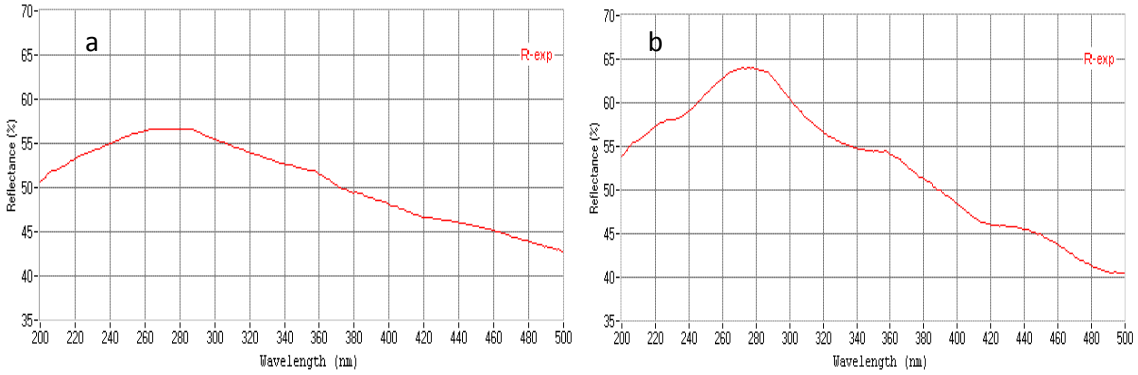

Figure 6.10 reflectance spectra of a-Si samples deposited on a thin Al layer a) with a furnace anneal @380°C b) with a furnace anneal @420°C

On the same samples we removed the Amorphous silicon Layer using a SF6 plasma etch in order to see how the aluminum surface under the film reacted. The result is showed in figure 6.11

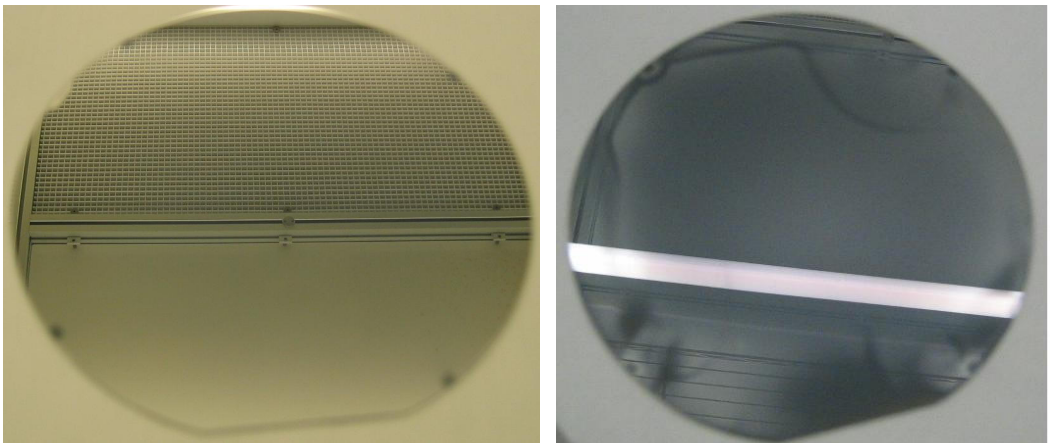

Figure 6.11: Result of the removal of the a-Si layer with a SF6 plasma etch from the samples with thin Al layer substrates

6.3.3.3 Comments

On all the samples the stress after furnace anneal was reduced. In this range of temperatures the thermal budged is probably high enough to induce a partial rearrangement of the film structure. At higher temperature (420°C) the resulting stress value was lower compared to lower values (380°C).

The substrate played a great role in the response of the system. The change in stress for pure silicon, silicon oxide and silicon with aluminum contamination are the same. This means that even if all the samples started from different stress values (as we have seen the Al contaminated samples showed a lower stress for example) the impact of the furnace anneal was the same. Is also important to notice that all the values remained compressive. The films that were sputtered on the thin aluminum films on the other hand, showed a different behavior. At 380°C the relaxation was greater than for all the other substrates, but the stress remained compressive. As the temperature reached 420°C on the other hand, the system changed, and the stress turned tensile. A removal of the amorphous silicon layer revealed that, on the 380°C sample no reaction occurred. The 420°C sample on the other hand reacted with the substrate, and this also deeply changed the internal structure of the amorphous silicon film.

The UV reflectance spectra of the two samples clearly show that, while at 380°C the system is still amorphous, after the 420°C treatment the two peaks that are characteristic of polycrystalline material appeared.

This first series of experiment we were able to gather some important information on our system, that will help during the next investigations:

- The substrate influences the starting stress level of sputtered amorphous silicon
- If a thin layer of aluminum is present under amorphous silicon, they react at temperatures above 400°C, giving
- A fast method to detect the reaction between aluminum and silicon is the compressive to tensile transition of the stress.
- When the stress turns tensile the material is deeply reorganizing its internal structure. The arise of a long range order, typical of a polycrystalline material can be seen looking at the UV reflectance spectra, and in particular at the 275 and 365 nm peaks.

Starting from this statements, we proceeded in the exploration of the system, focusing on stress evaluation and on the influence of different types of substrates.

6.3.4 Experiments 3 and 4: Stress response to interface type

6.3.4.1 Introduction

Two more experiments (we will call them Experiment 3 and 4) have been performed in order to study in deeper detail the influence of substrates and interfaces on the residual stress of sputtered amorphous silicon and its evolution in consequence of a furnace anneal. We will discuss them together for two main reasons: the samples had similar process flows and in order to compare the results. In experiment 3 the substrate employed for the amorphous silicon film deposition was aluminum, while on experiment 4 silicon with different types of contaminants was employed. In experiment 3 we investigated the aluminum microstructure (which was found to be related to the preclean-treatment employed before aluminum deposition), the hydration of the aluminum's surface, and the platinum presence (that was found to vary the behavior of aluminum). In experiment 4 aluminum was removed from the substrate before amorphous silicon deposition: the amorphous silicon was sputtered directly on the silicon substrate in order to test if a contamination of the surface (Aluminum, Platinum, or a combination of those material) could modify the stress.

6.3.4.2 Experimental

In order to evaluate the various structures, an experimental matrix has been appositely designed. A total of 22 wafers have been used: 12 on experiment 3 and 10 on experiment 4. On Table 6.13 is presented the list of samples and which process has been applied on each one. On Fig. 6.12 the schematic flow of each experiment is presented. Here are the process details:

On a substrate of Cz Si [100], a very thin layer (less than 100A) of platinum has been deposited on the backside of the wafers using e-beam evaporation at 100 °C. Before the deposition the samples were treated using a diluted HF (DHF) solution (1:100 HF:H2O) done at room temperature for 60 seconds. This cleaning step is necessary in order to remove native oxide that may interfere with the successive drive process. Diffusion of Pt in Si has been obtained by furnace annealing treatment at 950° for 60 minutes in

nitrogen atmosphere. Afterwards the samples were prepared for aluminum deposition. Since Al is very sensitive to the presence of oxygen at the interface, and this causes different microstructures to grow, two types of pre-cleaning has been applied: the same DHF treatment used before platinum evaporation, and the standard cleaning solution for silicon called RCA, which is the combination between SC1 (standard cleaning 1) and SC2 (standard cleaning 2) used respectively to remove particles and metallic contaminations. SC1 is a mixture of NH4OH:H2O2:H20 1:5:25 and SC2 is HCl:H2O2:H2O 1:5:25. Each bath time is 10 minutes at the temperature of 60°C. A very thin layer (less than 300 Angstrom) of Al-Si alloy (1% silicon) has been sputtered using a DC magnetron sputter (Varian 3290) in argon atmosphere at 7 mtorr for 2 seconds. The layer thickness was appositely chosen in order to avoid any variation of the initial curvature of the silicon substrate. In this way we can consider that the final curvature measure only depends on the successive amorphous silicon layer. On experiment 4 this layer was then removed with a commercial product (E6 by FFEM) followed by a "defreckle" etch to remove the silicon's particles that were present inside the Al-Si alloy. After having been Al covered and before the sputtering deposition of the amorphous silicon layer, the samples have been divided in three groups and submitted to three different treatments. The first two treatments did not involve any bath, but only the delay between aluminum and silicon deposition. Those times were respectively 48h and 5 minutes. All the processes have been performed in a ISO5 clean room with humidity @50% and temperature comprised between 19 and 21°C. The last group was cleaned with a DHF mixture for 1min, at room temperature. After those preparations amorphous silicon (a-Si) was sputtered in pure Argon atmosphere using a Varian DC magnetron sputter. The pressure during the deposition was 7 mtorr, on the deposition station the temperature was set at 150°C with a Power of 1 kW. On Experiment 2 two more samples were added, where no aluminum was deposited at all. This samples were used as a reference.

On both the experiments, at the end a furnace annealing at 420°C in nitrogen atmosphere for 60 seconds has been performed.

For all the samples after the process the stress has been measured using the substrate curvature method on a tencor FLX 2320. X-Ray Photoelectron Spectroscopy (XPS) was performed some interesting samples by means of a PHI 5000 VersaProbe - Physical Electronics system, equipped with an ion gun

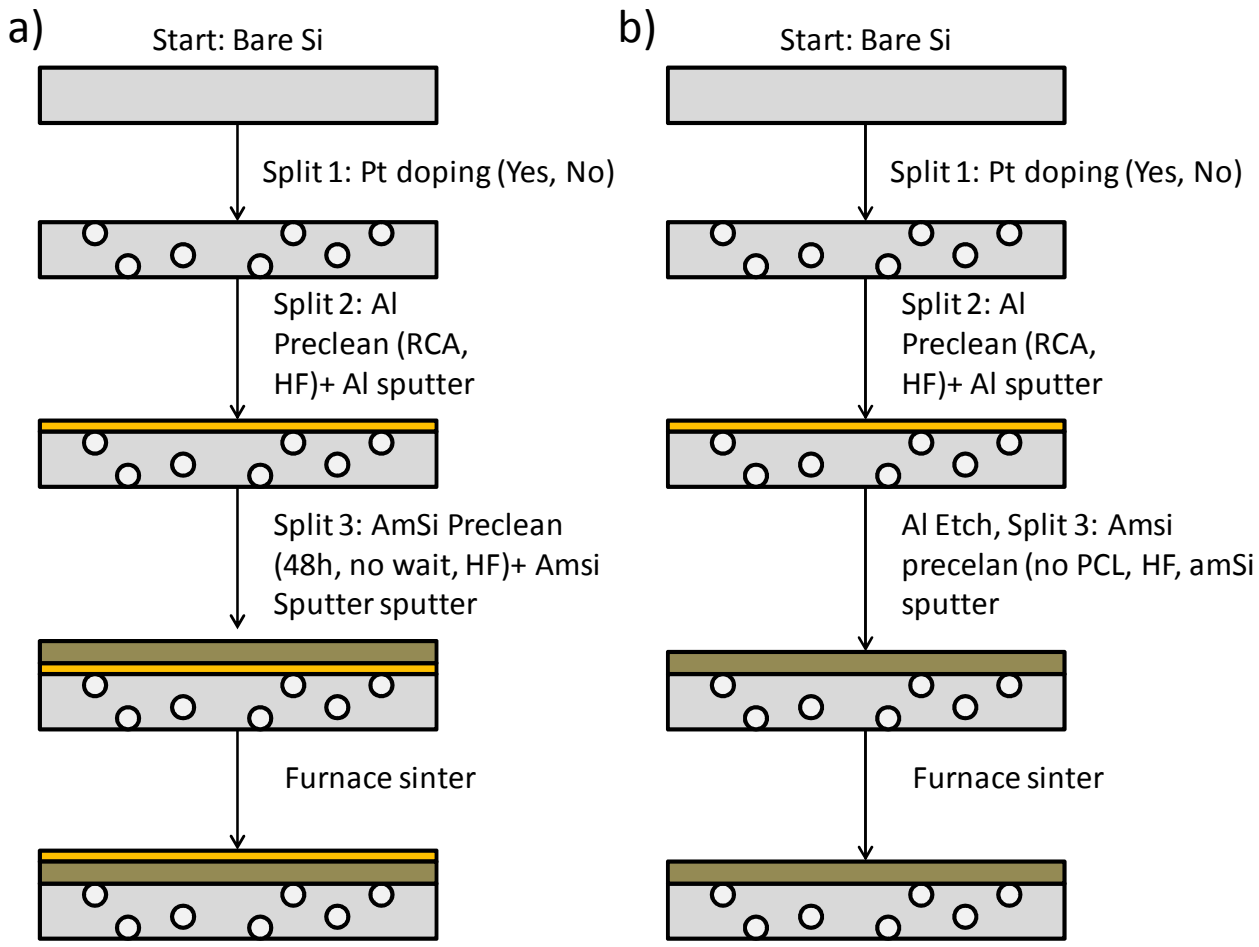

Figure 6.12: Experimental Flow for Experiment 1 (a) and Experiment 2 (b)

Experiment number	Sample ID	Pt Doping	Al Deposition	Al preclean	AmSi Preclean
1	1	Yes	Yes	HF	48h
1	2	Yes	Yes	HF	HF
1	3	Yes	Yes	HF	No wait time
1	4	Yes	Yes	RCA	48h
1	5	Yes	Yes	RCA	HF
1	6	Yes	Yes	RCA	No wait time
1	7	No	Yes	HF	48h
1	8	No	Yes	HF	HF
1	9	No	Yes	HF	No wait time
1	10	No	Yes	RCA	48h
1	11	No	Yes	RCA	HF
1	12	No	Yes	RCA	No wait time
2	13	Yes	Yes	HF	HF
2	14	Yes	Yes	HF	No precelan
2	15	Yes	Yes	RCA	HF
2	16	Yes	Yes	RCA	No precelan
2	17	No	Yes	HF	HF
2	18	No	Yes	HF	No precelan
2	19	No	Yes	RCA	HF
2	20	No	Yes	RCA	No precelan
2	21	Yes	No	RCA	No precelan
2	22	No	No	RCA	No precelan

Table 6.13: Process details for the two sets of experiments

6.3.4.3 Results

In figure 6.14 the stress values relative to a-Si film after the deposition (6.14a) and the sintering process (6.14b) are shown for experiment 3. The corresponding values obtained for Experiment 4 are reported in Fig. 6.15.

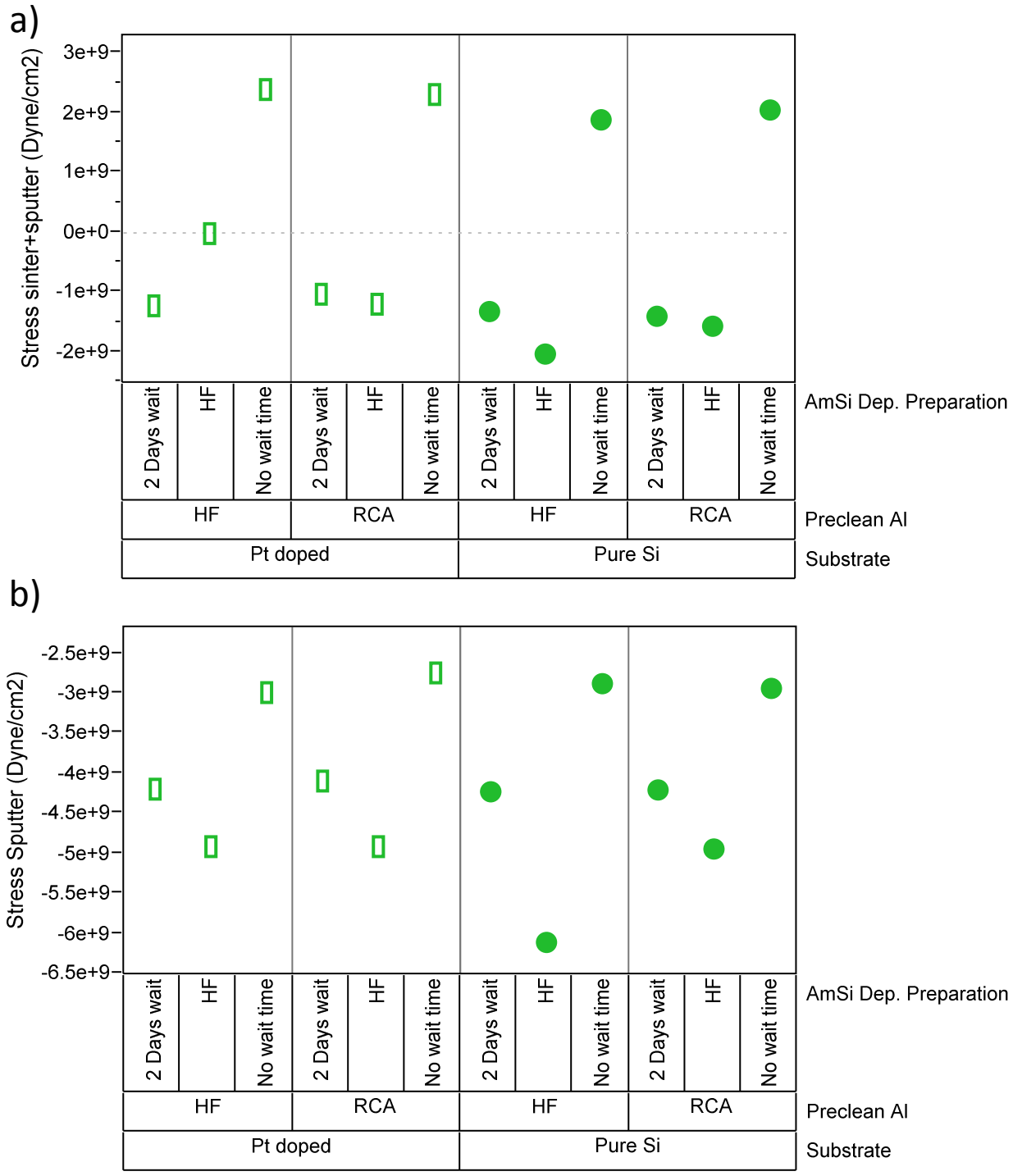

Figure 6.14. Experiment 3: a) a-Si stress after deposition b) a-Si stress after furnace sintering

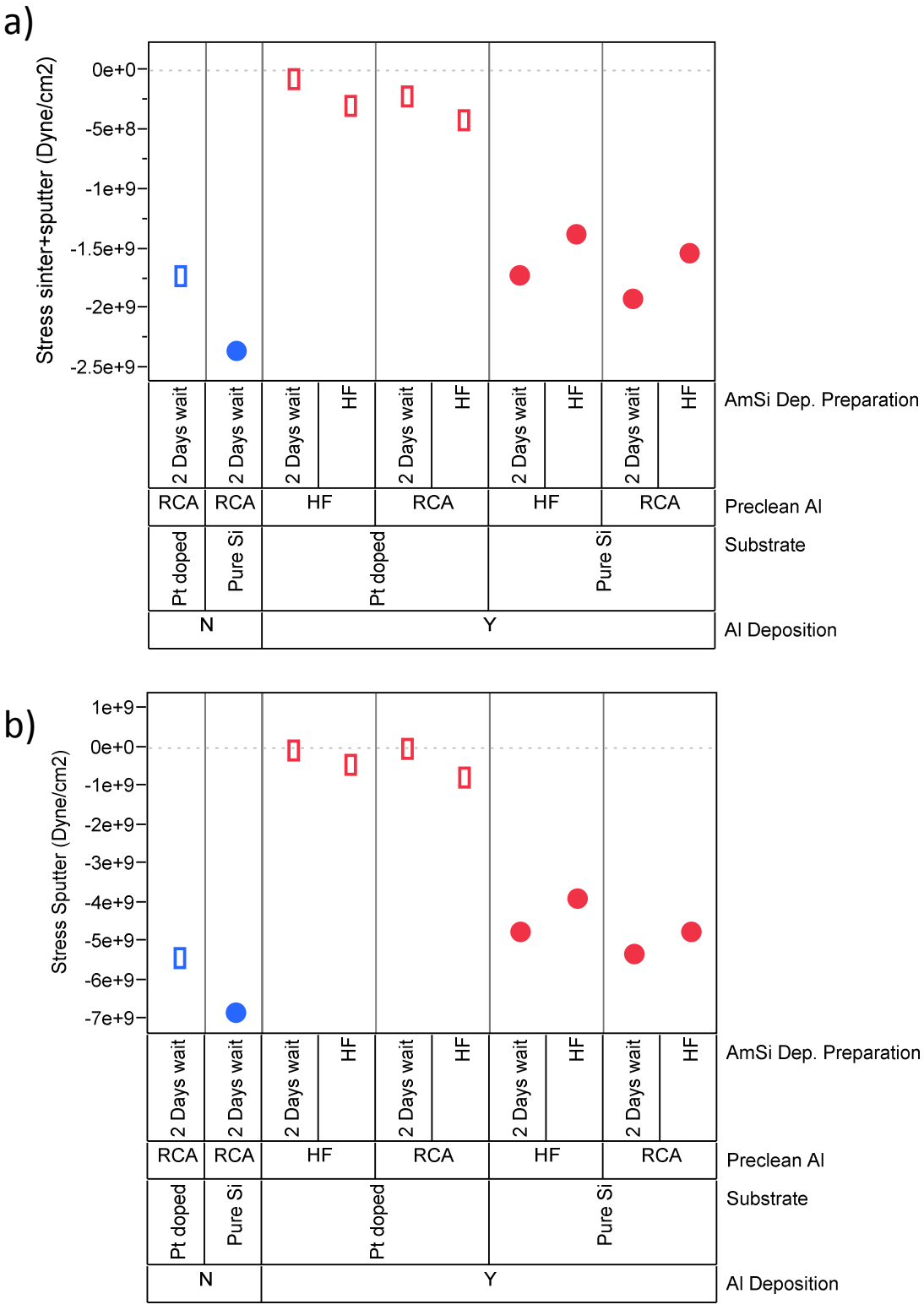

Figure 6.15. Experiment 2: a) a-Si stress after deposition b) a-Si stress after furnace sintering

The visual observation of the samples revealed that, in experiment 3, only 4 samples experienced a complete exchange between Aluminum and Silicon, and the Stress turned tensile.
In figure 6.16 is possible to see optical microscope pictures of two samples in exp 3, one with complete exchange (sample 12: no Pt on substrate, RCA as Al cleaning, and no wait time between Al and a-Si sputter) and the other (sample 11: no Pt on substrate, RCA as Al cleaning, and DHF cleaning between Al and a-Si sputter) without. In pictures 6.17 and 6.18 SEM and XPS analysis performed on the samples are reported.

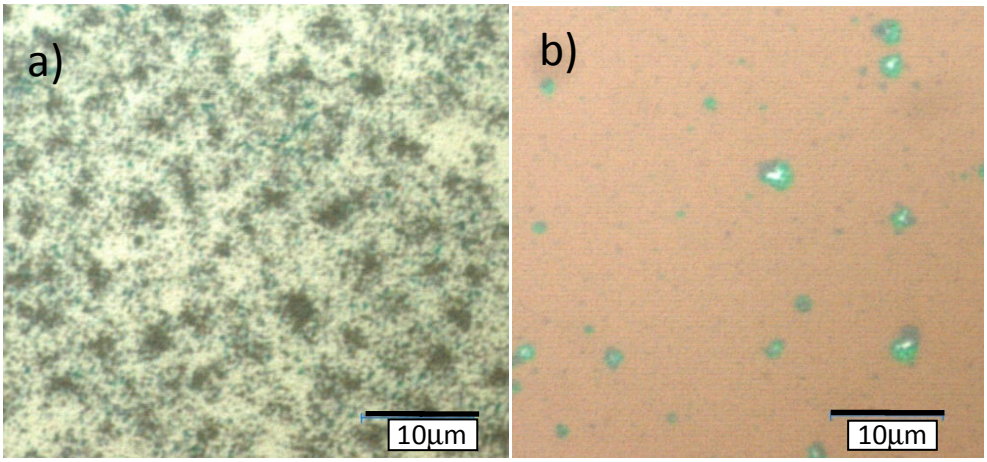

Figure 6.16: Images at optical microscope of sample 12(a) and sample 11(b). On the first sample aluminum exchanged with amorphous silicon and the stress turned tensile. Large Aluminum islands are visible on the surface giving arise to a metallic surface if inspected with bare eyes. On sample 11 only isolated traces of aluminum are visible on the surface, surrounded by a greenish material. The stress remained compressive even after the furnace sintering treatment.

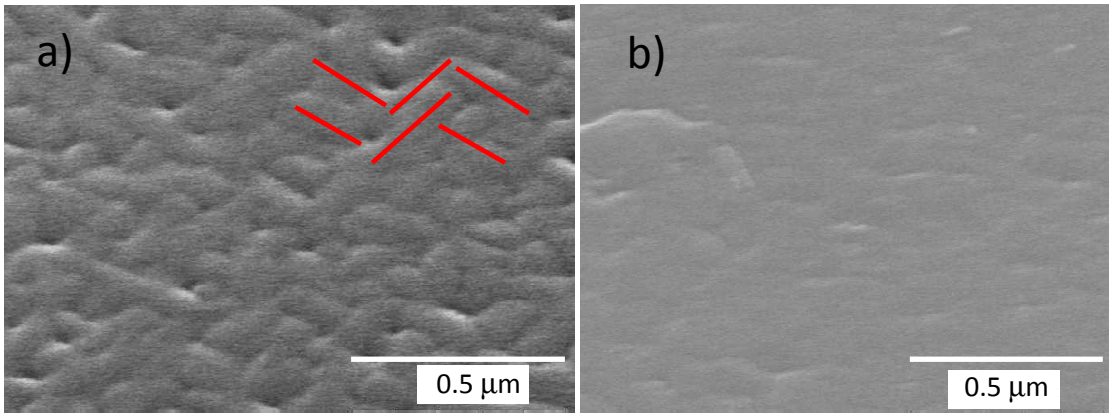

Figure 6.17: SEM pictures sample 12 (a) and sample 11 (b). On the first sample, where aluminum is on top, and the exchange took place, the surface's structure shows an ordered texture with 90° angles. The second sample (b) shows a disordered surface with limited surface's roughness.

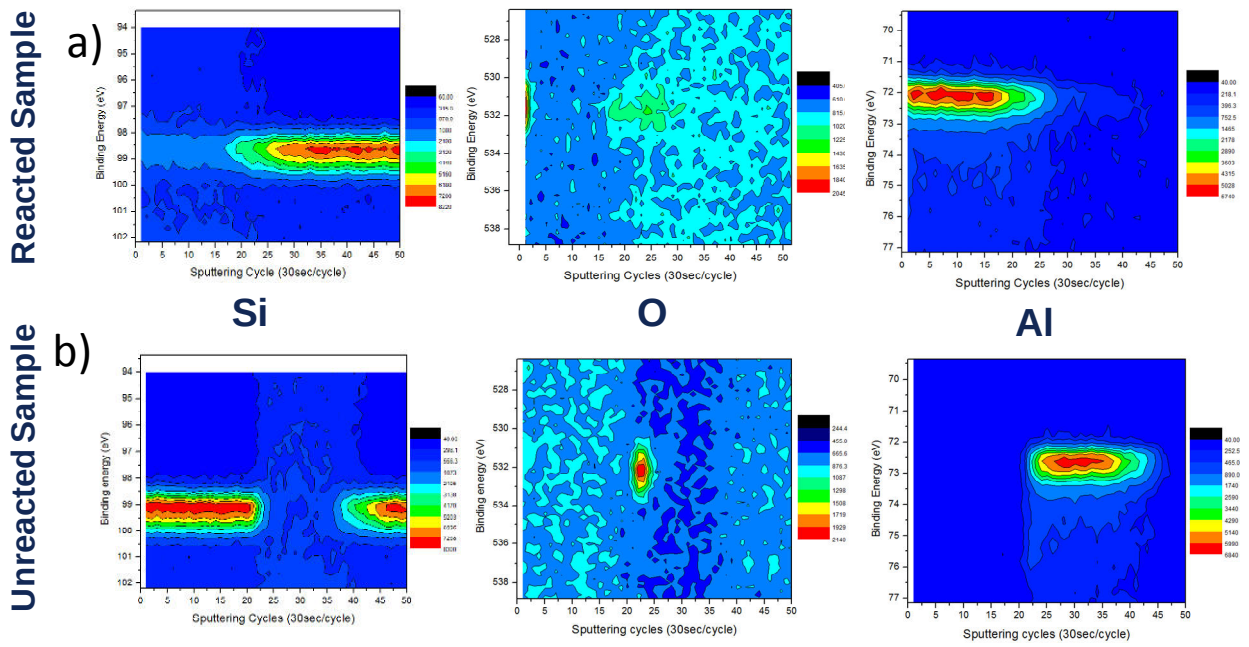

Figure 6.18: XPS depth profiles spectra for a sample where ALILE took place (a) and for a sample where no ALILE occurred (b). On the x axis the number of XPS sputtering cycles is reported, each cycle was 15" in argon pressure. On the y Axis the binding energy is reported, with a color scale to represent the counts value.

6.3.4.4 DISCUSSION

On experiment 3 we analyzed different types of interfaces between Al and a-Si. Is important to notice that a-Si is never deposited directly on the metallic aluminum, due to the presence of a very thin film of Aluminum oxide (Al_2O_3), which always grows and get hydrated after exposure to air (see details in chapter 2). The DHF solution (which is commonly used for aluminum cleaning in the semiconductor industry) can only partially remove this film, which is readily formed back when exposed again to air. Different preclean treatments were used in order to generate different types of Al microstructures. Moreover , since the Pt presence can change the potential of the Al_2O_3 top layer, also Pt enriched Si substrates have been employed. From the data we collected, reported in figure 6.14, it can be deduced that the stress of the a-Si films is mostly affected by the thickness and the composition of the alumina layer. From Fig.6.14a it is evident that the stress is minimal before annealing when only a very thin, native Al oxide layer was present. After the sintering in the furnace (fig 6.14b), in such films the stress changed from compressive (negative) to tensile (positive) and the ALILE phenomenon took place. Analyzing the XPS depth profiles spectra (fig. 6.18b), it is possible to see that on the sample where ALILE did not take place, the oxygen peak is very high and concentrated on the interface. This oxygen is bonded to aluminum as confirmed by the presence of a shoulder (73-76 eV) in the Al peak of the XPS spectrum. On the sample with ALILE on the other hand, it is possible to see that the a-Si and the

aluminum layer exchanged their position. The interface is in this case less abrupt, and the oxygen has been spread and diluted in the region where Silicon and aluminum have diffused one on the other. Looking at SEM pictures (Fig.6.17), it is possible to notice that on the reacted sample, after ALILE, the Al surface shows an ordered texture with elongated structures forming 90° angles. This effect is caused by the ALILE process. The lattices of Al and Si are compatible if they are 45° rotated one with respect to the other (the reticular mismatch is around 5% as we have seen in chapter 3). After aluminum migration through Silicon, both materials reorganize and they respectively use the other lattice as a template. In air-exposed samples, the presence of a thick amorphous oxide layer on the top of aluminum inhibits the exchange reaction: this amorphous and less ordered hydrated layer can act as a diffusion barrier. The role of Pt and the effect of cleaning treatment on the obtained stress values are not clearly visible(fig.6.14). However from a numerical analysis of the variance, the Pt effect on the stress is significant (t test gives probability >|t| = 1.9% using the a-Si preclean as a block and different types of preparations before Al deposition as repetitions) after the sintering treatment.

On experiment 4 the role of Pt on the other hand is clearly visible (fig 6.15a): in these samples Al is not present as a film, but as a surface contamination of the substrate. On all the samples where a metallic contamination is present, the stress of amorphous silicon is lower compared to pure silicon substrates. Moreover the stress values after the deposition are near to zero for the films in which platinum is present together with aluminum. In this experiment, the cleaning before the amorphous layer deposition has been found to give no effect. For none of the samples the stress sign turns to tensile values after sintering. This is due to the absence of a real Al layer.

6.4 Conclusions

In this chapter we have analyzed the variability of stress of a layer of sputtered amorphous silicon and the consequences of its interaction with different types of substrates. We have analyzed the reactions of the system to furnace annealing at temperatures in the range of 380/420 °C, paying attention to the role of interface. We have demonstrated that metallic contaminations change dramatically the initial stress of the sputtered amorphous silicon film, and that to generate a solid crystallization of the amorphous layer, we need to produce an exchange of layer between aluminum and silicon. A contamination is not enough for this purpose, since aluminum need to pass through a massive aluminum layer, in order to use its structure as a template to rearrange the lattice

7 Closing comments

7.1 Results summary

In this thesis, we explored the Al-Si system, paying particular attention to the effects that its characteristics produce on the structure of power diodes.

- The sputtering of a film of Al-Si (1% Si) on monocrystalline Si substrates, produces different crystal structures depending on the pre-treatment of the substrate
    - If native oxide is present on the silicon substrate the AlSi film doesn't show a preferential crystalline orientation
    - If the substrate is treated with HF, on (111) Si, the film grows with a preferential orientation that is 45° rotated with respect to the underlying lattice
- The microstructure of a sputtered Al-Si film varies with temperature and the result depends on the material's crystal structure
    - On films without a preferential orientation, the system relaxes the stress generating grains and grain boundaries
    - On films with a preferential orientation the film relaxes the stress generating big crystal domains, that at a XRD inspection result almost mono crystalline
- The SBH of Aluminum on silicon depends on the stress of the aluminum film. The higher is the stress, the higher is the SBH
- The SBH of aluminum on silicon can reaches almost 1 eV. This high value is caused by the reactions at the interface between the two materials: if thermal budget is applied, silicon is dissolved inside the aluminum, when it cools down re-crystallizes at the interface generating p-doped epitaxial formations.
- Amorphous silicon may be applied on the structure of devices in order to generate high efficiency SIPOS terminations
- Amorphous silicon on termination can be deposited with e-beam or by sputtering. Material produced with e-beam has superior characteristics
- The deposition conditions of sputtered amorphous silicon can be tuned in order to enhance its characteristics. In order to match the e-beam material, a certain amount of hydrogen must be injected together with the sputtering gas
- Amorphous silicon reacts with aluminum at temperatures above 400°C. The effect is a layer exchange between silicon and aluminum known as ALILE (aluminum induced layer exchange), during the exchange the solid crystallization of amorphous silicon occurs. The effect is known as aluminum induced crystallization (MIC)
- For the ALILE effect to occur, on the surface of aluminum only a thin layer of native oxide must be present.
- During the ALILE process, the stress changes turning tensile.

7.2 Industrial impact

The results obtained during the doctorate period, had a direct impact on the production of power diodes.

The understanding of the structure of aluminum, and the consequent tuning of production recipes, stabilized the optical appearance of the metallization layer. This allowed a high automatization of successive production steps.

The stabilization of aluminum SBH increased yields of products with this type of barrier, reducing the variability of final devices electrical parameters

The amorphous silicon obtained with sputter instead of e-beam, can be applied on devices, increasing in this way the productivity of the line

The deep comprehension of ALILE helped to solve many quality and reliability issues.

7.3 Future works

In the future we will continue to focus on the Al-Si system. In particular we will still work on amorphous silicon, in order to understand some differences that has been evidenced in reliability between e-beam and sputtered material. Work has still to be done on the marble effect: the objective is to find process condition that can produce a material without marble effect and with a low schottky barrier. Furthermore we will introduce platinum on the experiments, since this metal is important in fast diodes, and the interaction with aluminum and silicon may change the way the two materials react.

8 References

[1] A.R Forouhi and I. Bloomer, “Optical dispersion relation for amorphous semiconductors and amorphous dielectrics” phys rev B, 34, 7018 (1986)

[2] A.R Forouhi and I. Bloomer, “Optical Properties of Crystalline Semiconductors and Dielectrics” phys rev B, 38, 1875 (1988)

[3] C.Ayas, V. der Giessen “dislocation dynamics simulation of the relaxation of intrinsic stress in thin films” Philosophical magazine Vol 88 Nos 30-32 (2008)

[4] P.Riess, G.Ghibaudo, G.Pananakakis, J. Brini, G.Ghidini “electric field and temperature dependence of the stress induced leakage current”: Fowler-Nordheim or schottky emission?

[5] Howard C.Card, “Aluminum-Silicon Schottky Barriers and ohmic contacts in integrated circuits”, IEEE transactions of electronic devices, vol ED-23, no6, june 1976

[6] P. Van Mourik, E.J.Mittemeijer, Th. H. de Keijser “on precipitation in rapidly solidified aluminum silicon alloys” Journal of materials science 18 (1983) 2706-2720

[7] T. Stockmeier, K. Lilja “SIPOS-passivation for high voltage power devices with planar junction termination” Proceedings of the 3rd International Symposium on Power Semiconductor Devices and ICs, (1991) 145-148

[8] D. Dragomirescu, G. Charitat, F. Rossel and E. Scheid “Very high voltage planar devices using field plate and semi resistive layers: design and fabrication” International Semiconductor Conference, 2000. CAS 2000 vol1 (2000) 363-366

[9] D.Kim, B.Heiland, W.D. Nix, E. Arzi, M.D. Deal, J.D. Plummer “Microstructure of thermal hillocks on blanket Al Thin films” Thin solid films 371 (2000) 278-282

[10] P.R.Guduru, E.Chason, L.B. Freund “mechanics of compressive stress evolution during thin film growth” Journal of the mechanics and physics of solids 51 (2003) 2127-2148

[11] Y. Pang R. Huang “nonlinear effect of stress and wetting on surface evolution of epitaxial thin films” Physical review B 78, 075413 (2006)

[12] Y.F.Chen, S.F.Huang, W.S.Chen “kinetics of optically generated defects in hydrogenated amorphous silicon” Pysical rewiew B Volume 44 Nr 23 (1991)

[13] J.Dong, D.A.Drabold “atomistic structure of band-tail states in amorphous silicon” Physical review letters Volume 80, nr. 9 (1998)

[14] Y.Pan, F.Inam, M.Zhang, D.A.Drabold “atomistic origin of Urbach tails in amorphous silicon” Physiscal review letters PRL100 206403 (2008)

[15] Paul A.W.E. Verleg J.I.Dijkhuis “Resistance fluctuations in hydrogenated amorphous silicon: Thermal equilibrium” Physical review B Volume 58, Nr.7 (1998)

[16] S.Chakraborty, D.A. Drabold “static and dynamic properties of hydrogenated amorphous silicon with voids” Physical review B 79, 115214 (2009)

[17] H.M.Branz E.A.Schiff “Dangling bond relaxation and deep level measurements in hydrogenated amorphous silicon” Physical review B Volume 48 Nr.12 (1993)

[18] E.Pihan, A Slaoui, P. Roca I Cabarrocas, A. Focsa “Polycrystalline silicon films by aluminum –induced crystallization: growth process vs. silicon deposition method” Thin Solid Films 451-452 (2004) 328-333

[19] J. Shim, M. H. Lim, S. G. Jeong, J.H. Park, “Effects of annealing temperature and interfacial oxide thickness on layer exchange metal-induced crystallization” Journal of the Korean Physical Society, vol. 60, No. 5, March 2012, pp. L671-L673

[20] Y. Huang, F. Law, P. I. Widenborg, A. G. Aberle, “crystalline silicon growth in the aluminum indudec glass texturing process” Journal of Crystal Growth 361 (2012) 121-128

[21] M. Hosssain, H. M. Meyer III, H. H. Abu-Safe, H. A. Naseem, W.D. Brown “the effect of hydrogen in the mechanism of aluminum induced crystallization of sputtered amorphous silicon using scanning Auger microanalysis” Thin Solid Films 510 (2006) 184-190

[22] WANG ChengLong, FAN DuoWang, WANG ChengBin, GENG ZhongRong, MA HaiLin, MIAO ShuFan, “Poly-Si films with low aluminum dopant containing by aluminum induced crystallization” Science China, Vol. 53 January 2010 No.1: 111−115

[23] L. Cai, M. Zou, H. Abu-Safe, H. Naseem, W. Brown “Understanding the effects of stress on the crystallization of amorphous silicon” Journal of ELECTRONIC MATERIALS, Vol. 36 (2007) No. 3, 191-196

[24] H. Kim, Daewon Kim, G. Lee, Dongseop Kim, S. H. Lee “polycrystalline Si films formed by Al-induced crystallization (AIC) with and without Al oxides at Al/a-Si interface” Solar Energy Materials & Solar Cells 74 (2002) 323–329

Ringraziamenti

Vorrei ringraziare di cuore tutte le persone che mi sono state vicine, che mi hanno aiutato e supportato durante questa esperienza.

La Vishay, che mi ha permesso di intraprendere il percorso di dottorato, e che mi ha messo nelle migliori condizioni in questi anni per svolgere il mio lavoro.

Il mio relatore C.F. Pirri e tutte le persone del politecnico con cui è stato davvero un piacere svolgere il lavoro di ricerca.

Ringraziamenti particolari a due persone senza le quali questa avventura sarebbe stata molto diversa: Simone Cianchini, che mi ha sostenuto, supportato e aiutato, ma che soprattutto ha creduto in me e in questo progetto con una professionalità e un calore umano che davvero hanno fatto la differenza. Elena Tresso che, specie nell'ultimo anno, è stata una guida e un riferimento fondamentale per superare gli ultimi ostacoli grazie a una attenzione e una professionalità rare.

Infine ringrazio la mia famiglia. Tutto ha un senso grazie all'affetto delle persone più care.

… e poi certo … c'e' il correttore delle bozze